

**AFRL-VS-HA-TR-98-0049**

**SPECIAL EVENT DISCRIMINATION ANALYSIS:  
THE TEXAR BLIND TEST AND IDENTIFICATION  
OF THE AUGUST 16, 1997 KARA SEA EVENT**

**Douglas Baumgardt**

**ENSCO, Inc  
5400 Port Royal Road  
Springfield, Virginia 22152-2301**

**31 MARCH 1998**

**Final Report  
September 13, 1995 - January 31, 1998**

**19981016 026**



**DEPARTMENT OF ENERGY  
Office of Non-Proliferation  
and National Security  
Washington, DC 20585**



**AIR FORCE RESEARCH LABORATORY  
Space Vehicles Directorate  
29 Randolph Rd  
AIR FORCE MATERIEL COMMAND  
HANSCOM AFB, MA 01731-3010**

**DTIC QUALITY INSPECTED 4**

**DISTRIBUTION STATEMENT A**

**Approved for public release;  
Distribution Unlimited**

SPONSORED BY  
Department of Energy  
Office of Non-Proliferation and National Security

MONITORED BY  
Air Force Research Laboratory  
CONTRACT No. F19628-95-C-0203

The views and conclusions contained in this document are those of the authors and should not be interpreted as representing the official policies, either express or implied, of the Air Force or U.S. Government.

This technical report has been reviewed and is approved for publication.

Katharine Kadinsky-Cade  
KATHARINE KADINSKY-CADE  
Contract Manager

  
CHARLES P. PIKE, Deputy Director  
Integration and Operations Division

This report has been reviewed by the ESD Public Affairs Office (PA) and is releasable to the National Technical Information Service (NTIS).

Qualified requestors may obtain copies from the Defense Technical Information Center. All others should apply to the National Technical Information Service.

If your address has changed, or you wish to be removed from the mailing list, or if the addressee is no longer employed by your organization, please notify AFRL/VSOS-IM, 29 Randolph Road, Hanscom AFB, MA 01731-3010. This will assist us in maintaining a current mailing list.

Do not return copies of the report unless contractual obligations or notices on a specific document requires that it be returned.

# REPORT DOCUMENTATION PAGE

Form Approved  
CMB No. 0704-0188

Public reporting burden for this collection of information is estimated to average. 1 hour per response, including the time for reviewing instructions, searching existing data sources, gathering and maintaining the data needed, and completing and reviewing the collection of information. Send comments regarding this burden estimate or any other aspect of this collection of information, including suggestions for reducing this burden, to Washington Headquarters Services, Directorate for Information Operations and Reports, 1215 Jefferson Davis Highway, Suite 1204, Arlington, VA 22202-4302, and to the Office of Management and Budget, Paperwork Reduction Project (0704-0188), Washington, DC 20503.

|  |  |  |   |
|--|--|--|---|
| 1. AGENCY USE ONLY (Leave Blank)   | 2. REPORT DATE<br>March 31, 1998                         | 3. REPORT TYPE AND DATES COVERED<br>Final Report 9/13/95 - 1/31/98         |   |
| 4. TITLE AND SUBTITLE: Special Event Discrimination Analysis: The Texar Blind Test and Identification of the August 16, 1997 Kara Sea Event  |  | 5. FUNDING NUMBERS<br>F19628-95-C-0203<br>PE 6912OH<br>PR DENN TA GM WU AQ |   |
| 6. AUTHOR(S)<br>Douglas Baumgardt  |  |  |   |
| 7. PERFORMING ORGANIZATION NAME(S) AND ADDRESS(ES)<br>ENSCO, Inc.<br>5400 Port Royal Road<br>Springfield, VA 22152-2301  |  | 8. PERFORMING ORGANIZATION REPORT NUMBER                                   |   |
| 9. SPONSORING/MONITORING AGENCY NAME(S) AND ADDRESS(ES)<br>Air Force Research Laboratory<br>29 Randolph Road<br>Hanscom AFB, MA 01731-3010<br><br>CONTRACT MANAGER: Katharine Kadinsky-Cade/VSBS   |  | 10. SPONSORING/MONITORING AGENCY REPORT NUMBER:<br>AFRL-VS-HA-TR-98-0049   |   |
| 11. SUPPLEMENTARY NOTES: This research was sponsored by the Department of Energy, Office of Non-Proliferation & National Security, Washington DC 20585   |  |  |   |
| 12a. DISTRIBUTION/AVAILABILITY STATEMENT   |  | 12b. DISTRIBUTION CODE   |   |
| 13. ABSTRACT (Maximum 200 words)<br>The International Monitoring System (IMS) for the Comprehensive Test Ban Treaty (CTBT) faces the serious challenge of being able to accurately and reliably identify seismic events in any region of the world. Extensive research has been performed in recent years on developing discrimination techniques which appear to classify seismic events into broad categories of source types, such as nuclear explosion, earthquake, and mine blast. This report examines in detail the problem of effectiveness of regional discrimination procedures in the application of waveform discriminants to Special Event identification and the issue of discriminant transportability. |  |  |   |
| 14. SUBJECT TERMS<br>P/S amplitude-ratio discriminant, explosions, waveforms   |  |  | 15. NUMBER OF PAGES                               |
|  |  |  | 16. PRICE/CODE                                    |
| 17. SECURITY CLASSIFICATION OF REPORT<br>Unclassified  | 18. SECURITY CLASSIFICATION OF THIS PAGE<br>Unclassified | 19. SECURITY CLASSIFICATION OF ABSTRACT<br>Unclassified                    | 20. LIMITATION OF ABSTRACT<br>Unclassified<br>SAR |

## TABLE OF CONTENTS

|   |           |
|---|-----------|
| <b>1. INTRODUCTION .....</b>  | <b>1</b>  |
| <b>1.1 BACKGROUND .....</b>   | <b>1</b>  |
| <b>1.2 REPORT ORGANIZATION.....</b>   | <b>2</b>  |
| <b>2. A BLIND TEST OF SEISMIC EVENT DISCRIMINATION PROCEDURES FROM THE TEXAR CHALLENGE.....</b> | <b>4</b>  |
| <b>2.1 INTRODUCTION.....</b>  | <b>4</b>  |
| <b>2.2 OVERALL APPROACH TO THE BLIND TEST.....</b>  | <b>4</b>  |
| <b>2.3 WAVEFORM CHARACTERISTICS.....</b>  | <b>5</b>  |
| <b>2.4 DISCRIMINATION FEATURE EXTRACTION.....</b>   | <b>7</b>  |
| <b>2.4.1 Incoherent Beams.....</b>  | <b>7</b>  |
| <b>2.4.2 Pn/Lg Ratio.....</b>   | <b>9</b>  |
| <b>2.4.3 Frequency Dependence of Pn/Lg Ratio.....</b>   | <b>10</b> |
| <b>2.4.4 Spectral Discriminants.....</b>  | <b>10</b> |
| <b>2.4.4.1 Spectral Shape Discriminant.....</b>   | <b>12</b> |
| <b>2.4.4.2 Spectral Scalloping/Ripple Firing.....</b>   | <b>12</b> |
| <b>2.4.5 Other Miscellaneous Discriminant Features .....</b>                                    | <b>13</b> |
| <b>2.4.5.1 Rg Presence.....</b>   | <b>13</b> |
| <b>2.4.5.2 Pn Impulsiveness and Coda Shape.....</b>   | <b>13</b> |
| <b>2.5 REFERENCE EVENT SELECTION FOR PN/LG RATIO CHARACTERIZATION.....</b>                      | <b>14</b> |
| <b>2.6 INTER-REGION CHARACTERIZATION APPROACH USING PN/LG RATIOS.....</b>                       | <b>16</b> |
| <b>2.7 DISCRIMINATION RESULTS .....</b>   | <b>18</b> |
| <b>2.7.1 First Group of 10 Events.....</b>  | <b>19</b> |
| <b>2.7.2 Second Group of 10 Events .....</b>  | <b>30</b> |
| <b>2.8 SUMMARY OF DISCRIMINATION RESULTS .....</b>  | <b>39</b> |
| <b>2.9 OVERALL CONCLUSIONS.....</b>   | <b>41</b> |
| <b>3. CHARACTERIZATION OF THE AUGUST 16, 1997 KARA SEA EVENT .....</b>                          | <b>43</b> |
| <b>3.1 INTRODUCTION.....</b>  | <b>43</b> |
| <b>3.2 EVENT LOCATION AND RECORDING STATIONS .....</b>  | <b>44</b> |
| <b>3.3 INCOHERENT BEAMS AND OBSERVED REGIONAL PHASES.....</b>                                   | <b>47</b> |
| <b>3.4 SPECTRAL COMPARISONS OF KEV AND ARCESS.....</b>  | <b>49</b> |
| <b>3.5 PN/SN RATIO ANALYSIS AT KEV AND ARCESS .....</b>   | <b>50</b> |
| <b>3.6 PN/SN AMPLITUDE RATIOS AT SPITZBERGEN .....</b>  | <b>54</b> |
| <b>3.7 WAS THE KARA SEA EVENT AN UNDERWATER EXPLOSION? .....</b>                                | <b>57</b> |
| <b>3.8 OVERALL CONCLUSIONS.....</b>   | <b>62</b> |
| <b>REFERENCES.....</b>  | <b>63</b> |

## Illustrations

|     |   |    |
|-----|---|----|
| 1.  | Waveforms for blind test events plotted in distance order   | 6  |
| 2.  | Examples of incoherent beams in different frequency bands from the TEXAR recording of Event #3 (20 July 1996)   | 8  |
| 3.  | Spectra for the regional phases identified for Event #3 and the Pre- <i>Pn</i> noise in various display modes   | 11 |
| 4.  | ISEIS training set selection for Inter-Region Feature Comparisons   | 15 |
| 5.  | Comparison of the <i>Pn/Lg</i> ratios of the GERESS training set events with the TEXAR recordings for the blind test events   | 16 |
| 6.  | Comparison of the <i>Pn/Lg</i> ratios of the GERESS training set events with the TEXAR recordings for the blind test events   | 18 |
| 7.  | SMU Blind Test - Feature Extraction - Event #1 identified as earthquake   | 20 |
| 8.  | SMU Blind Test Feature Extraction - Event #2 that was identified as a blast   | 21 |
| 9.  | SMU Blind Test - Feature Extraction - Event #3 identified as a blast based on high and increasing <i>Pn/Lg</i> ratio, peaked spectra, and spectral scalloping indicating ripple fire                              | 22 |
| 10. | SMU Blind Test - Feature Extraction - Event #4, which was identified as a blast based on high and increasing <i>Pn/Lg</i> ratio, large <i>Rg</i> , peaked spectra, and spectral scalloping indicating ripple fire | 22 |
| 11. | SMU Blind Test - Feature Extraction - Event #5 identified as a blast based on large and increasing <i>Pn/Lg</i> ratios with frequency, and peaked and scalloped spectra   | 24 |

|     |  |    |
|-----|--|----|
| 12. | SMU Blind Test - Feature Extraction - Event #6 identified as a blast based on large $Pn/Lg$ ratios that increase with frequency, presence of $Rg$ , and scalloped spectra  | 24 |
| 13. | SMU Blind Test - Feature Extraction - Event #7 identified as earthquake based on low and frequency independent $Pn/Lg$ ratios and emergent $Pn$ with flat coda   | 25 |
| 14. | SMU Blind Test - Feature Extraction - Event #8 identified as blast based on increasing $Pn/Lg$ ratios with frequency, somewhat large $Pn/Lg$ values and spectral scalloping indicating ripple fire                           | 26 |
| 15. | SMU Blind Test - Feature Extraction - Event #9 identified as blasts based on weak evidence of ripple fire, and high $Pn/Lg$ ratios that follow blast trend at low frequency  | 26 |
| 16. | Event #9 Bandpass Filter Analysis - Interfering Local Event  | 27 |
| 17. | SMU Blind Test - Feature Extraction - Event #10 with questionable earthquake identification, based on large long-period surface wave   | 28 |
| 18. | Event 10 Filter Analysis   | 29 |
| 19. | Event 10 Spectra   | 29 |
| 20. | SMU Blind Test - Feature Extraction - Event #11 identified as earthquake based on flat $Lg$ spectrum and earthquake-like $Pn/Lg$ ratios  | 31 |
| 21. | SMU Blind Test - Feature Extraction - Event #12 identified as a blast based on large $Rg$ wave, impulsive $Pn$ wave, large and increasing $Pn/Lg$ ratio with frequency, and strong spectral scalloping caused by ripple fire | 32 |
| 22. | SMU Blind Test Feature Extraction - Event #13 which we classified as a blast based on large $Rg$ wave, large and frequency dependent $Pn/Lg$ ratios and spectral scalloping in all phase spectra.                            | 32 |

|     |  |    |
|-----|--|----|
| 23. | SMU Blind Test - Feature Extraction - Event #14 identified as a blast based on large $Rg$ wave, large and increasing $Pn/Lg$ ratios with frequency, and strong spectral scalloping caused by ripple firing | 33 |
| 24. | SMU Blind Test - Feature Extraction - Event #15 identified as earthquake based on earthquake-like $Pn/Lg$ ratios, emergent $Pn$ onset, and smooth spectra  | 35 |
| 25. | SMU Blind Test Feature Extraction - Event #16 identified as a blast-induced earthquake because it had unusual features characteristic of both blast and earthquake   | 35 |
| 26. | SMU Blind Test Feature Extraction - Event #17 identified as a blast-induced earthquake based on the same kinds of features as Figure 25  | 36 |
| 27. | SMU Blind Test - Feature Extraction - Event #18 identified as blast based on increasing $Pn/Lg$ ratio with frequency and weak evidence of scalloped spectra indicating ripple fire                         | 37 |
| 28. | SMU Blind Test - Feature Extraction - Event #19 identified as blast based on high $Pn/Sn$ amplitude ratios and weak evidence of scalloped spectra indicating ripple fire                                   | 38 |
| 29. | SMU Blind Test Feature Extraction - Event #20 identified as earthquake based on earthquake-like $Pn/Lg$ ratios and broad, smooth spectra   | 39 |
| 30. | Map showing propagation paths from the August 16, 1997 Kara Sea event to the stations used in this study   | 45 |
| 31. | Basemap showing locations of and great-circle propagation paths for events recorded at ARCESS that were used as a comparison reference set for the Kara Sea event recorded at KEV                          | 46 |
| 32. | Plots of filtered incoherent beams for the recordings of the August 16, 1997 Kara Sea event  | 47 |
| 33. | Comparisons of nuclear explosion spectra recorded at ARCESS and KEV  | 49 |

|     |  |    |
|-----|--|----|
| 34. | Plots of the log 10 $Pn/Sn$ ratios for discriminants for the August 16, 1997 event, recorded at KEV, with nuclear explosions, mine blasts, earthquakes, and an underwater event (Komsomolets submarine sinking) recorded at ARCESS                                 | 52 |
| 35. | Plots of the log 10 $Pn/Sn$ ratios for discriminants for the August 16, 1997 event, recorded at KEV, with nuclear explosions, mine blasts, earthquakes, and an underwater event (Komsomolets submarine sinking) recorded at ARCESS plotted versus filter frequency | 53 |
| 36. | Plots of the log 10 $Pn/Sn$ ratios for discriminants for the August 16, 1997 event, recorded at Spitzbergen  | 54 |
| 37. | Plots of the log 10 $Pn/Sn$ ratios for discriminants for the August 16, 1997 event, recorded at Spitzbergen and mid-Atlantic ridge earthquakes plotted versus frequency  | 56 |
| 38. | (a) Spectra for an event from the North Sea region near southern Norway recorded at FINESA. (b) Spectra for the same event recorded at NORESS. (c) Cepstra computed for the event in (a). (d) Cepstra computed for the event in (b)                                | 58 |
| 39. | Plots of array averaged spectra for the recordings of the August 16, 1997 Kara Sea Event at four recording stations.   | 59 |
| 40. | Cepstra for August 16, 1997 Kara Sea Event - 225 m Water Depth => 0.325 sec  | 60 |
| 41. | NRI incoherent beams (a) and Spectra (b) for propagation path east of the Kara Sea   | 61 |

# 1. INTRODUCTION

## 1.1 *Background*

The International Monitoring System (IMS) for the Comprehensive Test Ban Treaty (CTBT) faces the serious challenge of being able to accurately and reliably identify seismic events in any region of the world. This requirement extends to a very low magnitude threshold,  $mb=2.5$ , which is in the range of the sizes of local and regional seismic activity, both natural and artificial. Much research has been performed in recent years on developing discrimination techniques which appear to classify seismic events into broad categories of source types, such as nuclear explosion, earthquake, and mine blast. Ryall et al (1996) provides a review of many of these techniques and a discussion of some of their limitations. However, little effort has been directed toward assessing the utility of seismic event identification procedures in an actual operational setting.

In general, most seismic events can be identified quickly using some standard criteria for “screening” of events and not considered further. The most likely screening method would be location, which can identify most earthquakes on the basis of their being deep and/or located far out at sea. Such events need not be processed further.

Another type of event identification challenge that must be addressed in monitoring the CTBT is the “Special Event”, an event that cannot be quickly identified using screening methods. Special Events may be those that occur near known test sites or on land in aseismic areas, or near some other suspicious location. An example is the recent August 16, 1997 event that occurred near the Former Soviet Union test site at Novaya Zemlya. Special Events would require more in-detail analysis than standard screening methods. Furthermore, it’s very possible that the event may occur in a region for which there is little historical seismic record, and thus, reference events of known identity may be difficult to find that can be used as “training events” for identification of the special event. This would be particularly true for nuclear explosions, since most nuclear explosion testing has only occurred in certain geographic regions of the world. Under the CTBT, countries must be monitored that have never tested nuclear weapons in the past. Thus, it will be necessary to have discrimination methods that utilize events of known type in certain regions of the world to be applied as reference events in other regions. The concern is that geological and tectonic differences might not allow the “transporting” of regional discriminants from one region of the world to another region.

In previous studies (Baumgardt, 1995), we have argued that Special Events must be characterized using discriminants that are known to be transportable and using reference events of known type in other regions recorded perhaps at different stations. The latter approach is scientifically problematic since the effect of station structure and path difference on waveform discriminants may be unknown. Transportable discriminants would be those which are insensitive to such regional differences, can be corrected for propagation path effects, or applied to situations where site and propagation differences are known to be minimal. We may, for example, be able to transport path-sensitive regional discriminants between shield areas but not from a shield area to a tectonically active area.

## **1.2 Report Organization**

This report examines in detail the effectiveness of regional discrimination procedures in the application of waveform discriminants to Special Event identification and the issue of discriminant transportability.

In Section 2, we present the results of a blind-test study, arranged by Professor Eugene Herrin of Southern Methodist University, in which we were sent 20 events of unknown identity recorded at the TEXAR array in southern Texas. We were to use the discrimination techniques in the Intelligent Seismic Event Identification System (ISEIS) to determine how many events we could identify. We were provided no reference events of blasts and earthquakes recorded at TEXAR. Rather than collecting such a training-set database, we utilized features collected earlier in ISEIS for blasts and earthquakes recorded at the GERESS array. Thus, we are attempting to transport discriminants from a different region of the world for events recorded at a different station to identify the events at TEXAR. This is the kind of Special Event problem that may be confronted by the IMS, i.e., that events recorded in areas with limited or no historical record of seismic sources must be characterized in a timely manner. We show the results of this method, which we call *inter-region comparison*, applied to the 20 blind-test events.

Section 3 presents the results of our analysis of the August 16, 1997 Kara Sea event that occurred near the former Soviet test site at Novaya Zemlya. Because the ARCESS array was down at the time, we again had limited historical data to compare with this event. Some investigators (e.g., Richards and Kim, 1997) have studied this event by using a non-IMS station, KEV, to compare the Kara Sea event with nuclear explosions at Novaya Zemlya recorded at KEV. These studies could only investigate if the Kara Sea event was consistent or inconsistent with nuclear explosions. Other studies have used other stations

(e.g., NRI, Spitzbergen) which recorded the Kara Sea event, but had a limited historical record of the nuclear explosion data or had very poor quality data. In this report, we assume transportability and show that KEV and ARCESS have similar enough site and propagation effects that events at the two stations can be directly compared. Thus, we compared the KEV recording of the Kara Sea event with historical recordings of earthquakes, mine blasts, and nuclear explosions at ARCESS. We also consider the question of whether or not the August 16, 1997 event could have been an underwater explosion given that it was located offshore.

## **2. A BLIND TEST OF SEISMIC EVENT DISCRIMINATION PROCEDURES FROM THE TEXAR CHALLENGE**

### ***2.1 Introduction***

This study has arisen from a challenge given by Professor Eugene Herrin of Southern Methodist University to the seismic discrimination community to attempt to identify, using any variety of discrimination techniques, a set of seismic events recorded at the IMS array located in West Texas near Lajitas, called TEXAR. We decided to attempt to identify the events as a test of event identification methods for Special Events and the transportability of regional discriminants. Because TEXAR is a recently installed array to be part of the IMS, we have limited knowledge of the historical events in the region monitored by the array. We wanted to test our discrimination techniques, developed as part of the Seismic Event Identification System (ISEIS) (Baumgardt et al, 1991), and the application of the reference region approach to selecting reference events.

### ***2.2 Overall Approach to the Blind Test***

In the blind test, we were to identify 20 seismic events, presumed to be known by SMU, but unknown to us. We know that they were regionally recorded at TEXAR, and thus had to have occurred somewhere in the vicinity of the southwestern U.S. The following are the general conditions under which we took the blind test:

(1) Twenty seismograms of events recorded at the TEXAR array were provided by SMU. The first 10 events were received and processed in October, 1996. The second set of 10 were received and processed in August of 1997. These events were placed in the Oracle database. We utilized the standard database schema (Anderson et al, 1990) developed for the Center for Monitoring Research (CMR), formerly the Center for Seismic Research (CSS), that has served as the prototype for the International Data Center (IDC).

(2) We were generally not given much information about the event parameters in order to prevent the possibility that we could identify the events by other means. For the first 10 events, we were provided dates, times, locations, and magnitudes. Only the dates of the events were provided for the second 10 events. Because some of the discriminants used in this study, most notably the regional *P/S* ratio discriminant, required distance corrections, the distances of the events from TEXAR were provided. We placed dummy origins and

locations into the database in order to process them through ISEIS. We generally ignored the locations and magnitudes for the first 10 events, although in actual operational practice, this information would be useful for identification. In this study, however, we were interested in learning how well waveform discriminants performed without other information.

(3) No ground truth was provided. In essence, this dataset was the first we had ever studied at TEXAR, and thus, we had no historical data with which to compare these events, i.e., no training events recorded by the TEXAR array to do discrimination. This, of course, will be a fundamental problem which will have to be addressed by the IMS for new stations and arrays. Our solution was to seek out other events recorded at a different station in the absence of known events recorded at the TEXAR array. We discuss this approach below.

(4) No regional phase identifications were provided, so all phases had to be picked. Using ISEIS, we picked the phases *Pn*, *Pg*, *Sn*, *Lg*, and *Rg* on those waveforms where these phases could be observed. Since distances of the events from TEXAR were provided, we were able to make some predictions of travel times, and produce record sections, to aid in the actual identification of the regional phases.

(5) All discrimination features were extracted by the ISEIS system and placed in the Oracle database.

(6) All events were then identified by visual analysis of features. Although ISEIS has an expert system and we have developed Bayesian probabilistic decision trees for decision making about seismic discrimination (e.g. Baumgardt and Karafotis, 1995), we opted not to use these tools in this exercise.

### **2.3 Waveform Characteristics**

The events sent to us were all recorded on the short-period array elements of the Lajitas, Texas Seismic Array (TEXAR). TEXAR has ten short-period elements located in West Texas (Bonner et al, 1997). No magnitude estimates were included with the data. All the events were small, with  $mb < 4.0$ , and were thus primarily observed at regional distances.

Figure 1 (a) and (b) show record section waveform plots for the first and second set of 10 events, respectively. The waveforms shown are recordings at the TEXAR - TX02 array element. Each waveform has been passed through a 0.6 to 4.5 Hz Butterworth bandpass filter in order to enhance the recorded signals. All waveforms have been aligned to the first

arrival phase, assumed to be  $Pn$ , and the time scale is relative in seconds. The phase picks are indicated.

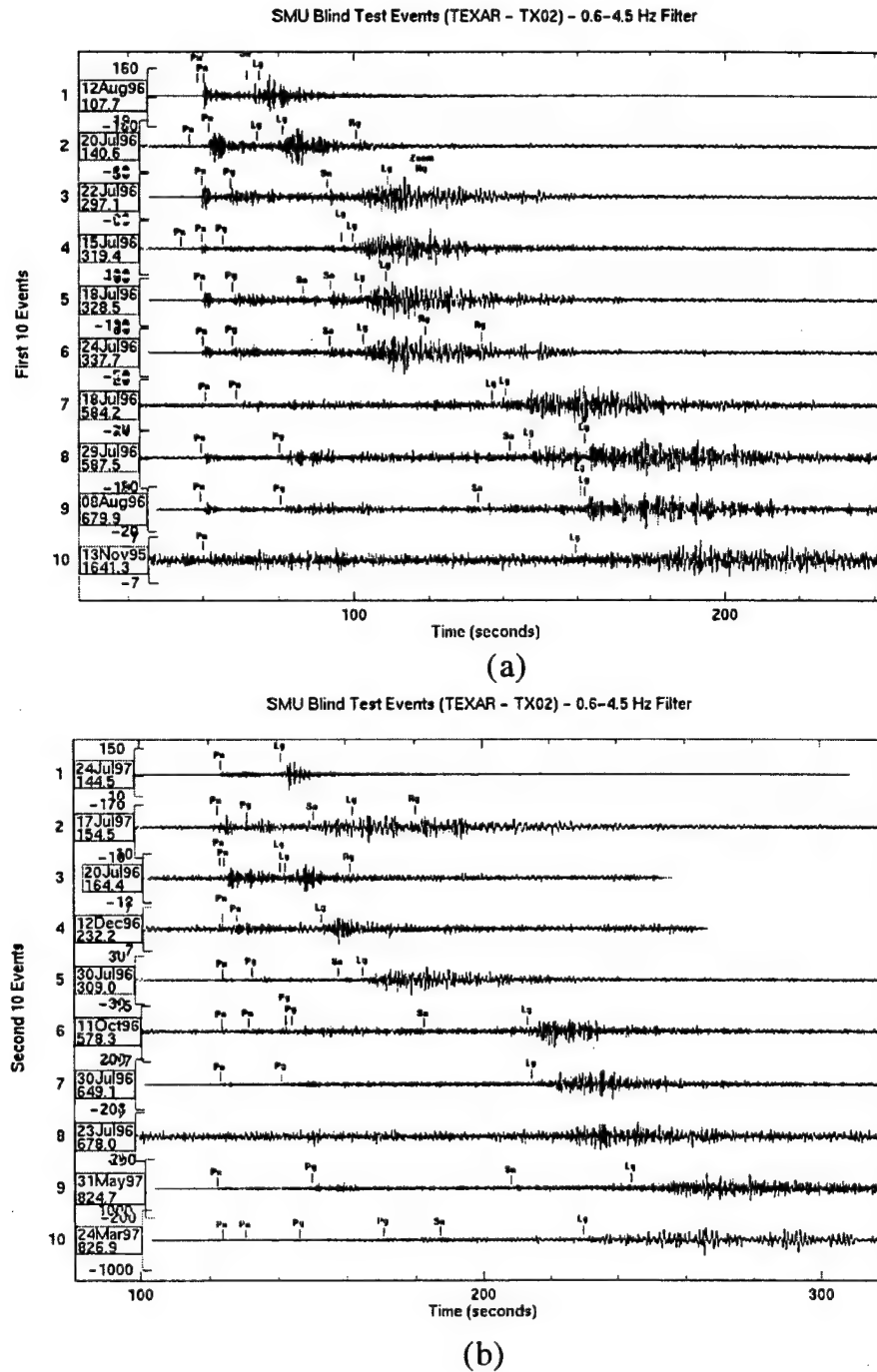


Figure 1 Waveforms for blind test events plotted in distance order. All events have been filtered from 0.6 to 4.5 Hz. (a) First 10 events; (b) Second 10 events.

In most cases, a regional  $Pn$  and  $Lg$  could be identified on all traces. It should be noted that many of these phases were picked on filtered waveforms in different bands than that in Figures 1 (a) and (b), and sometimes on incoherent beams, discussed in the next section. In a number of cases, long duration  $Lg$  codas and  $Rg$  phases were observed, primarily at low frequency (< 1 Hz). Also, interestingly, a number of  $Sn$  phases, commonly not thought to propagate efficiently in western U.S., were identified mainly on the basis of their arrival times relative to the other phases.

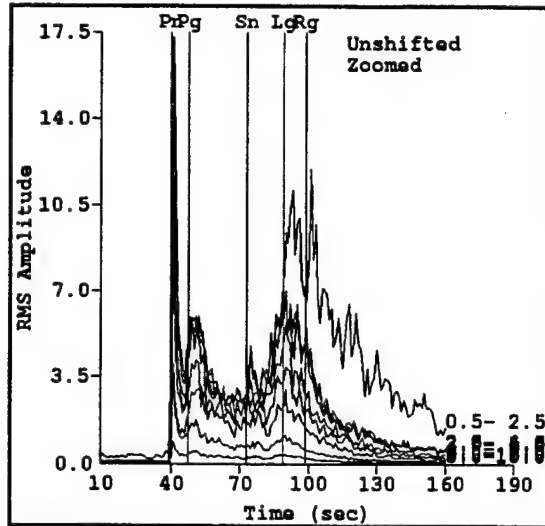
## 2.4 Discrimination Feature Extraction

To identify the events, we used features extracted by the Intelligent Seismic Event Identification System (ISEIS) (Baumgardt et al, 1991). We relied on a set of fundamental features that various research studies in the past have shown to be effective for the discrimination of explosions and earthquakes. Because these events are assumed to be very small, we relied principally on short-period discriminants, with the exception of Event #10. This event had some unusual properties that required looking at long period signals, which we discuss in more detail below.

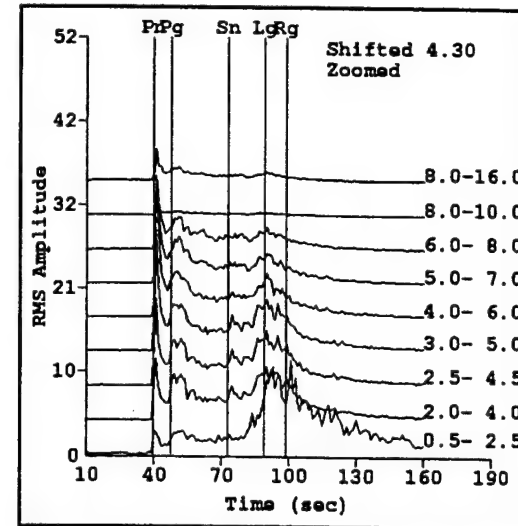
### 2.4.1 Incoherent Beams

Incoherent beams are averages across the TEXAR array of the average rms amplitude levels in 1-second time windows on waveforms. Each waveform was prefiltered in nine frequency bands, in Hz: 0.5-2.5, 2-4, 2.5-4.5, 3-5, 4-6, 5-7, 6-8, 8-10, and 8-16, prior to the averaging. Incoherent beams provide a smoothed representation of the envelope of the regional seismic waveform in the different filter bands.

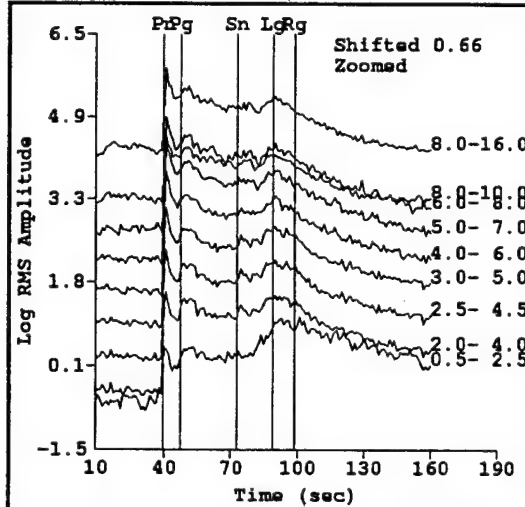
Examples of different ways of displaying the incoherent beams are shown in Figure 2 for Event #3 of 20 July 1996. In Figures 2 (a), (b), and (c), the phase picks, made on the original waveforms, are shown as vertical lines. In the case of this event, five phases,  $Pn$ ,  $Pg$ ,  $Sn$ ,  $Lg$ , and  $Rg$ , were identified on the waveforms, and they appear as envelope peaks on the incoherent beams. In Figure 2(a), incoherent beams are plotted on an absolute scale whereas in Figure 2(b) they are shown shifted. Displaying the beams on an absolute scale shows variations in signal-to-noise ratios in different frequency bands, but sometimes results in overlapping traces that can be confusing. Shifting the incoherent beams makes it easier to see important differences in the shapes of the incoherent beams in different frequency bands. Sometimes, phases are easier to identify on incoherent beams than on the waveforms themselves. In this example, a weak  $Sn$  phase can be seen



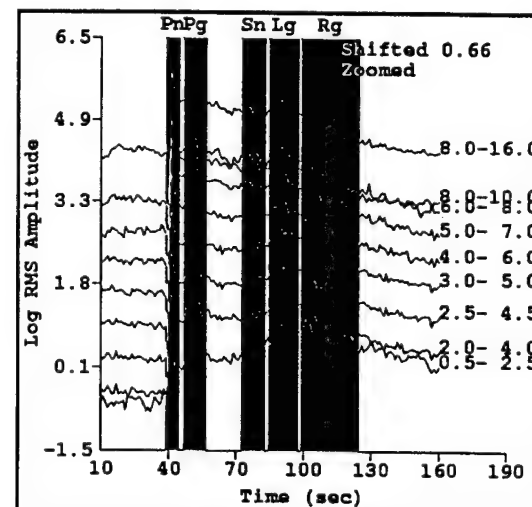
(a)



(b)



(c)



(d)

Figure 2: Examples of incoherent beams in different frequency bands from the TEXAR recording of Event #3 (20 July 1996). (a) Beams plotted on the same rms amplitude scale. Phase picks from waveforms are shown. (b) Same as (a) but the beams have been shifted vertically for display purposes. (c) Beams plotted as log10 rms. (d) Black regions indicated phase windows for phase amplitude measurements.

somewhat enhanced on the 2-4 Hz, 2.5-4.5 Hz, and 3-5 Hz filter bands. Sometimes it is better to view the incoherent beams as log10 rms, as shown in Figure 2(c). In Figure 2(b), the  $S_n$  and  $L_g$  phases are hard to make out on the high-frequency bands because of the large amplitude differences between the  $P_n$  and  $S_n, L_g$  phases. Taking the log of the incoherent beams decreases the dynamic range between the highest and lowest levels in the display which reveals more subtle coda shape variations not observable on the unlogged plots.

Regional phases,  $P_n$ ,  $P_g$ ,  $S_n$ , and  $L_g$ , that are picked on the waveforms, are also picked on the incoherent beams in each filter band. Each phase is defined as a time window, beginning at the phase pick onset time, within which the maximum rms amplitude is measured for each frequency band. These windows are shown as the black regions in Figure 2 (d). A window for pre- $P_n$  noise is also defined, and the average rms noise level is computed. The black region, which is called a “phase selection” in ISEIS, is meant to represent the time interval over which the phase energy arrives, including the first arrivals and later coda phases. Sometimes, the maximum energy comes in at a later time than the onset time. All information about the phase pick windows, including maximum and average rms amplitude for each filter band, is stored in the database. The various amplitude estimates for each phase are later used for computing amplitude ratio features and time intervals in the phase selection are used for defining windows for spectral estimates.

#### 2.4.2 $P_n/L_g$ Ratio

The regional P/S amplitude-ratio discriminant, primarily  $P_n/L_g$  amplitude ratios, has been studied extensively recently and found to be effective for discriminating explosions and earthquakes. The discriminant seems to work best for identifying earthquakes because they usually produce very large  $L_g$  waves at high frequency and hence have small  $P_n/L_g$  ratios. Nuclear explosions apparently produce little  $L_g$  energy at high frequency and hence  $P_n/L_g$  ratios increase as frequency increases. Presumably, the low-frequency  $L_g$  energy produced by nuclear explosions results from  $Rg$ -to- $L_g$  mode conversion. However, as we have pointed out in numerous earlier studies (e.g., Baumgardt, 1996), ripple-fired mine blasts may not discriminate from earthquakes since they may generate shear waves and resemble earthquakes. In the blind test, we looked for small  $P_n/L_g$  ratios as direct indications of earthquakes.

In ISEIS, the maximum rms amplitudes in each phase selection window (black regions in Figure 2(d)) are computed and stored in the database. These amplitudes are then read from the database and used to compute amplitude ratios. For the analysis in this study, both the numerator and denominator amplitudes are computed in the same frequency band.

It should be noted that in the Southwestern U.S., the primary shear wave is  $Lg$ , and  $Sn$  is often not observed.  $Pn/Sn$  ratios can be used for discrimination, such as in the Novaya Zemlya region (Baumgardt, 1993b), and we did observe  $Sn$  for some events at TEXAR, as can be seen in Figures 1 and 2. Moreover, ratios involving the  $Pg$  phase, such as  $Pg/Lg$  ratios, have also proven useful for discrimination, and most of the events at TEXAR had observable  $Pg$  phases. However, to maintain consistency with the reference-event analysis, we relied on  $Pn/Lg$  ratios, where  $Pn$  is the earliest arriving phase at TEXAR.

#### 2.4.3 Frequency Dependence of $Pn/Lg$ Ratio

Goldstein (1995) has found that the frequency dependence of the  $Pn/Lg$  ratio may serve as a discriminant. Generally,  $Pn/Lg$  tends to increase with frequency for explosions but is relatively frequency independent for earthquakes. A possible explanation for this relates to the fact that most shear waves may originate for explosions by  $Rg$  mode conversion at low-frequency, but that this conversion is less efficient at higher frequency. However, earthquakes may produce significant  $Lg$  energy across the entire frequency band, depending on the source mechanism. Hence, we might expect to see low  $Pn/Lg$  ratios at both low and high frequency.

It has usually been thought that this discriminant requires broadband data, with frequencies higher than the 20 Hz Nyquist of the TEXAR dataset. However, in our earlier studies (Baumgardt, 1995), we have found that this discriminant can sometimes be applied with limited bandwidth data, generally as a positive indication of earthquakes.

#### 2.4.4 Spectral Discriminants

Spectral discriminants, including spectral shape and ripple fire scalloping, utilize spectra computed for the phase picked on waveforms and incoherent beams. Smoothed spectral estimates are taken on each channel of the array, using the phase selection windows as the FFT windows on the waveforms, and the spectra for each channel are then averaged across all elements of the array.

Examples of spectra for Event #3, showing the different spectral display modes available in ISEIS, are shown in Figure 3. Figure 3(a) shows the original spectra for five phases,  $Pn$ ,  $Pg$ ,  $Sn$ ,  $Lg$ , and  $Rg$ , and noise plotted on the same scale. This kind of plot shows signal-to-noise ratios, but it is sometimes hard to see all the spectra. In Figure 3 (b), the spectra have been shifted in order to make them more visible individually. However, information about the relative spectral levels and noise are lost in this display.

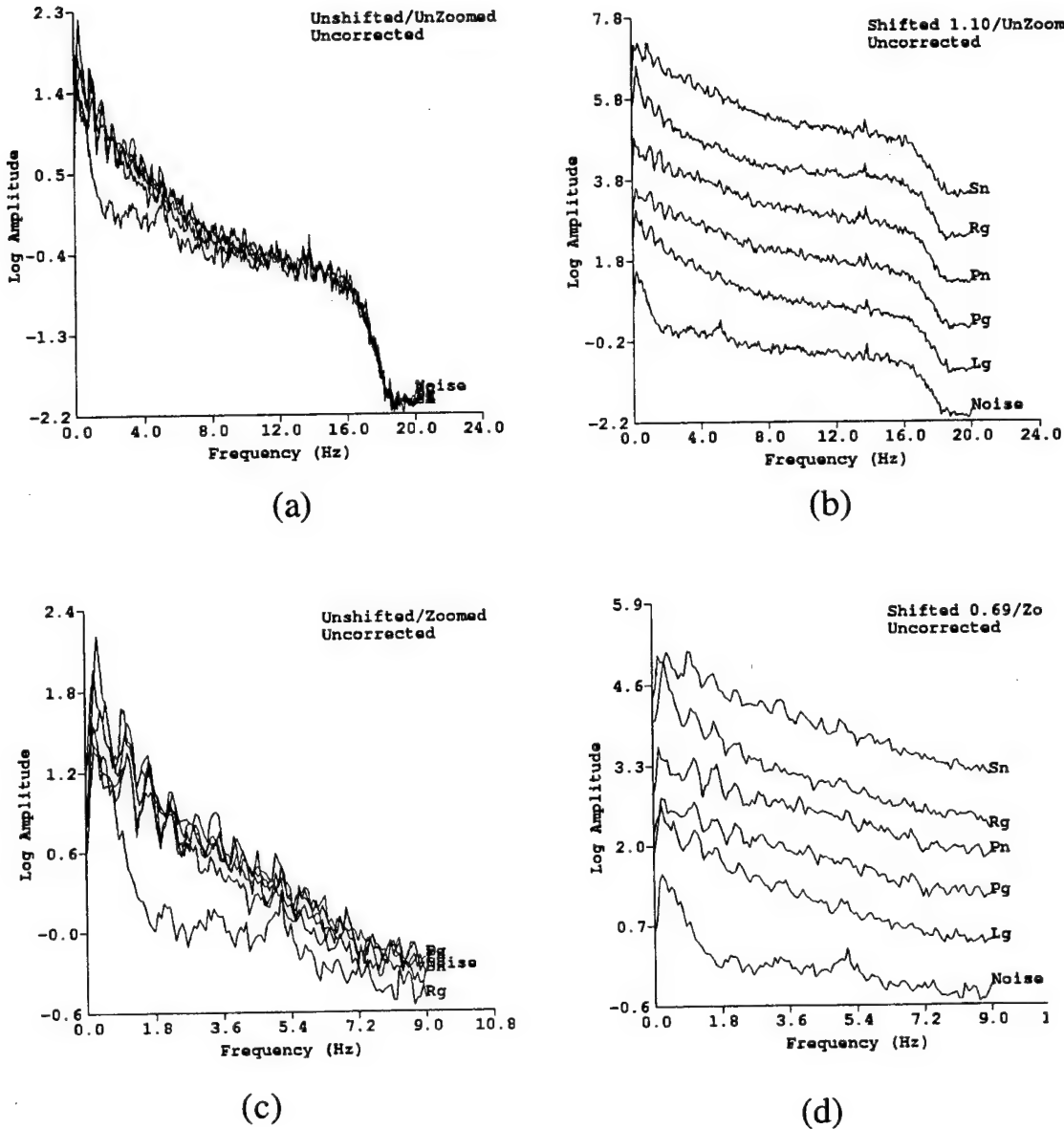


Figure 3: Spectra for the regional phases identified for Event #3 and the Pre- $Pn$  noise in various display modes. (a) Original spectra (b) Original spectra shifted for display (c) Original spectra zoomed from 0 to 10 Hz, (d) Spectra zoomed and shifted.

Figure 3 (a) shows that best spectral signal-to-noise ratio is evident in the spectral band from about 0 to 9 Hz. Figure 3 (c) shows a frequency zoom on this band that makes this band more clear. This plot reveals spectral scalloping of all the phase spectra at frequencies around 1.8 Hz. Finally, Figure 3 (d) shows the spectra zoomed and shifted which makes it easier to see the spectral scalloping around 1.8 Hz.

These different ways of displaying spectra are used to enhance and identify different features. The two main discriminants we have examined are the *spectral shape* and *spectral scalloping*.

**2.4.4.1 Spectral Shape Discriminant.** Some previous studies (e.g., Murphy and Bennett, 1982) have suggested that earthquakes tend to have flat spectra whereas nuclear explosions have peaked spectra. This is usually quantified in terms of the spectral ratio between low-frequency and high-frequency bands of the spectrum. Most commonly, the  $Lg$  spectral ratio is utilized. In earlier studies, we have also found this discriminant to work for mine blast and earthquake discrimination (Baumgardt, 1993 a) for some regions of the world, specifically, the Vogtland mining district of Germany (Wuster, 1993). Shallow mine blasts appear to have peaked spectra, whereas earthquakes have relatively flat spectra. In this blind test, we also looked at spectra of all regional phases, and look for the same diagnostic, i.e., flat spectra indicate earthquakes, peaked spectra indicate explosions.

Although in our study we did extract the spectral ratio measurements for all regional phases, we decided not to actually use the spectral ratio discriminant directly since this discriminant requires path corrections. Instead, spectra were analyzed visually and the spectral shape was characterized as either being “explosion-like” or “earthquake-like.” We will show a number of examples of this later.

It should be noted that this discriminant requires significant bandwidth to be useful. The example in Figure 3 has somewhat limited bandwidth, although within the band of relatively high signal-to-noise ratios, the spectrum slopes down rapidly with frequency rather than being flat. This kind of shape is more typical of mine blasts than earthquakes.

**2.4.4.2 Spectral Scalloping/Ripple Firing.** Time-independent spectral scalloping appearing in two or more phases is usually an indication of ripple firing, which identifies the event as a blast (Baumgardt and Ziegler, 1988). This discriminant has been implemented in ISEIS as a cepstral analysis peak finder. However, for this study, we mainly focus on the spectra themselves and look for indications of identical spectral scalloping in all phases observed for an event.

An example of time-independent spectral scalloping was pointed out above in Figure 3. It should be emphasized that the key feature to look for in identifying ripple firing is consistent scalloping in frequency bands where the signal-to-noise ratio is high enough. This can be clearly seen in Figure 3 where the best spectral signal-to-noise ratio band is from 0 to 9 Hz. Even weak scalloping, due to shot delay variations or complex, extended ripple fire patterns can still be identified if it is consistently observed in spectra for both P and S type phases at different times. We also check the spectra of the noise selection ahead of the  $P_n$  onset to determine that the scalloping only appears in the signal at all times and not in the noise ahead of the first arrival  $P_n$ .

#### **2.4.5 Other Miscellaneous Discriminant Features**

Two other features which can sometimes be used to augment the discriminants discussed above are *Rg Presence*, *Pn Impulsiveness*, and *Coda Shape*

**2.4.5.1 Rg Presence.** If *Rg* is observed, it usually implies that the event is shallow, and hence, is a mine blast. We just require the observation of an *Rg* with significantly high signal-to-noise ratio at low frequency to identify the event as "shallow" and hence, "blast-like." This discriminant cannot be considered as a sole indication of explosion since earthquakes can also generate large *Rg* waves if they are shallow. However, it can be used to support other positive indications of explosions from other discriminants.

**2.4.5.2 Pn Impulsiveness and Coda Shape.** *Pn* impulsiveness is a feature we have observed in many mine blasts and was discussed by Baumgardt and Young (1990). We found that mine blasts in Scandinavia observed at the NORESS regional array had impulsive *Pn* waves observed across the entire frequency band. Earthquakes, on the other hand, had somewhat emergent onsets that tended to be more enhanced at high frequency than at low. The coda shape discriminant was first suggested by Blandford (1993) and is related to *Pn* impulsiveness. In essence, regional seismograms of earthquakes have emergent *Pn* onsets accompanied by a relatively flat coda. Explosions differ in that they have more impulsive onsets and sloping coda levels. These two features probably relate to the source mechanism difference between explosions and earthquakes. These two features have not yet been coded into ISEIS, although they can be observed most clearly on incoherent beam plots.

## 2.5 Reference Event Selection for Pn/Lg Ratio Characterization

ISEIS was originally designed to be a Special Event identification system. The focus is on one or multiple Special Events to be identified. To identify the Special Event, reference events of known source type and comparable distance from the station are selected. Ideally, these reference events should be from the same region as the Special Event, be located at comparable distance, and be recorded at the same stations.

As mentioned earlier, Special Event identification may require reference events to be selected from different regions and perhaps at different stations than that of the Special Event itself. This is the case for the blind test events at TEXAR, because we have no reference events at TEXAR. Rather than to try to seek out reference events of known source type at TEXAR, which of course might be the best approach in operation, we decided, as an operational experiment, to treat TEXAR as if it was a new station, and we choose reference events from another region and station.

We utilize the *inter-region comparison* and regionalization scheme, described in Baumgardt and Der (1994), and designed to obtain reference events to identify a Special Event where the reference events and Special Event are in different parts of the world and recorded at different stations. This method combines a geographic regionalization of reference events as well as tectonic regionalization to try to obtain reference events that have common station-source distances and tectonics. The primary assumption is that the reference events and Special Event will have comparable propagation-path and receiver effects on the discrimination features.

Figure 4 shows an example of the regionalization display from ISEIS used to select reference events for classifying a Special Event recorded at TEXAR. For the 20 events from TEXAR, the paths have been classified tectonically as *orogenic* and *basin-and-range*, as shown in the select table in Figure 4 (a). There are no reference events recorded at TEXAR to use for comparison, so the user selects All Stas, to get all the stations from other reference regions in the world recorded at other stations. In Figure 4 (b), the regions found are shown in the table for other regions classified as *orogenic hercynian*.. Other kinds of tectonic regions, including *shield*, *caledonian*, *ocean\_continents*, and *phanerozoic\_platform*, have been defined, but they are not selected.

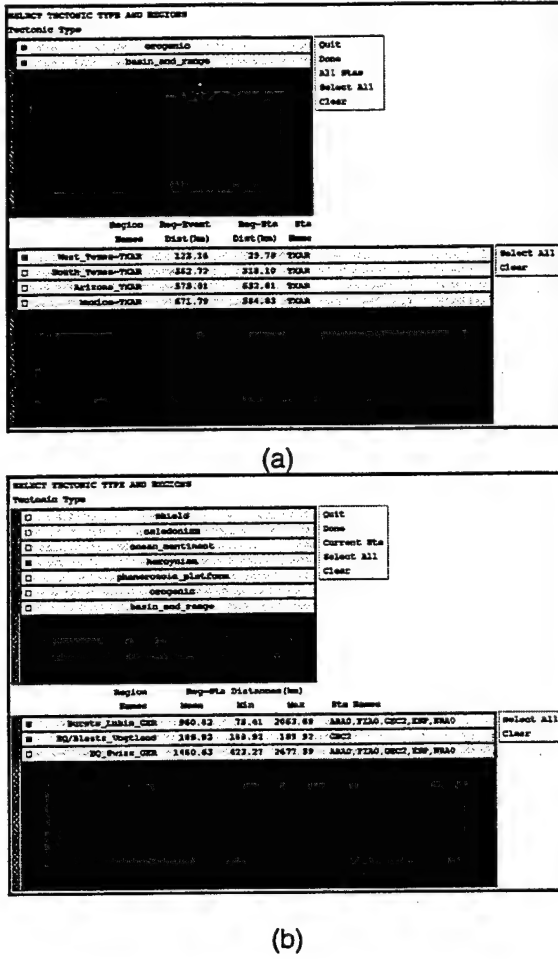


Figure 4: ISEIS training set selection for Inter-Region Feature Comparisons. (a) TEXAR reference region selections. (b) GERESS reference region selections. GERESS recordings of earthquakes, mine blasts, and mine tremors in Germany and Poland used as training events for TEXAR recordings of southwestern US events because of similarities of path structure, distances, and recording instrumentation

We see in Figure 4 (b) that two reference regions, *Bursts\_Lubin\_GER*, *Eq/Blasts\_Vogtland*, and *EQ\_Swiss\_GER* were recorded at the array GERESS (GEC2), in addition to other sensors. The first region contains mine tremors in Poland recorded at GERESS. The second region, *EQ/Blasts\_Vogtland*, includes a group of known explosions and earthquakes first studied by Wuster (1993). The third region, *EQ\_Swiss\_GER*, includes events from an earthquake swarm in Switzerland recorded at GERESS. Both the Vogtland earthquakes and Lubin mine tremors are similar and can represent earthquake-type sources, and the twelve Vogtland mine blasts are a reasonably large sample for mine blasts. Because the GERESS and TEXAR instrumentation are similar, and the distances of the events from the stations and tectonic classification of the propagation paths are simi-

lar, we selected the GERESS recordings of the Vogtland, Lubin and Swiss events as the reference events to classify the events recorded at TEXAR.

## 2.6 Inter-Region Characterization Approach using $Pn/Lg$ Ratios

Our approach to Special Event analysis is to compare the features of the event to be identified, called the Current Event, with the features of the referenced events from the selected regions.

Figure 5 shows a comparison of the  $Pn/Lg$  amplitude ratios measured for the events in the selected regions with one of the TEXAR events, Event #1 (12 Aug 96).

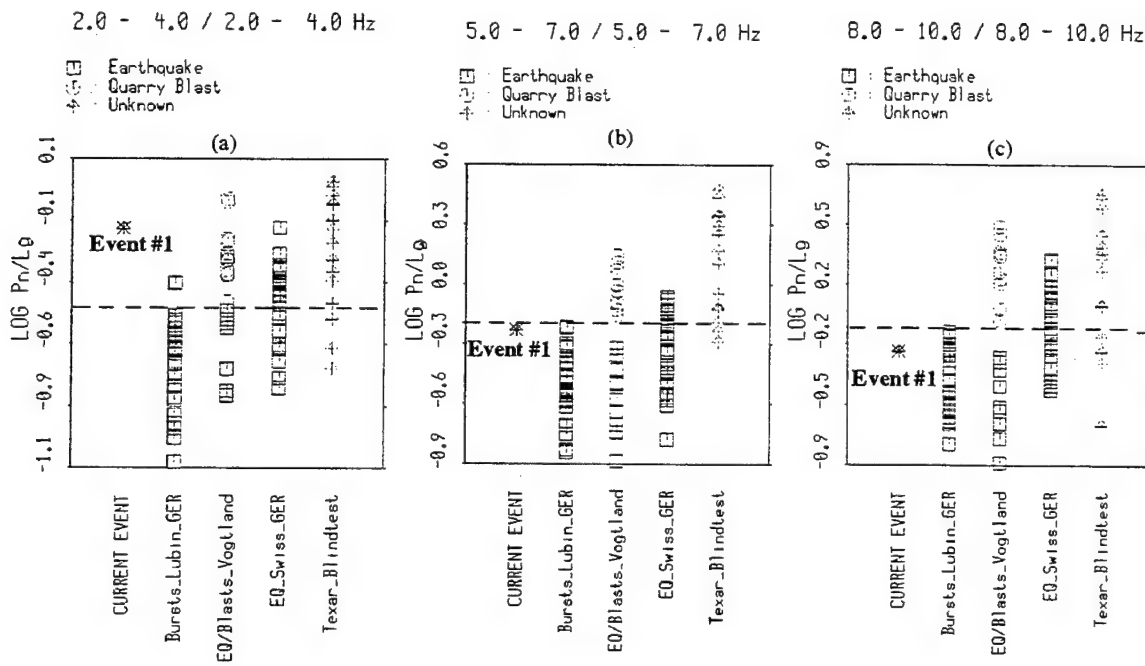


Figure 5: Comparison of the  $Pn/Lg$  ratios of the GERESS training set events with the TEXAR recordings for the blind test events. Event #1 is shown as Current Event. Event numbers for the other TEXAR events are indicated. The triangles indicate the values for the other TEXAR blind test events. Dashed line is separation of Vogtland blasts and earthquakes. (a) 2-4 Hz filter (b) 5-7 Hz filter (c) 8-10 Hz filter

The ratios are shown in 3 frequency bands, 2-4 Hz (a), 5-7 Hz (b), and 8-10 Hz (c). In these plots, different symbols represent different source types, as indicated in the legends above each figure. The triangle symbols, identified as "Unknown", represent the 20 TEXAR events that we want to identify. The Vogtland explosions and earthquakes, recorded at GERESS, clearly separate, with mine blasts having high ratios and earthquakes having low ratios and with the horizontal dashed line showing the possible separation point

in the different frequency bands. The Lubin mine tremors generally fall below this line and resemble Vogtland earthquakes. However, the Swiss earthquake swarm contains events that fall above and below the line. This large scatter in the Swiss events may be due to variations in the source mechanisms of the earthquakes. We note that the TEXAR events also fall both above and below the line.

We desire to use this decision line, defined by the GERESS recordings of Germany and Poland, to classify the events recorded by TEXAR in Southwestern U.S. This is what we refer to as event identification by "inter-region comparison" of events and the "transporting" of a regional discriminant from GERESS to TEXAR. TEXAR Event # 1, for example, clearly falls in well above the line on the 2-4 Hz plot but below the line in the 5-7 Hz and 8-10 Hz bands. So, Event #1 might be identified as a blast at low frequency and an earthquake at high frequency. Clearly, a single frequency band cannot be relied on to identify the event.

Figure 6 (a) shows all the  $Pn/Lg$  ratios in the 5-7 Hz band plotted versus distance of the events from their respective recording stations. The events cluster in the distance range of 100 to 800 km. However, most of the GERESS recordings fall in an even smaller range of about 100 to 300 km. With the exception of the one event at TEXAR, Event #10, which was at 1641 km, most of TEXAR and GERESS events were at comparable distances. Because frequency-dependent distance corrections are not yet available for Southwestern U.S., Germany, and Poland, we decided not to make any corrections for distance since these events are closely located. Event #10 may require a distance correction, however, but there were other problems with this event that we will discuss later.

Figure 6 (b) shows all the measurements in all the frequency bands plotted versus frequency. Each symbol now is an average for the frequency band over all the GERESS events in the category of blast or earthquake, and the triangle symbols are the averages over all the TEXAR events. The bars on each symbol are the standard deviations of the measurements about the means. The asterisks symbol shows the values measured for the Current Event, Event # 1. This plot shows that the explosions and earthquakes recorded at GERESS clearly separate on the values of the  $Pn/Lg$  ratios and the frequency dependence of the ratios. Also, the spectral trends are different with the blasts increasing with frequency whereas the earthquakes stay constant to about the 4-6 Hz band and then increase. The Current Event # 1 seems to be in the mine blast category at low frequency but then turns down to the earthquake category at high frequency. The TEXAR events as a group tend to follow the  $Pn/Lg$  amplitude-ratio frequency trend corresponding to quarry blasts,

but they have large standard deviations, which indicates that there are probably both blasts and earthquakes in the group.

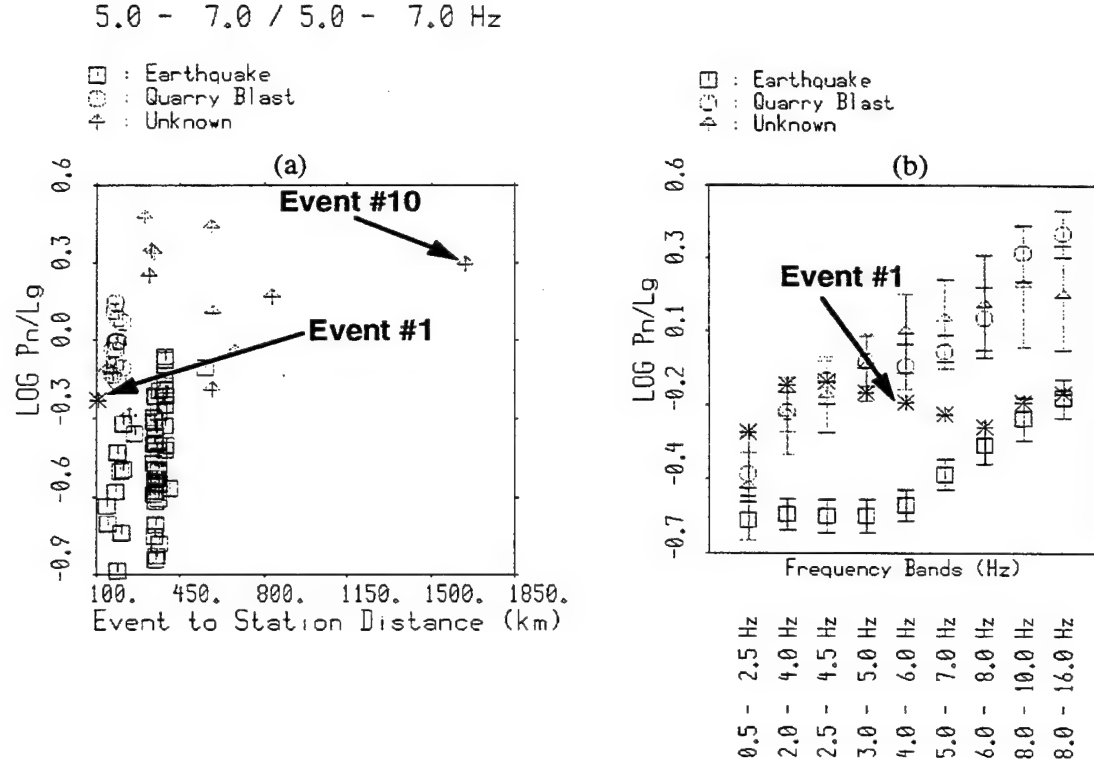


Figure 6: Comparison of the  $P_n/L_g$  ratios of the GERESS training set events with the TEXAR recordings for the blind test events. (a) Ratios plotted versus distance. (b) Ratios plotted versus frequency band of filter.

Our conclusion from this analysis is that the TEXAR events, which we assume as a group are comprised of both earthquakes and blasts, are very similar to the GERESS recorded blasts and earthquakes. This gives us some degree of confidence that the events are similar in terms of source-receiver propagation path and station effects.

In order to characterize these events, it would be possible to cluster the two categories and identify the events using a supervised classification scheme, like likelihood ratios or outlier methods. We have in fact done this in some other studies (Baumgardt and Karafotis, 1995). However, in this blind test, we decided to characterize the events visually rather than automatically.

## 2.7 Discrimination Results

Each event was processed through ISEIS and discriminants discussed above were extracted. We then visually analyzed the features, made identifications, and sent the results to

SMU. The judgments about the identity of the events and whether we were correct or not were made by Professor Herrin.

For each of the 20 TEXAR events, we show plots of the features extracted for each of the events. In the following figures, the incoherent beams are on the left, the  $Pn/Lg$  ratios versus frequency, compared with those of the GERESS recorded events, are plotted in the center and the spectra are plotted on the right. For the  $Pn/Lg$  ratios, the ratios for each event are shown individually on the same plot as the ratios for the GERESS reference events, as in Figure 6 (b). The spectra and incoherent beams are displayed in different display modes (i.e., zoomed or unzoomed, shifted or unshifted, rms or log10 rms) shown in Figures 3 and 4 depending on what is being emphasized in each case.

The next two sections discuss in detail our reasoning on the identification of each of the events and whether or not the original identification was correct in each case, indicated in the parentheses.

### 2.7.1 First Group of 10 Events

#### (1) Event # 1 - Earthquake (Correct)

The features for Event 1 are shown in Figure 7, which is also the event we discussed in the previous section. The incoherent beams have the very distinctive shapes of earthquakes, with large  $Lg$  at high frequency. The phase selection windows are shown as the black regions on the incoherent beam plots. The  $Pn/Lg$  ratios follow the earthquake trend, and are very small at high frequency. There might be some uncertainty here because of the low values of the  $Pn/Lg$  ratio at low frequency. This might be caused by a regional site effect difference between TEXAR and GERESS, which could be more evident at low frequency than at high frequency. However, the bending down of the  $Pn/Lg$  ratio trend at high frequency is an earthquake-like feature, never seen in explosions, and the low values at high frequency convince us that the event is an earthquake. The spectra are essentially flat out to the highest frequency observable, which is about 17.5 Hz. Beyond this frequency the spectra of both signals and noise drop off rapidly with frequency, due to the instrument anti-alias filter cutoff. Also, there is no evidence of ripple fire.

The event was identified as an earthquake, which is correct.

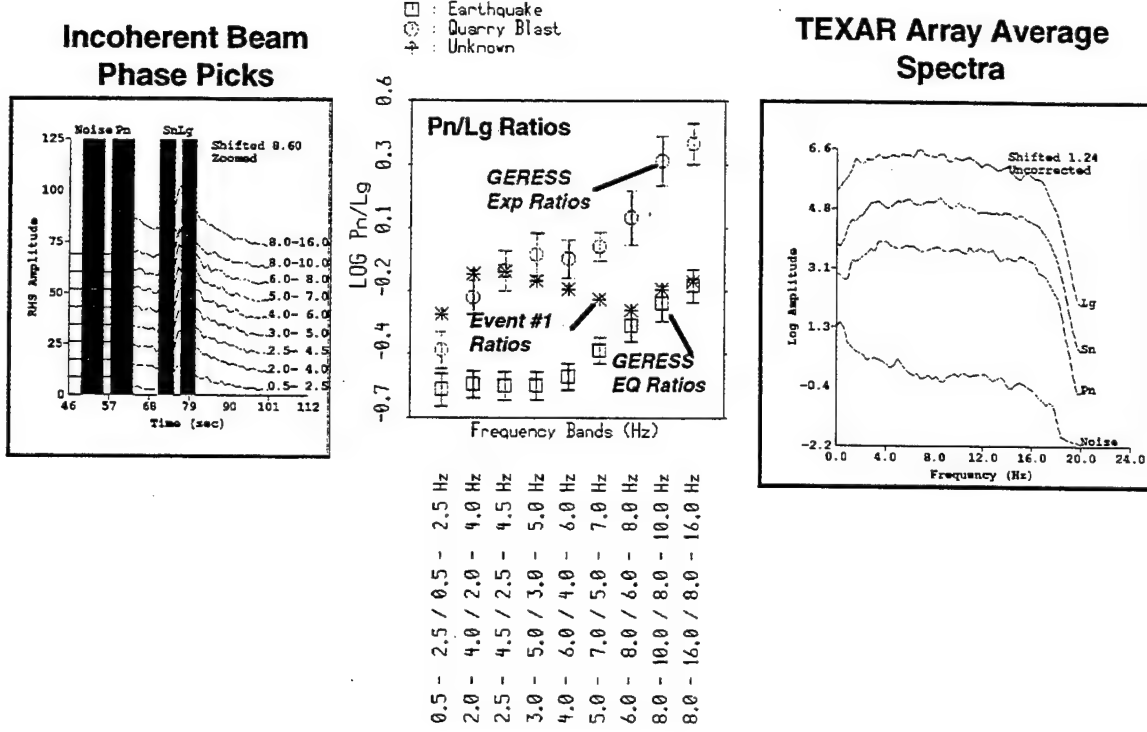


Figure 7: SMU Blind Test - Feature Extraction - Event #1 identified as earthquake. Incoherent beams (left),  $Pn/Lg$  ratios versus frequency (middle), and regional phase spectra (right). Earthquake identification is based on the spectra of  $Lg$  and other phases being flat, and low and frequency dependent  $Pn/Lg$  ratios which fall into the GERESS earthquake group at high frequency. The phase selection windows used to compute the spectra are shown on the incoherent beams on the left.

#### Event #2 - Blast (Correct)

Figure 8 shows that this event is distinctively different than Event #1. Again, the black regions on the incoherent beams indicate the phase selection windows. The  $Pn$  is larger than  $Lg$  at high frequency. The  $Pn/Lg$  ratio is large, and follows the blast trend with frequency. The  $Pn$  has a sharp onset. The spectra have clear, although rather irregular, spectral scalloping not observed in the noise spectra. We conclude that the scalloping was caused by ripple firing.

We identified the event as a blast, which is correct.

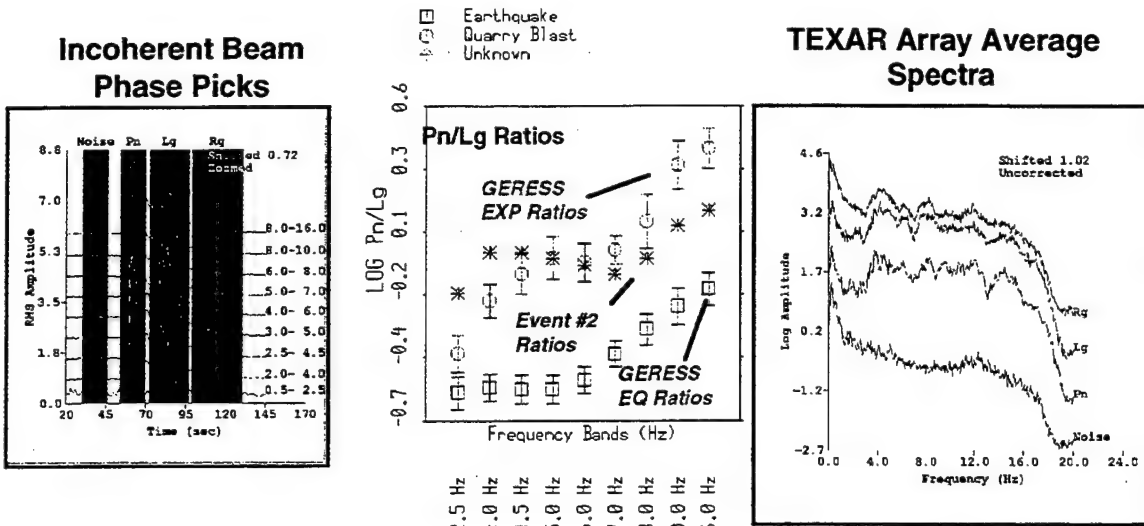


Figure 8: SMU Blind Test Feature Extraction - Event #2 that was identified as a blast. Blast identification based on  $Pn/Lg$  ratios falling in GERESS explosion group and evidence of spectral scalloping caused by ripple firing in the spectra on the right.

#### *Event #3 - Blast (Correct)*

The unlogged incoherent beams are shown in Figure 9 which exhibit a sharp onset  $Pn$ . From this point on, we only show the phase picks on the incoherent beams, not the phase-selection windows. In the middle and high frequencies, the  $Pn/Lg$  ratios become very large, well in excess of the training set events. The spectrum of this event was discussed earlier in connection with spectral display options in Figure 3. We concluded that the event had ripple fire spectral scalloping at lower frequency where the signal-to-noise ratio is high. The  $Pn/Lg$  ratios tend to be quite high through most of the frequency band from 3 to 8 Hz, where the signal-to-noise ratios are high.

We identified the event as a blast, which is correct.

#### *Event #4 - Blast (Correct)*

As shown in Figure 10, Event #4 has very large  $Pn/Lg$  ratios which increase with frequency, a very strong explosion-like feature. The incoherent beams in Figure 10 are unlogged and show strong energy following the  $Lg$  at low frequency. This feature may be caused by an  $Rg$  arrival which is more evident on the incoherent beams than on the

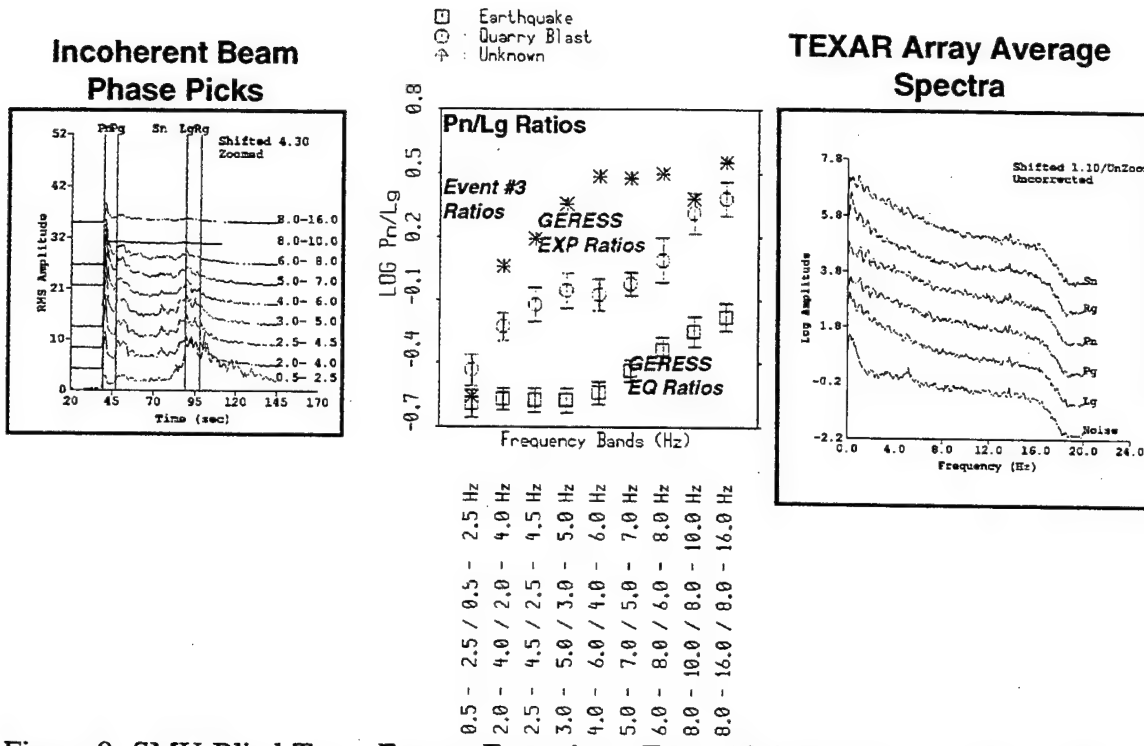


Figure 9: SMU Blind Test - Feature Extraction - Event #3 identified as a blast based on high and increasing  $Pn/Lg$  ratio, peaked spectra, and spectral scalloping indicating ripple fire.

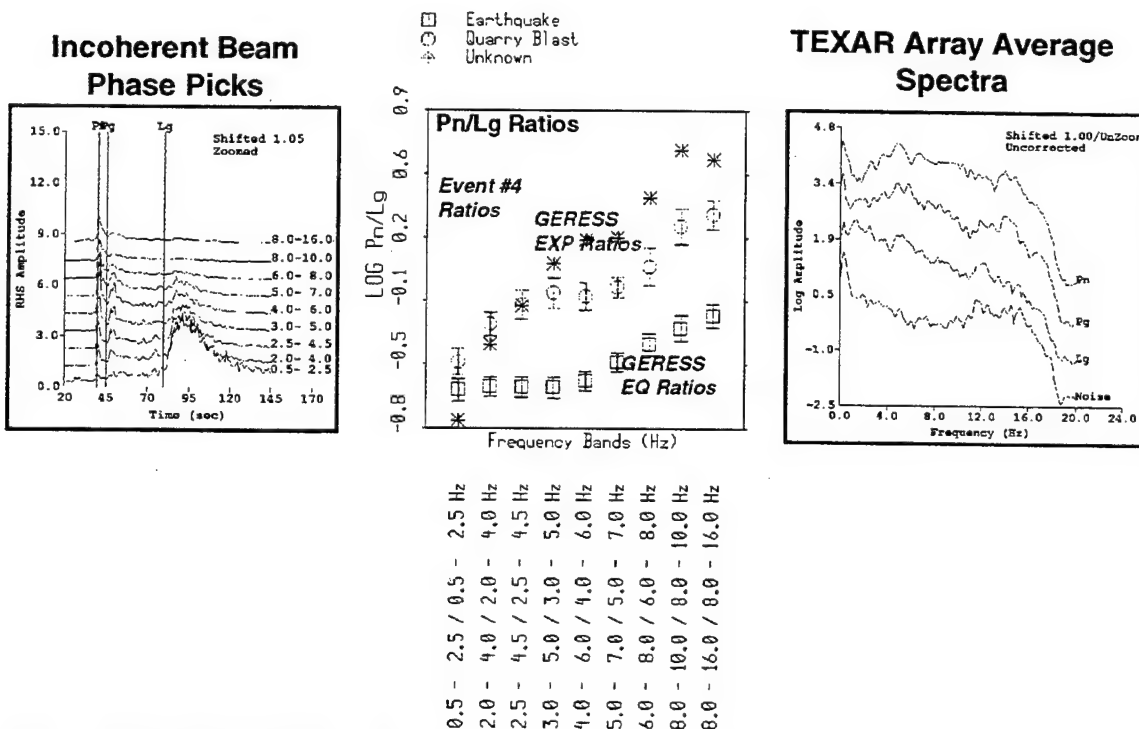


Figure 10: SMU Blind Test - Feature Extraction - Event #4 which was identified as a blast based on high and increasing  $Pn/Lg$  ratio, large  $Rg$ , peaked spectra, and spectral scalloping indicating ripple fire.

waveforms. The spectra show some evidence of modulation patterns and a peaked spectrum at low frequency.

We identified the event as a blast, primarily based on the  $Pn/Lg$  ratio features, which is correct.

*Event #5 - Blast (Correct)*

As shown in Figure 11, Event #5 has very large  $Pn/Lg$  ratios that increase strongly with frequency and fall within Vogtland mine blast category. The spectra are peaked at low frequency, or at about 4 Hz, and show spectral modulations due to ripple fire.

The event was identified as a blast, which is correct.

*Event #6 - Blast (Correct)*

As shown in Figure 12, Event #6 has very large  $Pn/Lg$  ratios which increase strongly with frequency and fall within the Vogtland mine blast category. The spectra are peaked at low frequency, and very strong spectral scalloping is evident, caused by ripple firing.

The event was identified as a blast, which is correct.

*Event #7 - Earthquake (Correct)*

The features for Event #7, shown in Figure 13, are somewhat ambiguous. The signal-to-noise ratios are low, and the signal features are weak. The  $Pn$  arrival is very emergent and has a somewhat flat coda. The  $Pn/Lg$  ratios increase with frequency, but it should be noted that the spectra show that the signal level drops to the noise level above about 6 Hz. So,  $Pn/Lg$  ratios above the 4-6 Hz band should not be considered. In the bands up to 4-6 Hz, the  $Pn/Lg$  ratios are flat and fall in the earthquake category. The spectra show no evidence of scalloping.

We identified the event as an earthquake, although with low confidence, which is correct.

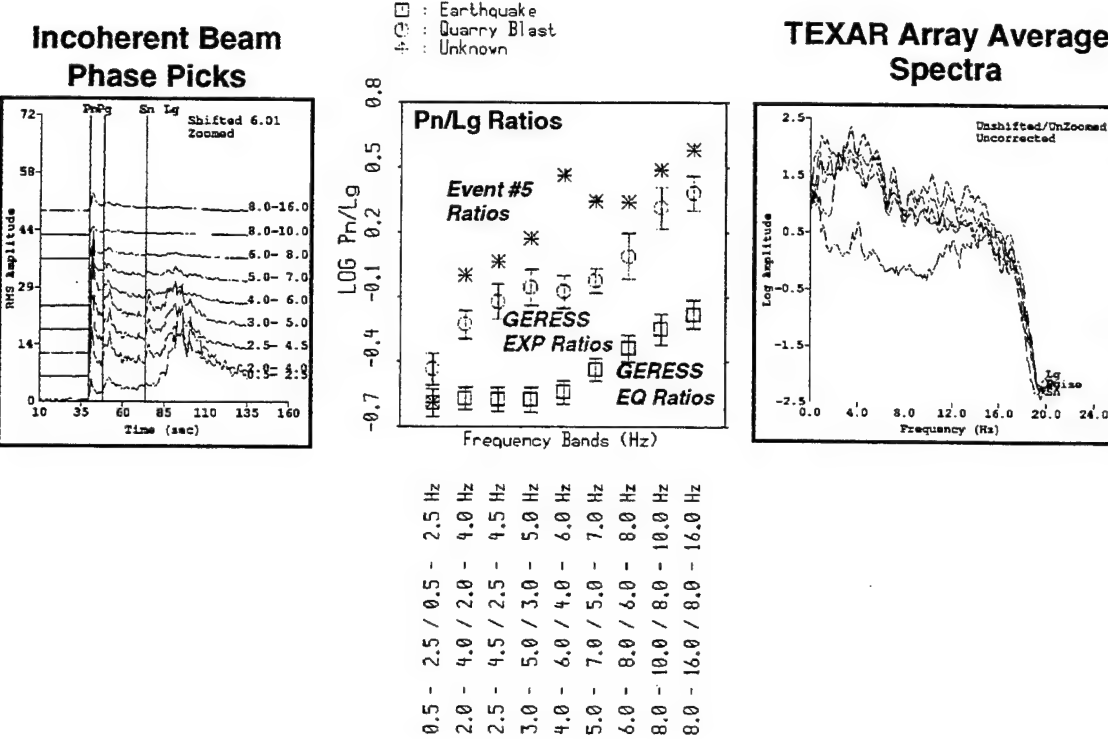


Figure 11: SMU Blind Test - Feature Extraction - Event #5 identified as a blast based on large and increasing Pn/Lg ratios with frequency, and peaked and scalloped spectra.

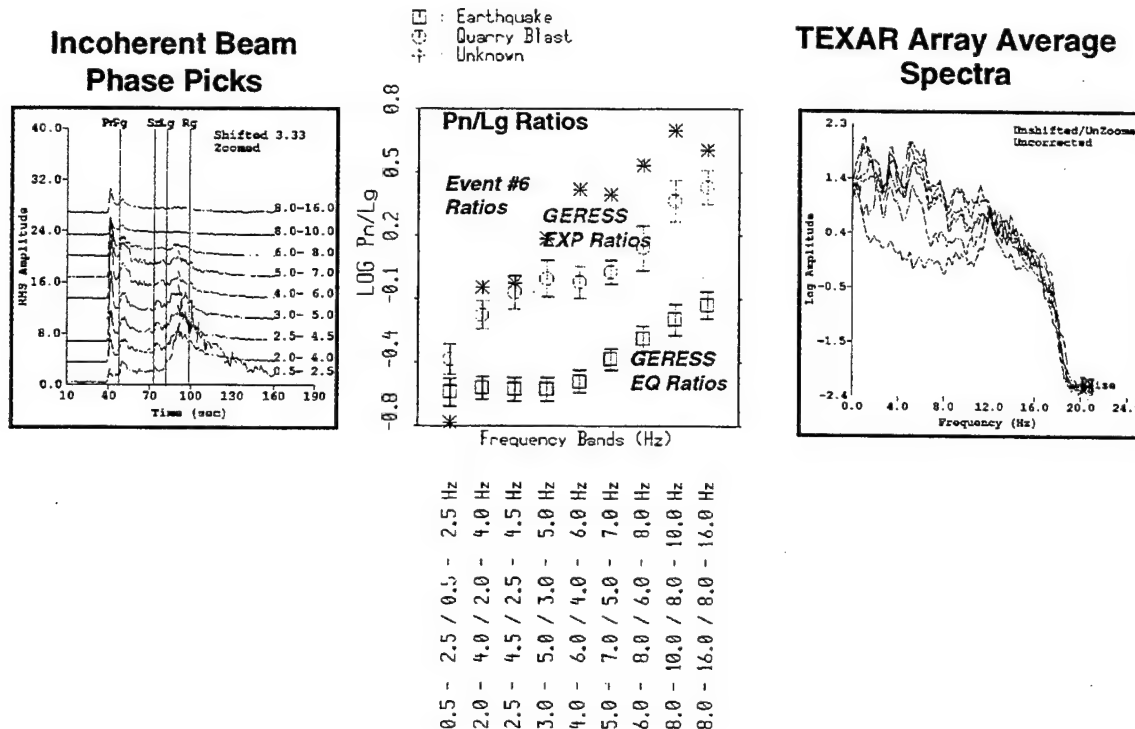


Figure 12: SMU Blind Test - Feature Extraction - Event #6 identified as a blast based on large Pn/Lg ratios that increase with frequency, presence of Rg, and scalloped spectra.

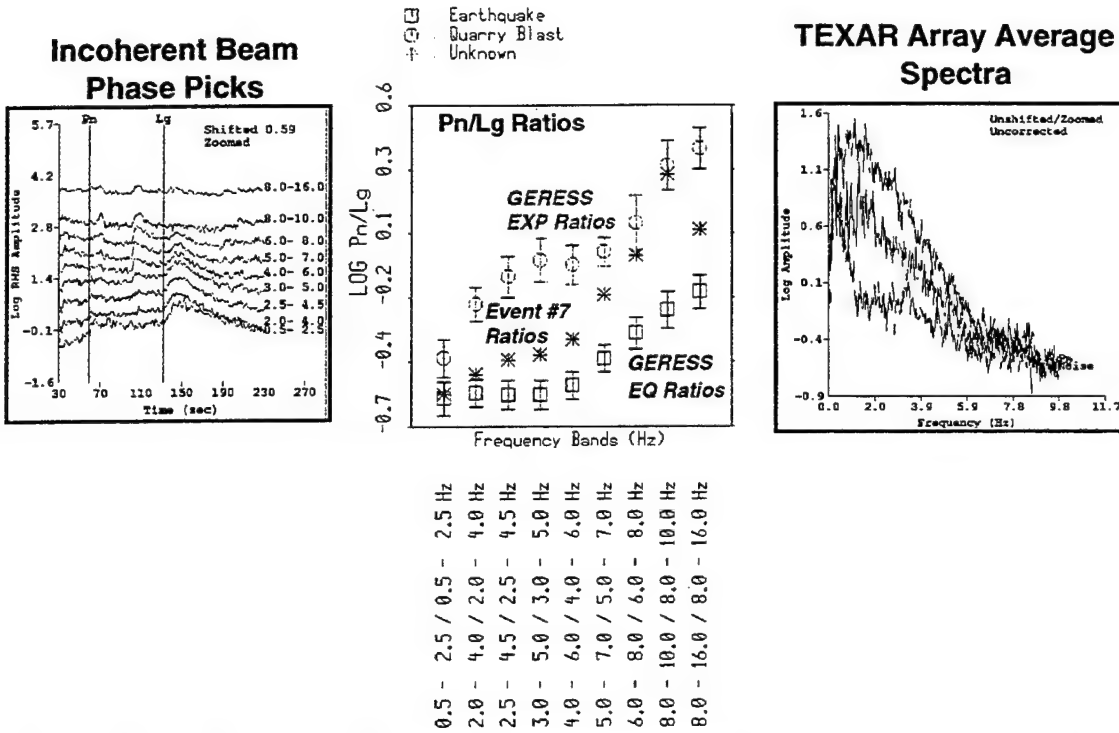


Figure 13: SMU Blind Test - Feature Extraction - Event #7 identified as earthquake based on low and frequency independent  $Pn/Lg$  ratios and emergent  $Pn$  with flat coda.

#### *Event #8 - Blast (Correct)*

The features for Event #8, shown in Figure 14, have frequency dependent  $Pn/Lg$  ratios that tend to increase with frequency. The spectra in Figure 14 are zoomed from 0 to 9 Hz, which is the band where the signal exceeds the noise. Weak scalloping can be made out at low frequency. Also, the peaked feature can be seen at around 1.8 Hz, most strongly evident for  $Lg$ , an explosion-like feature.

We identified the event as a blast, which is correct.

#### *Event #9 - Blast (Correct)*

The features for Event #9, shown in Figure 15, are very unusual. The  $Pn/Lg$  ratios increase at low frequency, seemingly in the Vogtland blast category, and then suddenly drop to very low values at high frequency. Looking at the incoherent beams in Figure 15, a strong signal is evident at high frequency following the  $Lg$  onset time. However, the signal is double peaked, and seems to be a  $P$  and  $S$  from a local event.  $Lg$  wave amplitudes do not usually increase so sharply with frequency.

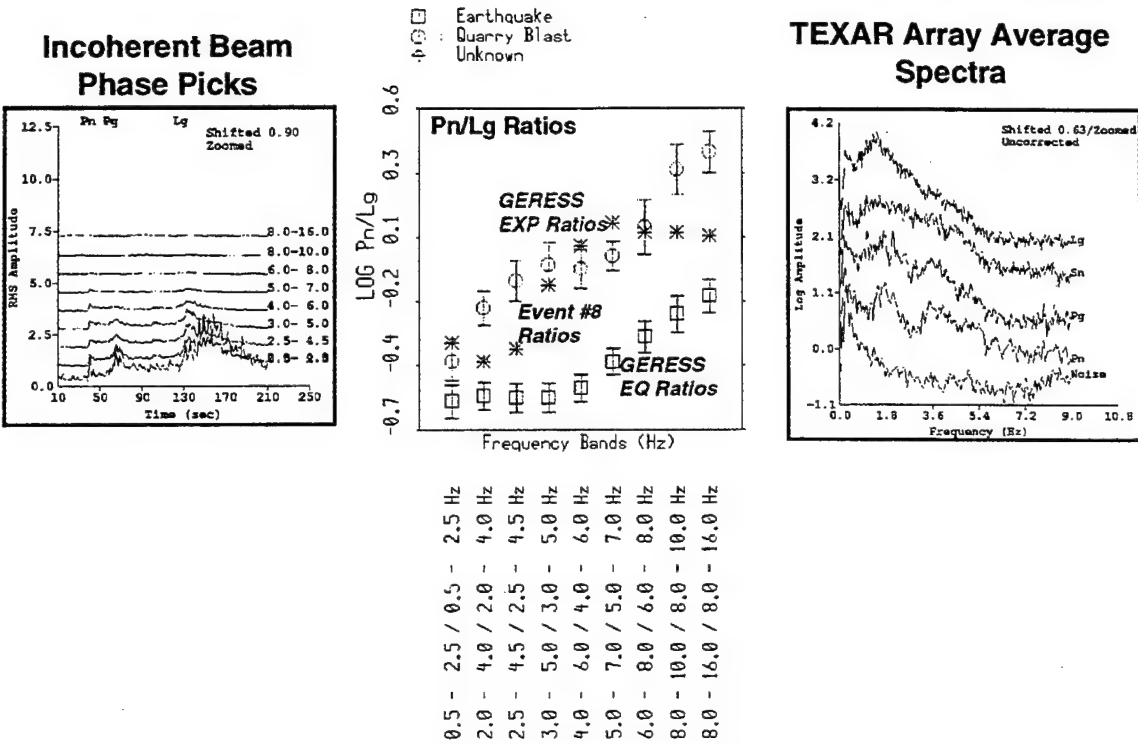


Figure 14: SMU Blind Test - Feature Extraction - Event #8 identified as blast based on increasing  $Pn/Lg$  ratios with frequency, somewhat large  $Pn/Lg$  values and spectral scalloping indicating ripple fire.

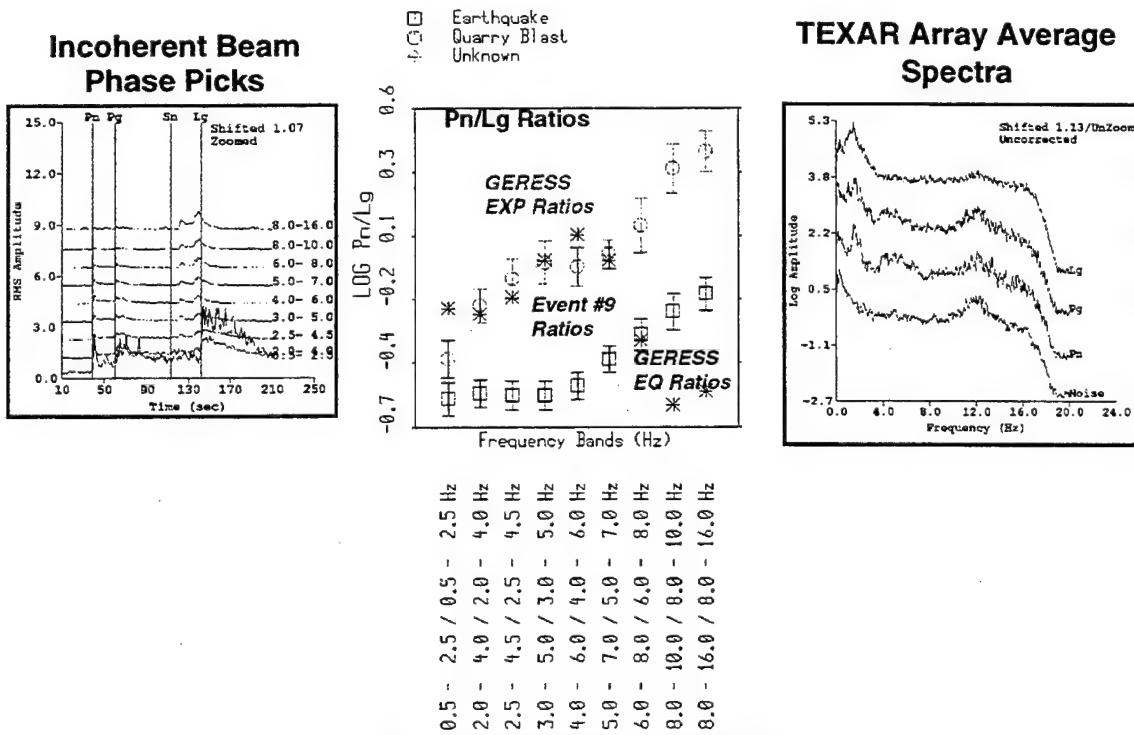


Figure 15: SMU Blind Test - Feature Extraction - Event #9 identified as blasts based on weak evidence of ripple fire, high  $Pn/Lg$  ratios that follow blast trend at low frequency. The earthquake-like values at high frequency are caused by contamination by a local event.

Figure 16 shows plots of the waveforms filtered in several frequency bands, and the local event arrivals can be clearly seen on the high-frequency filtered traces. Also, we have done frequency-wavenumber analysis on this signal, using the array, and the event has a different bearing than the primary signal. Based on the fact that the  $Pn/Lg$  ratios are clearly blast-like at low frequency, we identified the event as a blast with coda contaminated by a local event. Both of these conclusions were correct.

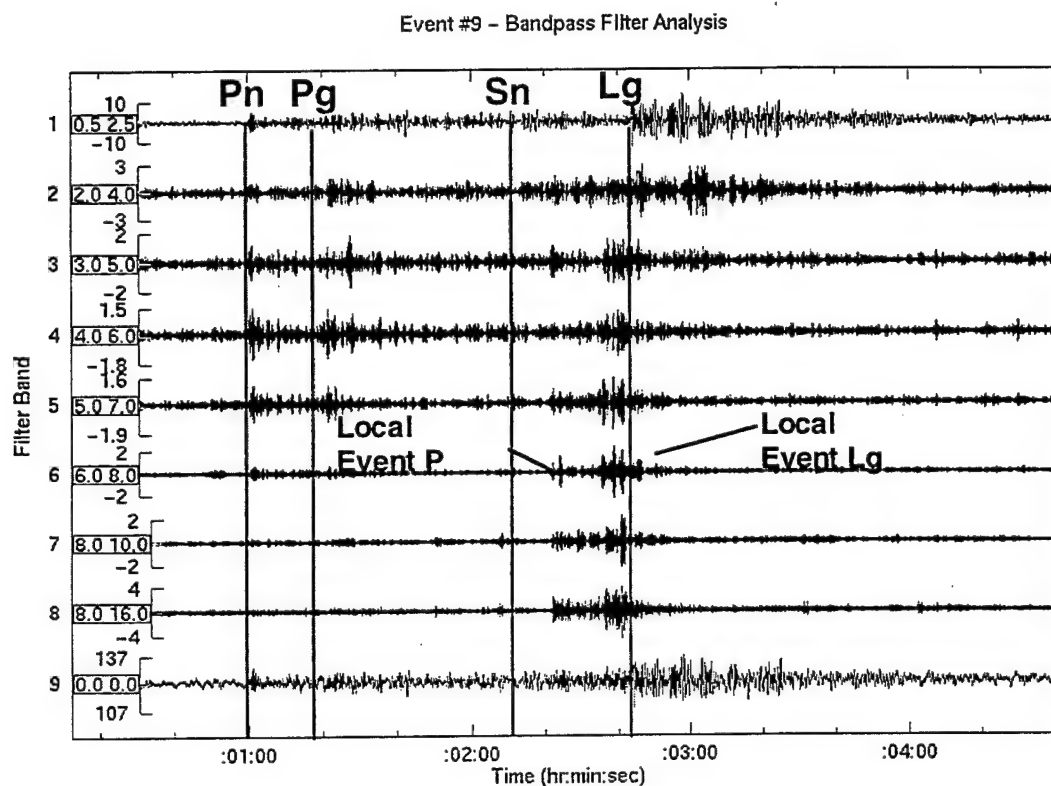


Figure 16: Event #9 Bandpass Filter Analysis - Interfering Local Event. The filter bands in Hz are shown on the left of each of the traces.

#### *Event #10 - Earthquake (?) ( Incorrect)*

As we discussed earlier, Event #10 was located at the greatest distance of all the events from TEXAR, probably outside the distance range where our reference events are valid without applying distance corrections. Figure 17 shows the incoherent beams and  $Pn/Lg$  ratios versus frequency. We discuss the spectra in detail below. Looking at the incoherent beams, a strong  $Lg$  at low frequency and some  $Pn$  energy at high frequency can be seen, but overall, the signals are weak and very complex looking. The  $Pn/Lg$  ratios increase with frequency, as expected for blasts. But, the incoherent beam plots show that no  $Lg$  energy is evident at high frequency. So, the increased  $Pn/Lg$  ratio with frequency is actually caused

by the increase of  $Pn$  energy relative to noise and has nothing to do with the  $Lg$  amplitude, which is below noise level at high frequency.

In Figure 18, we show the waveforms in different filter bands that again show the signals to be very weak at high frequency. The top plot shows the broadband signal with a strong arrival identified as  $Rg$ . Moreover, SMU provided a low-pass filtered waveform that showed this phase to be very large at low frequency. The weakness of  $Pn$  and the strength of the presumed  $Rg$  would suggest a large Ms-mb, characteristic of earthquake.

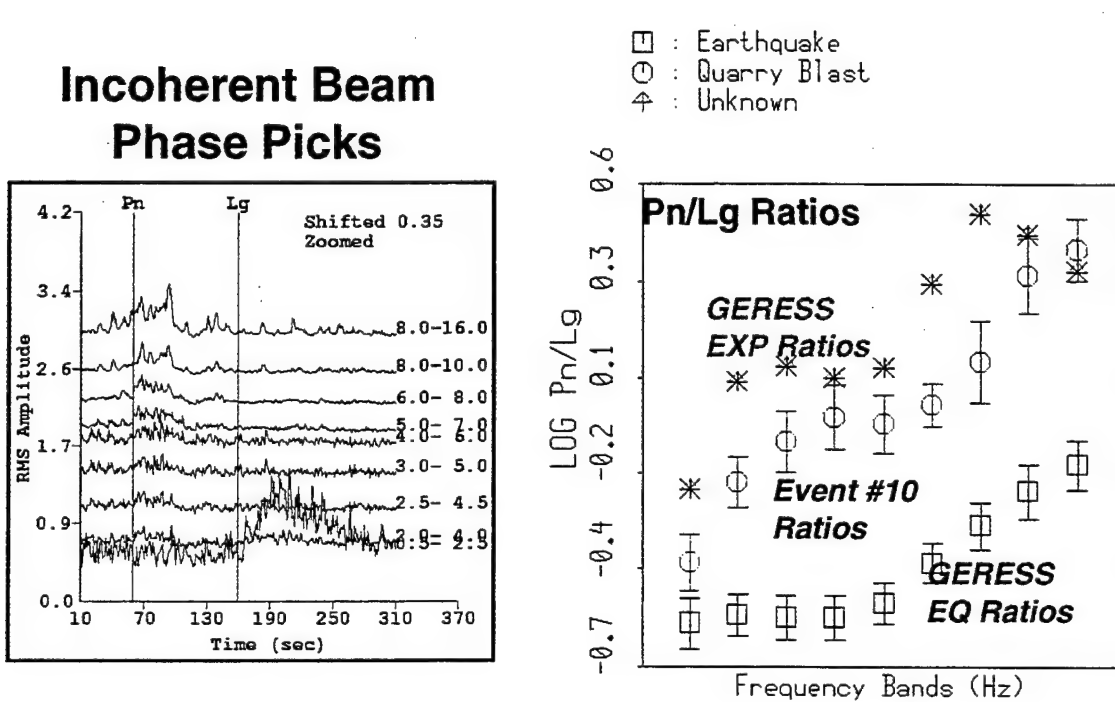


Figure 17: SMU Blind Test - Feature Extraction - Event #10 with questionable earthquake identification, based on large long-period surface wave.  $Pn/Sn$  ratios are more blast like, but they are low signal-to-noise ratio.

Event #10 – Bandpass Filter Analysis

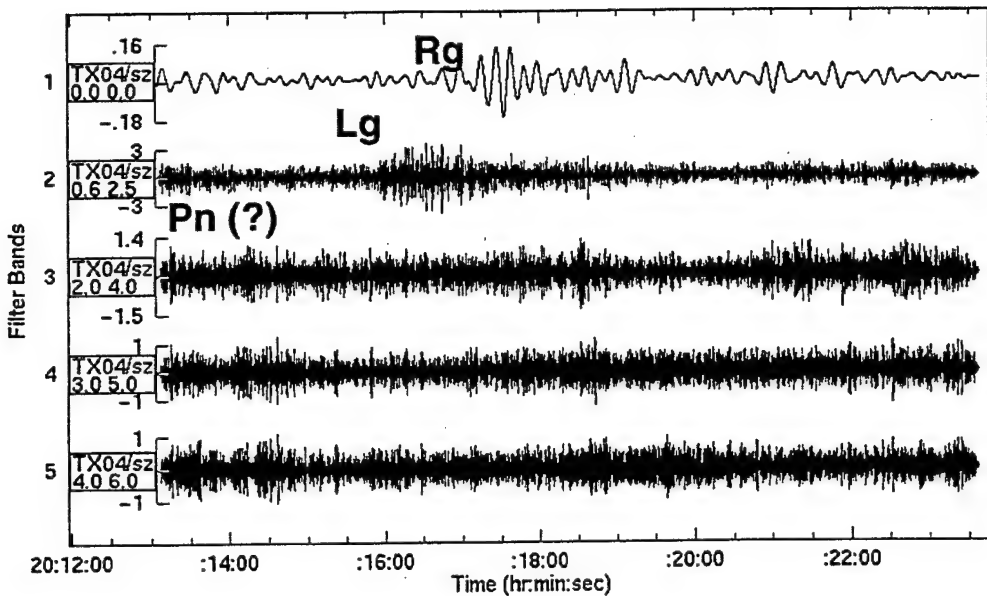


Figure 18: Event 10 Filter Analysis. This event appears to be earthquake on basis of Ms/mb. However, the event is actually an extended mine blast with  $M_I=3.5$ . Large extent builds up low-frequency  $Rg$  and reduces high-frequency  $Pn$ .

Figure 19 (a) shows that the spectra have high signal-to-noise ratios in two frequency bands, 0 to 1 Hz and 2.7 to 4.2 Hz. These two bands are shifted and zoomed in Figures 19 (b) and (c). There may be very weak spectral modulations in both  $Pn$  and  $Lg$  that could have been caused by ripple firing. However, we decided the signals were too weak to make a conclusive identification.

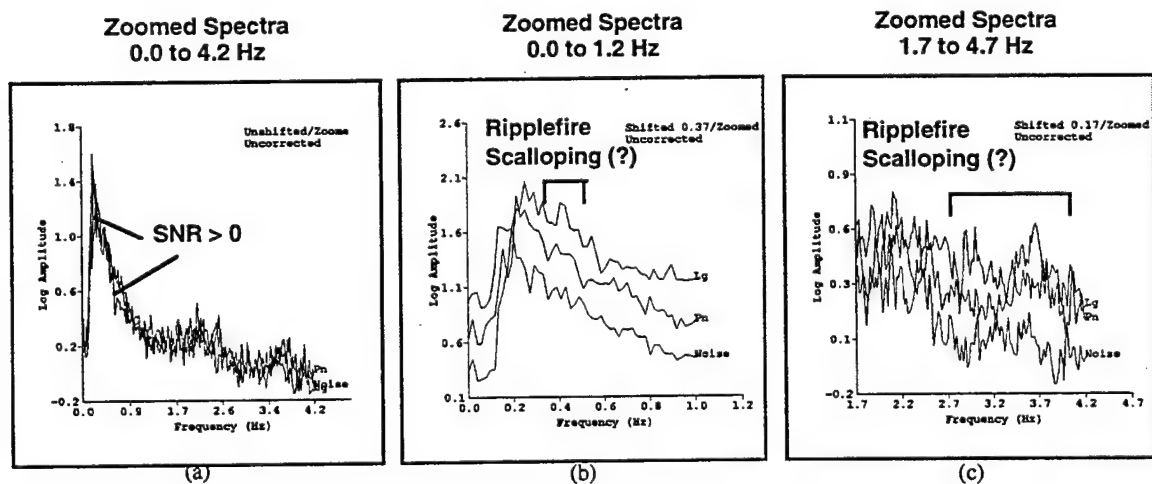


Figure 19: Event 10 Spectra. (a) Spectra from 0 to 4.2 Hz. Spectral bands where log-SNR exceeds 0 are indicated. (b) Low band where log-SNR > 0. (c) High band where log-SNR > 0.

We made no identification of the event since the high-frequency signals were too weak to conclusively apply the ISEIS high-frequency discriminants. However, based on the large low-frequency  $Rg$  and the Ms-mb argument (strong  $Rg$ , weak  $Pn$ ), we concluded that the event might be an earthquake. This identification was incorrect.

In fact, the event was an extended cast shot of 13 November 1995 in the Black Thunder mine in the Powder River Basin of Wyoming. Stump and Pearson (1997) studied Pinedale Array recordings of this event, at a distance of 360 km, that also showed the enhanced surface waves at low frequency that we observed at TEXAR at 1641 km distance. However, they also observed more explosion-like characteristics at high frequency that we could not conclusively observe at TEXAR because of low signal-to-noise ratios at the larger distance. Stump and Pearson (1997) argued that this low-frequency surface wave enhancement is a common feature of both single-fired and cast shots at the mine.

In hindsight, it is apparent we had more evidence that the event was an explosion than an earthquake. We based a possible earthquake identification on the observation of the large Ms, but this is a common feature of large mine blasts. We could have made a more conclusive, and probably correct, identification if we had had the data from Pinedale at closer distance than TEXAR.

### 2.7.2 Second Group of 10 Events

The second group of 10 events (Event # 11 through 20) were analyzed after the first group. This second set of events had some unusual “exotic” events never seen before so the identification of these events was problematic at best. However, a CTBT monitoring system will have to be able to handle such exotic events, either to call them “unusual” or not on the realm of current experience.

#### *Event #11 - Earthquake (Correct)*

The features for Event #11 shown in Figure 20 are very characteristic of earthquakes. The incoherent beams have stronger  $Lg$  energy through the entire frequency band, and the  $Pn/Lg$  ratios clearly fall on the GERESS earthquake group. The spectra are relatively flat like those for Event #1 in Figure 7.

This event was identified as an earthquake, which is correct. SMU identified the event as the Chihuahua Earthquake.

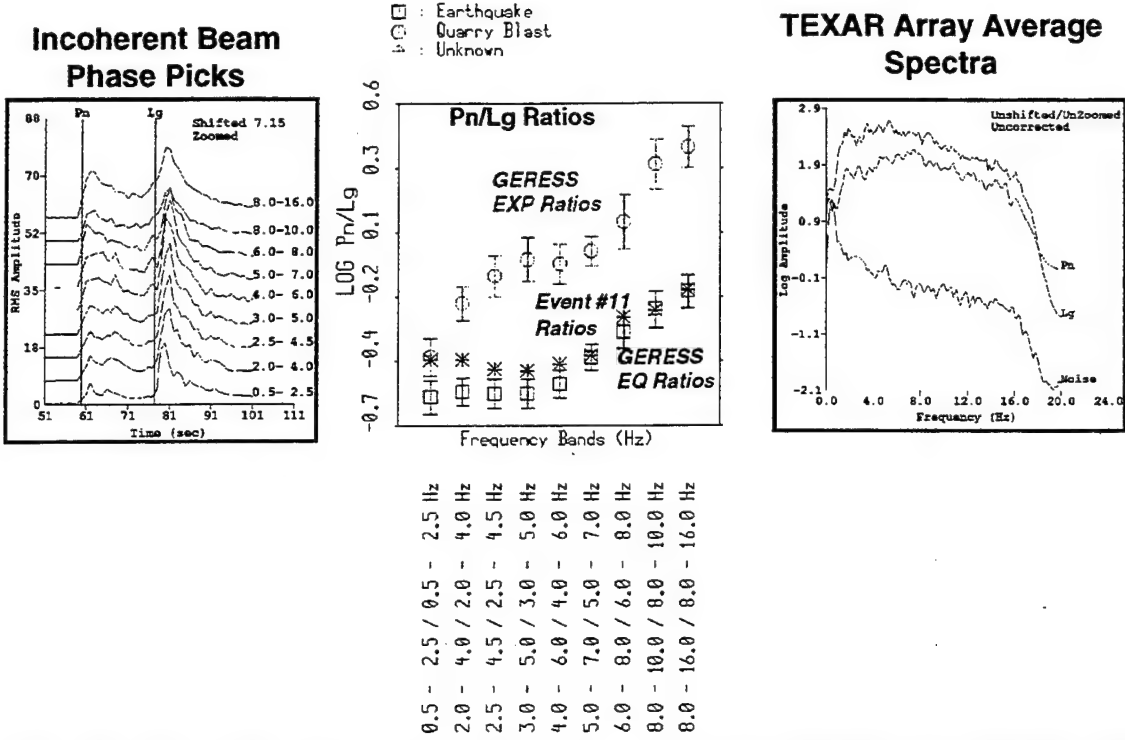


Figure 20: SMU Blind Test - Feature Extraction - Event #11 identified as earthquake based on flat Lg spectrum and earthquake like Pn/Lg ratios.

#### Event #12 - Blast (Correct)

The features for this event in Figure 21 are very characteristic of blasts. Spectral modulation due to ripple firing is evident in the spectra. The  $Pn/Lg$  ratios follow the trend for the GELESS mine blasts closely. Also, as can be seen on the incoherent beams, an  $Rg$  phase was observed at low frequency.

This event was identified as a blast, which is correct. SMU identified the event as a Hercules mine blast.

#### Event #13 - Blast (\*)

This event had features similar to blasts, but not conclusively so. The incoherent beams in Figure 22 show a very strong  $Rg$  arrival at low frequency. The  $Pn/Lg$  ratios tend to fall between the blast and earthquakes, but seem to follow the blast trend more closely. The spectra had very clear scalloping although somewhat different from spectra we have seen previously for ripple fired mine blasts.

We identified the event as a blast. However, this event was one of the exotic events, identified by SMU as a “Shuttlequake.” The signals are seismic waves produced by the

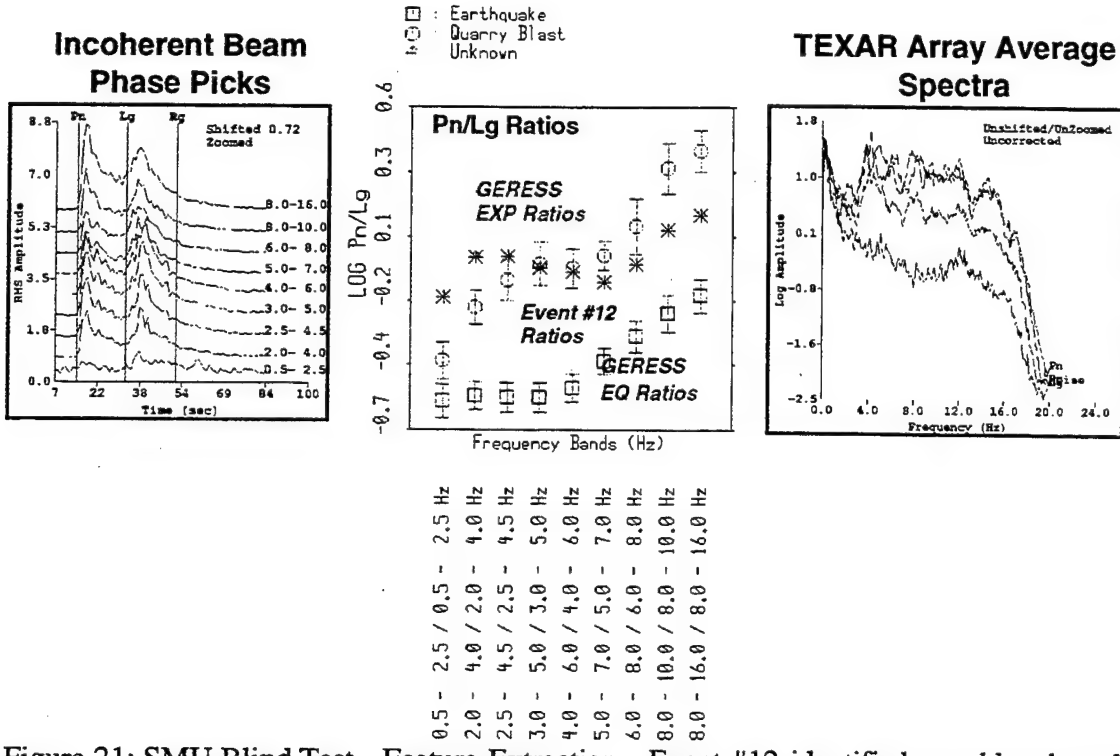


Figure 21: SMU Blind Test - Feature Extraction - Event #12 identified as a blast based on large  $R_g$  wave, impulsive  $P_n$  wave, large and increasing  $P_n/L_g$  ratio with frequency, and strong spectral scalloping caused by ripple fire.

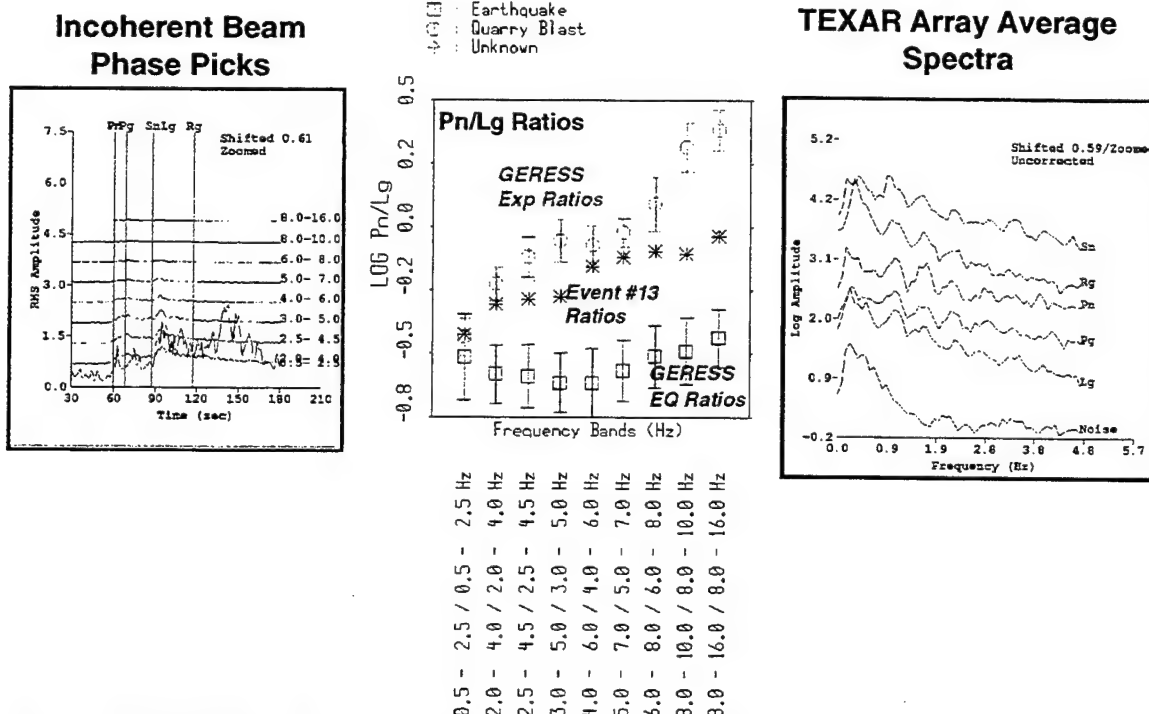


Figure 22: SMU Blind Test Feature Extraction - Event #13 which we classified as a blast based on large  $R_g$  wave, large and frequency dependent  $P_n/L_g$  ratios and spectral scalloping in all phase spectra. In fact, the event was a "Shuttlequake" or seismic signals produced the Mach cone of the space shuttle reentering the atmosphere.

bow shock of the Space Shuttle reentry about 150 km north of TEXAR. It is interesting that the event had strong characteristics of blast. Because the event is atmospheric, it would be easily detectable by means of infrasound sensors. The cause of the spectral scalloping may be that the reentry shock consisted of more than one shock front, possibly including one from the bow and one from the tail.

#### *Event # 14 Blast (Correct)*

This event had very clear characteristics of blast, as can be seen in Figure 23. The  $Pn/Lg$  ratios fall above the mine blast group at high frequency but below the earthquakes at low frequency. The incoherent beams in Figure 23 show that the  $Lg$  wave is very strong at low frequency, however, at high frequency, the  $Pn$  wave dominates the signal. The spectra show clear indications of spectral scalloping due to ripple firing.

We identified the event as a blast, which was correct. SMU identified the event as the Mi-care mine explosion.

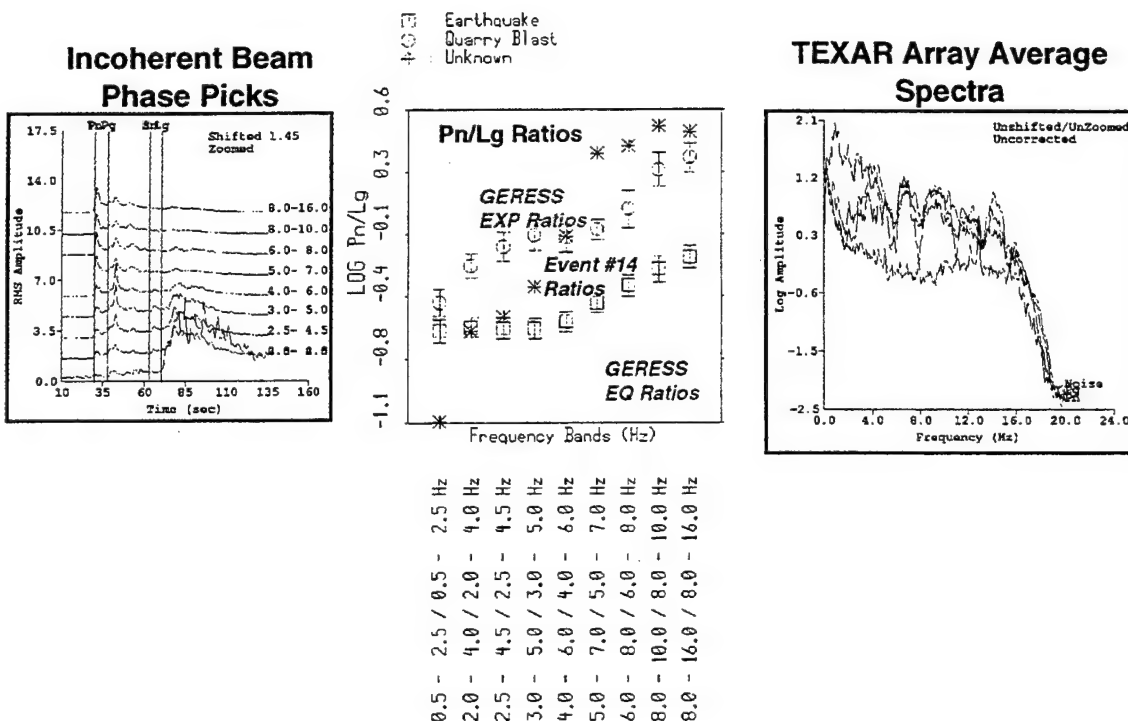


Figure 23: SMU Blind Test - Feature Extraction - Event #14 identified as a blast based on large  $Rg$  wave, large and increasing  $Pn/Lg$  ratios with frequency, and strong spectral scalloping caused by ripple firing.

*Event #15 Earthquake (Correct)*

The features for this event shown in Figure 24 are most consistent with earthquakes. The  $Pn/Lg$  ratios are low and follow the frequency dependence of the GERESS earthquakes. The spectra are peaked but smooth with no indication of ripple fire.

We identified the event as an earthquake which was correct. SMU identified the event as the Mazatlan Earthquake.

*Event #16 Earthquake (1/2 Correct)*

The features for this event, shown in Figure 25, are somewhat mixed. The  $Pn/Lg$  ratio increases with frequency, which indicates explosion, but the values are very low except at high frequency. The  $Lg$  and  $Pg$  spectra are somewhat peaked at low frequency, which is explosion like, but the  $Pn$  and  $Sn$  spectra are flatter like earthquakes. The  $Lg$  spectrum has a peak near 12 Hz which can also be seen in the noise spectrum.  $Lg$  is extremely large, relative to the  $Pn$ , at low frequency which is evident on the incoherent beam and the  $Pn/Lg$  ratio plots.

Based on the mixed results, we identified the event as probable earthquake, but maybe a blast and mine tremor. This conclusion was only half correct as the event was an earthquake. SMU identified the event as the Greenville earthquake located near Dallas.

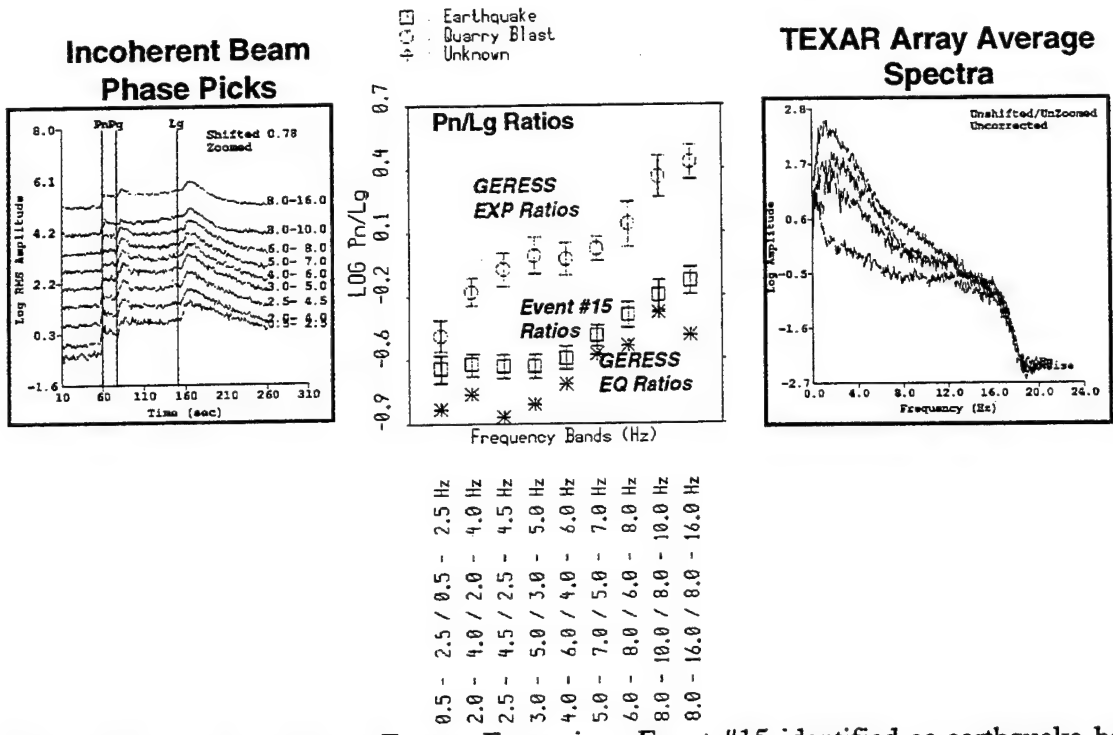


Figure 24: SMU Blind Test - Feature Extraction - Event #15 identified as earthquake based on earthquake like  $Pn/Lg$  ratios, emergent  $Pn$  onset, and smooth spectra.

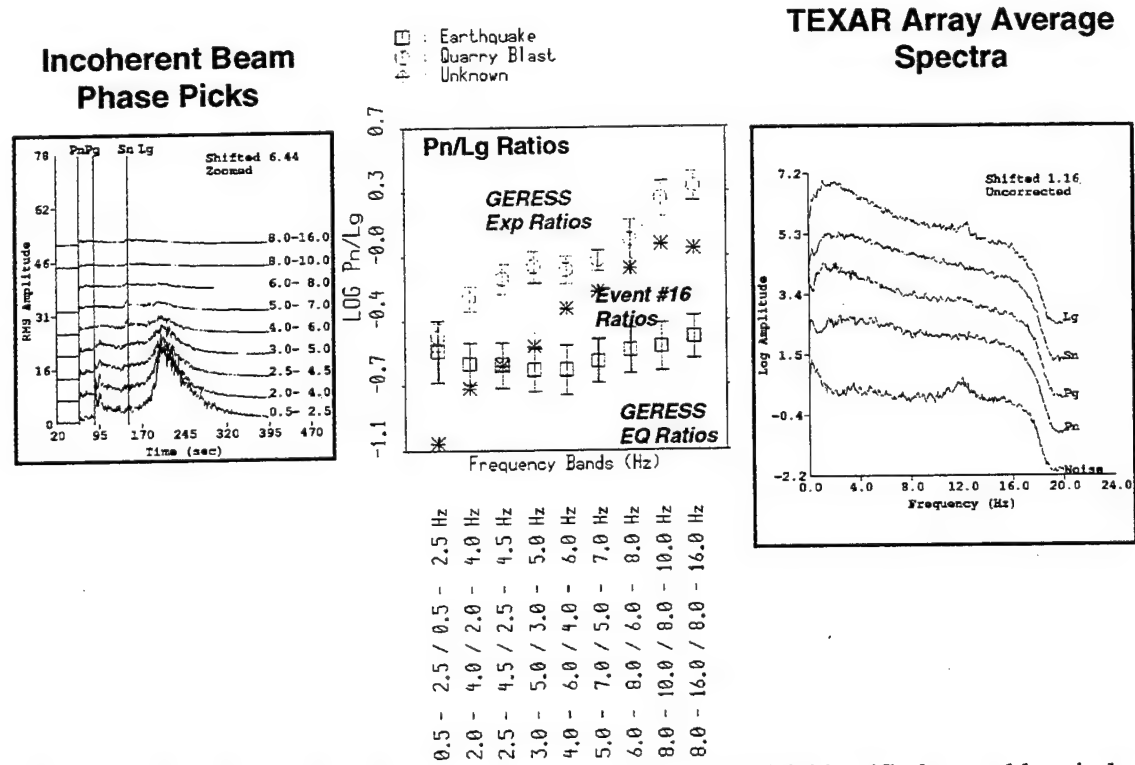


Figure 25: SMU Blind Test Feature Extraction - Event #16 identified as a blast-induced earthquake because it had unusual features characteristic of both blast and earthquake.  $Pn/Lg$  ratios increase with frequency, like blasts, but have very low values characteristic of earthquakes.

### *Event #17 Blast Induced Tremor (Correct)*

The features for Event #17 in Figure 26 are very similar to those of Event #16 discussed previously. The  $Pn/Lg$  ratios are very low at low frequency, indicating earthquake, but blast-like at high frequency. The spectra are peaked at low frequency, like blasts, and roll off quickly with frequency. As in the case of Event #16, there appears to be a spectral peak near 12 Hz in the  $Pg$ ,  $Sn$ , and  $Lg$  phases.

Based on the mixed results, we identified the event as probable earthquake, but maybe a blast and mine tremor as we did for Event #16. This turned out to be correct in that SMU identified the event as a South Texas induced earthquake.

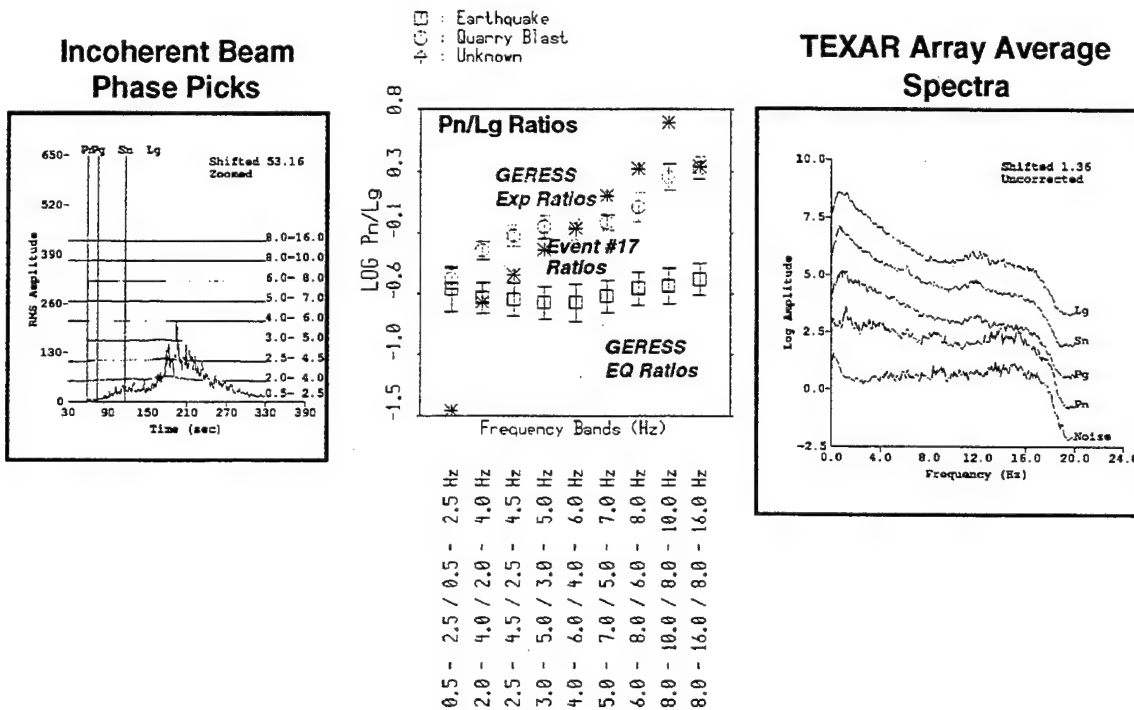


Figure 26: SMU Blind Test Feature Extraction - Event #17 identified as a blast-induced earthquake based on the same kinds of features as Figure 25.

### *Event #18 Blast (Correct)*

The features for this event shown in Figure 27 are unusual but most strongly resemble those of blasts. The  $Pn/Lg$  ratio, though very small at low frequency, rapidly increases with frequency and is well above the GERESS mine blast group. The spectra are peaked at low frequency and there is evidence of some spectral scalloping, primarily in  $Sn$  and  $Lg$ . The  $Pn$  spectrum looks unusual and seems to have different scalloping than  $Pg$ ,  $Sn$ , and  $Lg$ .

We identified the event to be an mine blast, which was correct. SMU identified the event as the Tyrone Mine explosion. Bonner et al (1997) have studied Tyrone earthquakes in some detail and suggest that the  $Pn$  wave is actually  $PnPn$ . This complexity might explain the unusual scalloping of the  $Pn$  spectrum in Figure 27.

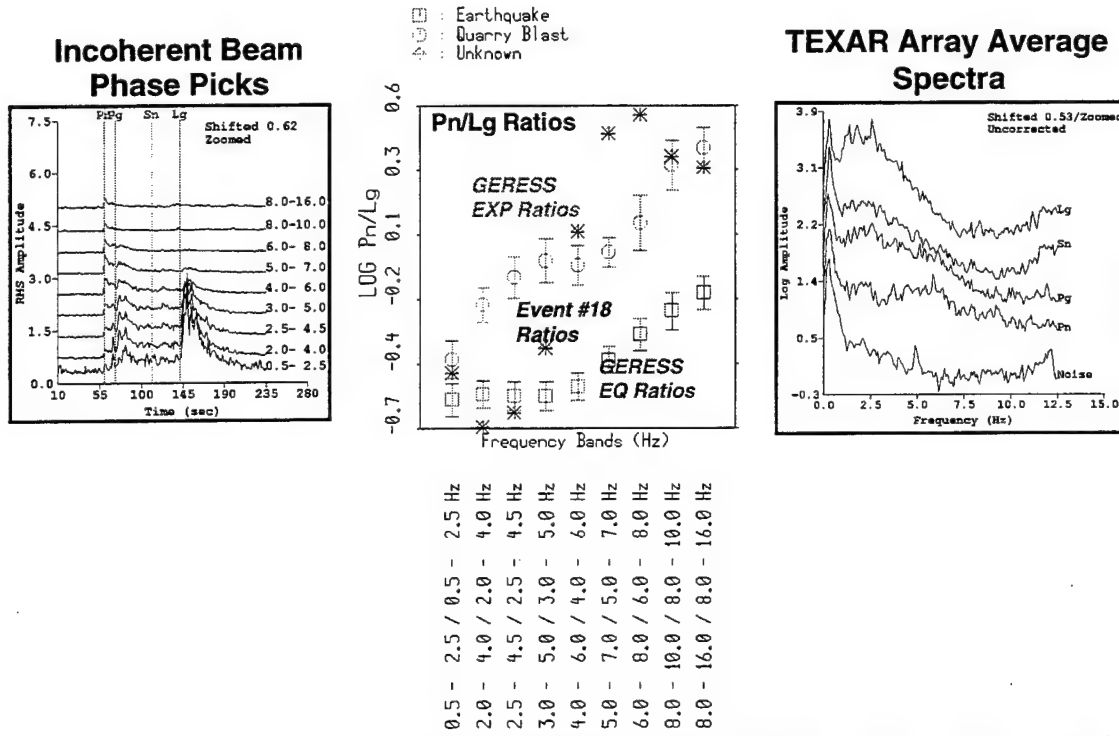


Figure 27: SMU Blind Test - Feature Extraction - Event #18 identified as blast based on increasing  $Pn/Lg$  ratio with frequency and weak evidence of scalloped spectra indicating ripple fire.

#### *Event #19 Blast (Correct)*

The features for this event shown in Figure 28 are also unusual but are most consistent with mine blast. The  $Pn/Lg$  ratios increase sharply with frequency and have values comparable to the Vogtland blasts. The spectra of all phases have a broad peak at about 12 Hz which we explained as being caused by ripple firing.

We identified the event as a blast, which is correct. SMU identified the event as the Morenci Mine explosion.

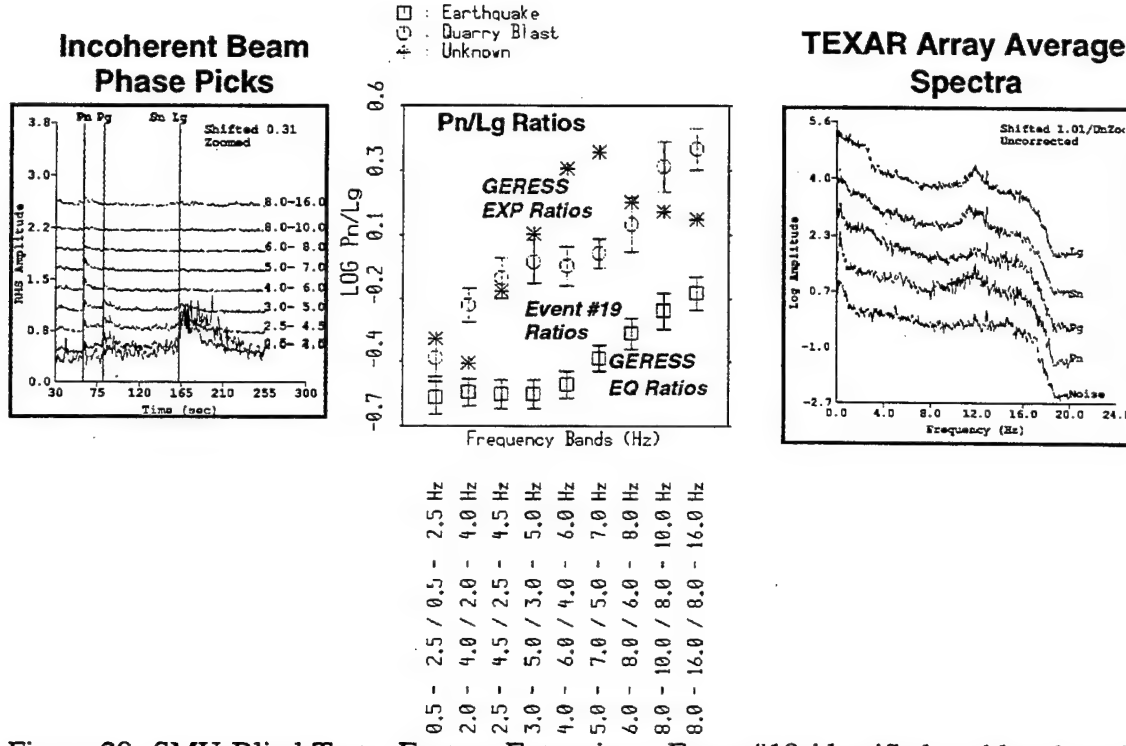


Figure 28: SMU Blind Test - Feature Extraction - Event #19 identified as blast based on high  $Pn/Sn$  amplitude ratios and weak evidence of scalloped spectra indicating ripple fire.

#### Event #20 - Earthquake (Correct ?)

This final event, whose features are shown in Figure 29, seemed to be earthquake-like. The  $Pn/Lg$  ratios are indicative of earthquake in that they are small, with  $Lg$  larger than  $Pn$  across the entire frequency band, and the spectra are smooth. Both the  $Pn$  and  $Lg$  spectra are flat and smooth, which are features of earthquakes.

We identified the event as an earthquake. SMU identified the event as being associated with a meteor shower and thus correct (i.e., meteorquake), which is another unexpected exotic event. The identification of meteorquake is based on the correlation in the time of the event and the known occurrence of the Geminid meteor shower, as discussed by Bonner et al (1997). The event may have produced an infrasound event. Thus, the seismic signals may have been produced by atmospheric shock fronts produced by the meteor shower. However, this event has none of the features of the Shuttlequake signals known to be produced by a shock front. The signals seem to be much more like an earthquake-like. At present, without more definitive ground truth, we would have to characterize the event as being unknown but probable earthquake.

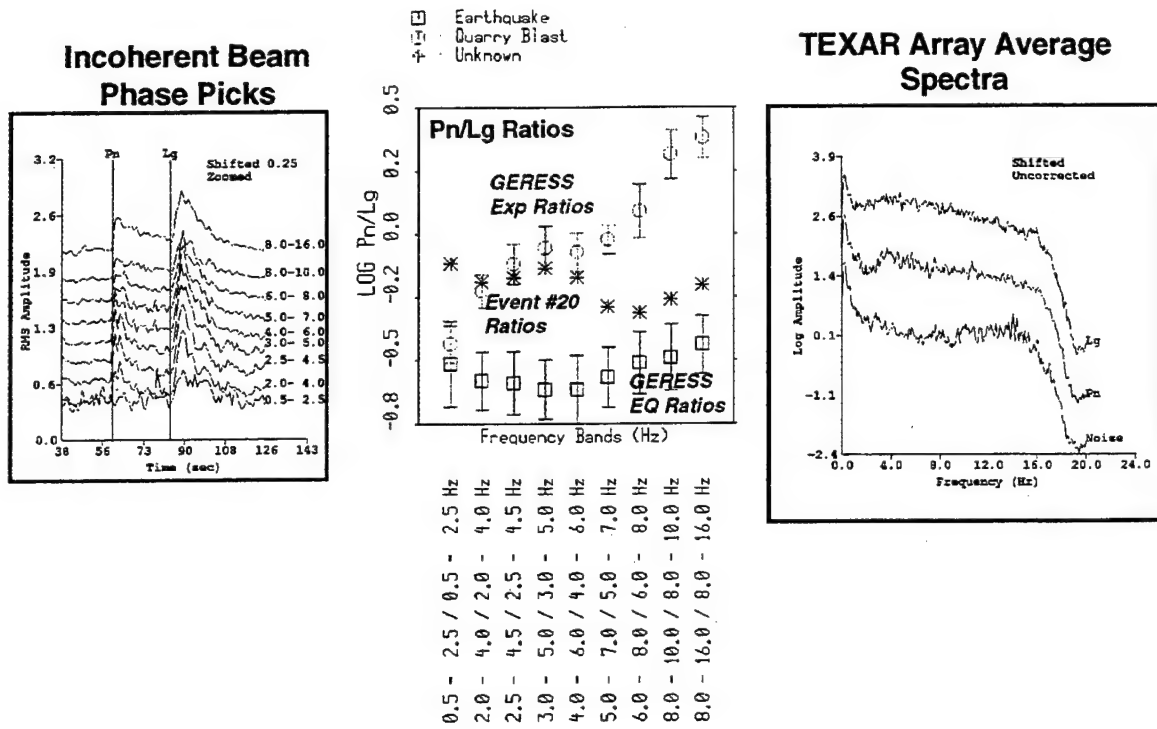


Figure 29: SMU Blind Test Feature Extraction - Event #20 identified as earthquake based on earthquake-like  $Pn/Lg$  ratios and broad smooth spectra. This event is of uncertain origin, perhaps associated with meteorite shower.

## 2.8 SUMMARY OF DISCRIMINATION RESULTS

Tables 1 and 2 tabulates the results of the discrimination analysis, how we classified each event, and whether or not the identification was judged correct or incorrect by SMU.

Of the first group of 10 events in Table 1, we identified 9 correctly and 1 incorrectly. However, regarding the incorrect identification, Event #10, we note in Table 1 that our actual decision was that ISEIS could not identify it because of poor high-frequency signal-to-noise ratios. In hindsight, we might have identified the event correctly as blast if we had believed our  $Pn/Lg$  discriminant and spectral scalloping results and discounted the large low-frequency surface wave as an earthquake indicator.

For the second set of 10 events in Table 2, Events #7 and #8 were judged half correct since we suggested a combination of explosion and earthquake characteristics. Event #6 was an earthquake and Event #7 a blast-induced earthquake. However, these events were so similar that we suspect they are both blast induced. All the normal events were identified correctly, and we were given credit for the exotic events, Event #13 (Shuttlequake) and Event #20 (Meteorquake ?). However, it should be noted that the IMS will have access to

Table 1 : SMU Blind Test Results - First 10

- Event #1 - Earthquake - flat Lg spectrum, low and frequency independent Pn/Lg ratios - Correct
- Event #2 - Blast - peaked Lg spectrum, high and increasing Pn/Lg with frequency, ripple fired, Rg present - Correct
- Event #3 - Blast - peaked spectrum, high and increasing Pn/Lg with frequency, ripple fired Correct
- Event #4 - Blast - high and increasing Pn/Lg with frequency, ripple fired, Rg present - Correct
- Event #5 - Blast - peaked Lg spectrum, increasing Pn/Lg with frequency, ripple fired - Correct
- Event #6 - Blast - increasing Pn/Lg with frequency, ripple fired, Rg present - Correct
- Event #7 - Earthquake - Low and frequency independent Pn/Lg at low frequency. ( Note: Weak signal, Pn had flat coda which is eq like) - Correct
- Event #8 - Blast - increasing Pn/Lg with frequency, ripple fired (?) - Correct
- Event #9 - Blast - Ripple fired (?), high Pn/Lg ratios and increasing with frequency to 5 Hz, where local event interferes - Correct
- Event #10 - Earthquake (?) (Note: ISEIS can't identify. Long-period surface wave for this event, no P a 1 Hz,

Table 2: SMU Blind Test Results - Second 10

- Event #11 - Earthquake - flat Lg spectrum, earthquake like Correct - Chihuahua Quake
- Event #12 - Blast - peaked Lg spectrum, high and increasing Pn/Lg with frequency, ripple fired, Rg present - Correct - Hercules Min Ex.
- Event #13 - Blast - high and increasing Pn/Lg with frequency, peaked spectra, Rg - \*Shuttlequake
- Event #14 - Blast - high and increasing Pn/Lg with frequency, Ripple fired, impulsive Pn Correct - Micare Mine Ex.
- Event #15 - Earthquake - Pn/Lg earthquake like, onset earthquake like, smooth spectra - Correct - Mazatlan Quake
- Event #16 - Blast-Induced ? - increasing Pn/Lg with frequency, earthquake and explosion like, spectral peak at 12 Hz, blast and tremor - 1/2 Correct - Greenville Quake, Near Dallas
- Event #17 - Blast-Induced ? - increasing Pn/Lg with frequency, earthquake and explosion like, spectral peak at 12 Hz, blast and tremor - 1/2 Correct - S. Texas Induced Quake
- Event #18 - Blast - increasing Pn/Lg with frequency, ripple fired (?) - Correct - Tyrone Mine Ex.
- Event #19 - Blast- Ripple fired (?), high Pn/Lg ratios - Correct - Morenci Mine Ex
- Event #20 - Earthquake - Pn/Lg earthquake like, broad smooth spectrum - Correct - Meteorquake

infrasound data to identify exotic events like this. In fact, the TEXAR infrasound array was used to identify these events.

## 2.9 OVERALL CONCLUSIONS

To our knowledge, this may be the first attempt at a blind test of discrimination techniques. A comprehensive blind test would of course require many more events involving data collected at different stations in different regions of the world. However, this preliminary study has provided a number of insights on the problems that will be confronted by the operational IMS for the identification of Special Events.

The following are our overall conclusions from this study:

- Events recorded at TEXAR are very similar to earthquakes/tremors and mine blasts recorded by GERESS in Germany and Poland.
- Inter-region comparison analysis identified all but two of the 20 test events. Generally, mine blasts can be best identified by looking for increasing  $Pn/Lg$  ratios with frequency, log10 ratios greater than 0 at high frequency, and spectral scalloping due to ripple fire. Earthquakes generally have low, frequency-independent  $Pn/Lg$  ratios. Earthquake spectra can be flat, smooth, and lacking in any kind of scalloping. However, not all earthquake spectra are flat, depending on the bandwidth of the signals.
- One event, the Thunder Mountain Cast shot, was judged unidentifiable based on weak signals at TEXAR. This event had very large  $Rg$  waves at low frequency, but this appears to be a typical characteristic of mine blasts there. If we had had access to a closer station, such as Pinedale, the event could have been correctly and conclusively identified.
- Application of single discriminants can be fooled by interfering events if care is not taken to detect mixed signals. The one example we had, Event #9, had  $Pn/Lg$  features that have never been observed, i.e., sharply increasing  $Lg$  amplitude with frequency. The CTBT IMS must be able to check such anomalies.
- Discrimination may be fooled by exotic events. Typical events we were sent by SMU include Shuttle and aircraft shock fronts and possible events associated with meteor showers. However, as discussed by Bonner et al (1997), having a collocated infrasound array should be able to handle most of these kinds of events.

Our overall conclusion is that blind tests such as this are effective ways of testing the reliability of Special Event identification methods. We are encouraged by the overall success of

ISEIS to identify most of the events, and that the GERESS events served well as a reference events even though they occurred in a different part of the world. This points to the robustness of the  $Pn/Lg$  ratio, and that it appears to be relatively insensitive for receiver effects. Perhaps this is due to the fact that the features were averaged over arrays, instead of at single sensors, and that this might have averaged out receiver structure effects. More such tests are recommended in the future as the IMS is developed and tested.

### **3. CHARACTERIZATION OF THE AUGUST 16, 1997 KARA SEA EVENT**

#### ***3.1 Introduction***

On August 16, 1997, a seismic event occurred near the Kara Sea in the vicinity of the Former Soviet Union test site at Novaya Zemlya. This event has received a great deal of attention, and a number of studies of this event have been published that have indicated that the event was probably an earthquake (e.g., Richards and Kim, 1997). However, it occurred in a relatively aseismic region near a known test site and was initially identified as a possible explosive event.

This event poses two problems for identification: (1) lack of earthquakes in the region, although there is a history of recorded nuclear explosions at Novaya Zemlya and (2) at the time of the event, one of the key stations, ARCESS, was not operating. However, the event was recorded at the non-IMS station Kevo (KEV) as well as a number of earlier nuclear explosions at the test site. Richards and Kim (1997) studied the event there and showed that the multiple frequency  $P/S$  ratios of the August 16, 1997 event were significantly different than those of the nuclear explosions recorded at the same site. However, no consideration could be given to whether it was, in fact, an earthquake or a chemical blast, because no historical record of these kinds of sources was available at KEV. Also, since the event was located offshore, no consideration was given in the earlier studies of whether the event could have been an undersea explosion.

In our characterization of the Kara Sea event, we make two fundamental assertions:

(1) Seismic events recorded at stations in other regions and at other stations can be used as reference events for characterization of Special Events if it can be shown that site and path effects are comparable.

This argument is controversial because most seismologists would require that reference events should occur in the same region as the Special Event and be recorded at the same station. However, this is often not possible for aseismic regions or stations located in new regions that have limited historical data. Thus, it may be necessary to utilize reference events in different regions perhaps recorded at a different station. We argued this point in the last section where we identified events in the southwestern US recorded at TEXAR using reference events in Germany and Poland recorded at GERESS. In this section, we will show that the site and path characteristics of seismic events recorded at KEV and ARCESS

are almost identical. Thus, it should be possible to combine features at the two stations, using the KEV data for the Kara Sea event, and the ARCESS recordings of historical earthquakes and mine blasts.

(2) Seismic events should utilize the best data available, and should not combine data for poor quality or of demonstrably inferior discrimination capability in the identification of Special Events.

This argument counters the view that all data should be used in characterizing seismic events. In the case of discrimination, this approach is unnecessary and can give incorrect information about the identity of seismic events if high and low quality data are combined. Stated another way, we would argue many stations are not necessary for the identification of seismic events; only one high-quality station would be sufficient. "High-quality" means that the station records broadband signals at high signal-to-noise ratios and that the discriminants are known to perform well there. In the case of identifying earthquakes using the frequency-dependent  $P/S$  ratio, we suggest that only one high-quality station with a low value of  $P/S$  ratio at high frequency would be required to identify an earthquake.

In this section, we discuss these two assertions in connection with the characterization and identification of the Kara Sea event and Special Events in general. We also consider the possibility of whether or not the event could have been an underwater explosion given that it was located offshore.

### ***3.2 Event Location and Recording Stations***

Figure 30 shows a map of the location of the Kara Sea event and the propagation paths to some of the stations that recorded it. The location near the former Soviet test site at Novaya Zemlya originally raised suspicions that the event might have been a nuclear blast. However, the seismic locations of the event in the Reviewed Event Bulletin (REB) of the PIDC, discussed by Richards and Kim (1997) and Israelsson et al (1997), placed the event offshore in the Kara Sea beneath 225 m of water. Based on location alone, and the lack of any other evidence for testing activity, it was suggested strongly that the event was an earthquake.

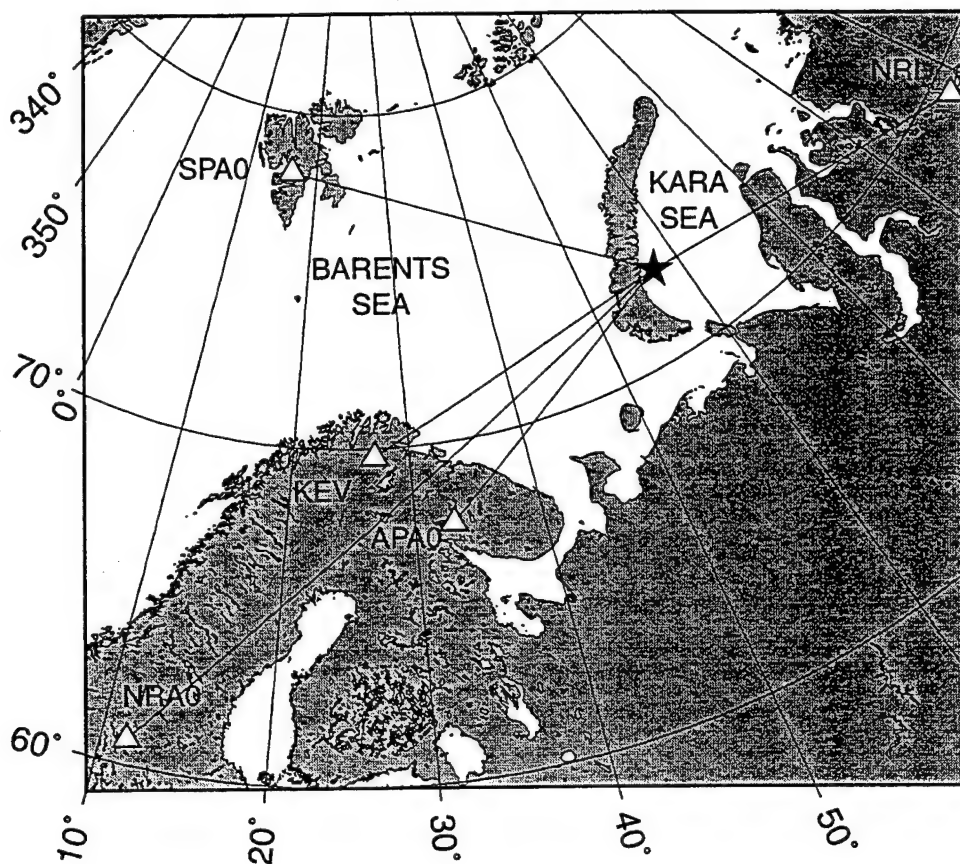


Figure 30: Map showing propagation paths from the August 16, 1997 Kara Sea event to the stations used in this study.

The inter-region reference-event comparison method, discussed in the last section, was used to characterize this event because of the missing earthquakes in the region and the failure of the ARCESS array at the time of the event. The Finnish station, Kevo (KEV), was identified as a surrogate station since it is located near ARCESS and thus in the same overall tectonic region. However, the data history for KEV was limited, although historical seismic data was available for KEV for nuclear explosions.

This event was processed through ISEIS and the  $Pn/Sn$  amplitude ratios were compared with other events, using KEV recordings of the August 16, 1997 event and historical nuclear explosions, and ARCESS recordings of earthquakes, nuclear explosions, and mine blasts in surrounding regions. Figure 31 shows a map of the locations and propagation paths of events recorded at ARCESS that we have used in this comparison. The earthquakes were near Spitzbergen and included the Steigen earthquakes of northern Norway, the mine blasts on the Kola Peninsula, and the nuclear explosions at Novaya Zemlya. The same Novaya Zemlya nuclear explosions were also recorded at KEV and were the ones studied earlier by Richards and Kim (1997) and Israelsson et al (1997). These events were

also analyzed in this study. All the ARCESS and KEV historical-event features were stored in the ISEIS database and were called up in the manner described above for the TEXAR data. The KEV data were obtained more recently but processed in the same way as the ARCESS data.

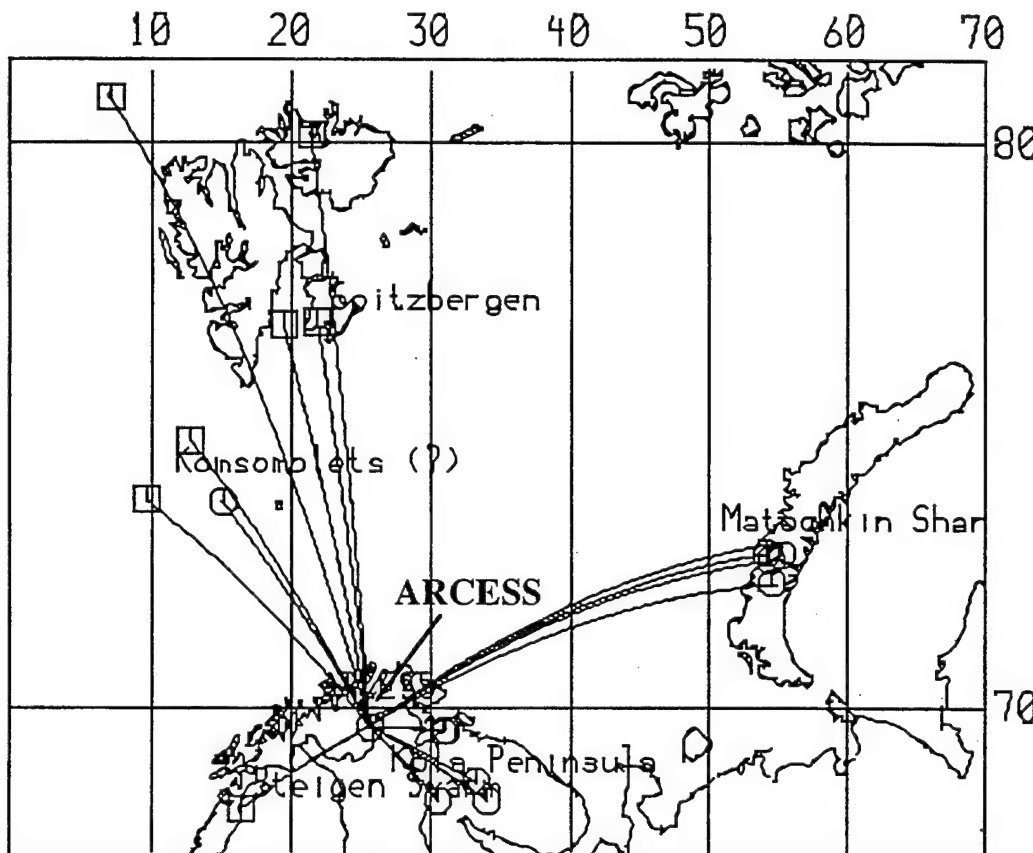


Figure 31: Basemap showing locations of and great-circle propagation paths for events recorded at ARCESS that were used as a comparison reference set for the Kara Sea event recorded at KEV.

We thus make the assumption that KEV and ARCESS are interchangeable stations and compared events recorded at the two stations as if they were the same station. This, in turn, rests on the assumptions that the recording instrumentation of KEV and the crustal structure effects beneath the two stations are similar. The former assumption is not totally valid since KEV and ARCESS have different sampling rates (KEV is 20 Hz and NORESS is 40 Hz), and also have different instrumentation. However, using same-band amplitude ratios and array averages for the ARCESS features should make our  $Pn/Sn$  ratios partially insensitive to differences in the recording instrumentation. The validity of the assumption that the stations have similar sites will be addressed later.

### 3.3 Incoherent Beams and Observed Regional Phases

As shown in Figure 30, this event was recorded at three regional arrays, NORESS, Spitzbergen, and Apatity, and the single stations KEV. Waveforms of these events have been shown by Israelsson et al (1997). Figure 32 shows “incoherent beams” computed for the Kara Sea event at KEV, Apatity, Spitzbergen, and NORESS. As in the previous section, we display all the incoherent beams shifted vertically for display purposes with the lower frequency filters on the bottom. The filter bands in Hz for incoherent beams are labeled on the sides. The rms amplitude scale on the vertical axis should be considered relative. Note that the KEV, Spitzbergen, and NORESS records are in log10 rms units whereas the Apatity records are unlogged rms amplitude units. The phase identifications for  $Pn$  and  $Sn$ , picked on waveforms, are shown on the incoherent beams.

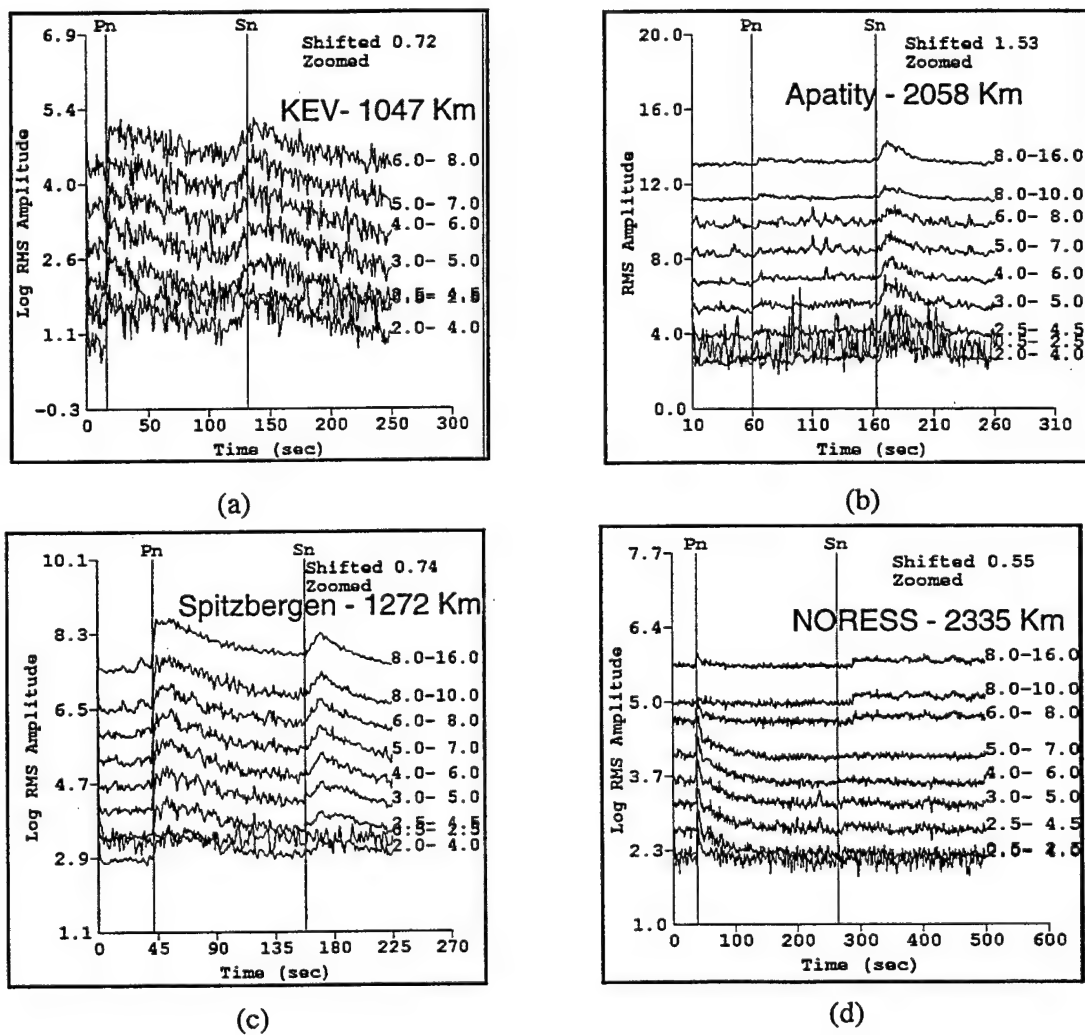


Figure 32: Plots of filtered incoherent beams for the recordings of the August 16, 1997 Kara Sea Event. (a) Kevo, (b) Apatity, (c) Spitzbergen, (d) NORESS

Note that at KEV and Apatity, the  $S_n$  energy exceeds that of  $P_n$  at the highest frequencies. At Spitzbergen, which is over 200 km more distant than KEV and Apatity, the  $P_n$  amplitude exceeds the  $S_n$  energy. However, it is notable that significant  $S_n$  energy appears on all three of these sensors to frequencies up to 8 Hz. Only NORESS, at 2335 km, failed to record an  $S_n$  of any significant size, although a very weak, emergent onset could be made out at high frequency. Of course, NORESS is at 2335 km and even the  $P_n$  wave is just barely observable.

As we discussed in the previous section, the incoherent beams are used to obtain amplitudes for the different phases in different frequency bands that, in turn, are used to compute the  $P_n/S_n$  amplitude ratios.

It should also be noted that no  $L_g$  waves are observed for propagation paths coming out of this region that cross the Barents and Kara Seas. An explanation for the blockage of  $L_g$  from Novaya Zemlya explosions, originally given by Baumgardt (1990, 1996), is that thick sediment accumulations in the Barents Sea cause a breakdown in the  $L_g$  propagation waveguide in the shallow crust. In an earlier study of Russian PNEs recorded at NORSAR (Baumgardt, 1991),  $L_g$  was observed to also be blocked for paths that crossed the Kara Sea, another region underlain by a sedimentary basin. Baumgardt (1996) has suggested that sedimentary basins may be a principal cause of  $L_g$  blockage in continental cratons.

However, in spite of the non-existence of  $L_g$ , strong  $S_n$  waves have been observed in the region. Baumgardt (1996) has suggested that in many regions there may be a tradeoff between  $S_n$  and  $L_g$  excitation and blockage; i.e., where  $L_g$  is blocked,  $S_n$  is strong, and vice versa. In the case of the Barents and Kara Seas, most of the  $L_g$  energy appears to have been blocked and the shear wave energy generally propagates as  $S_n$ . Thus, the  $P_n/S_n$  and  $P_n/L_g$  ratios may be used as interchangeable discriminants, and  $P_n/S_n$  would be best used in regions where  $L_g$  is blocked. The same argument may also be made about the tradeoff in  $P_n$  and  $P_g$  propagation. However, for most regions of the world, we usually observe efficient  $P_n$  type propagation, although high-frequency filtering is often required to observe  $P_n$ . Because  $P_n$  is the first arrival phase, we use it as the  $P$  phase for regional  $P/S$  ratios even when  $P_g$  is the stronger phase. However, for all the observations from the Kara Sea/Novaya Zemlya region, only  $P_n$  and  $S_n$  phases could be observed. Like in our earlier studies of discrimination in the region, we principally analyze the  $P_n/S_n$  amplitude ratio discriminant.

### 3.4 Spectral Comparisons of KEV and ARCESS

To check possible effects of differences in site on the features at KEV and ARCESS, we now compare the spectra for the two stations recording the same events. In Figure 33, we compare the spectra for two Novaya Zemlya nuclear explosions recorded at ARCESS and KEV for two common nuclear explosions in Figure 33 (a) and (b). Also, in 33 (c), we compare the ARCESS spectra for an earlier Special Event near Novaya Zemlya, the 31 December 1992 New Years Eve event (Baumgardt, 1993b), with the idea that these events may be similar. The  $Pn$  spectra are plotted in blue, the  $Sn$  in red, and pre- $Pn$  noise in black. Each of the spectra were computed for 20 second windows starting at the onset times for  $Pn$  and  $Sn$  on incoherent beams. All spectra were smoothed using the Parzen window. The same bandwidths (1 to 10 Hz) are shown in each case. The instrument response has been deconvolved in all cases.

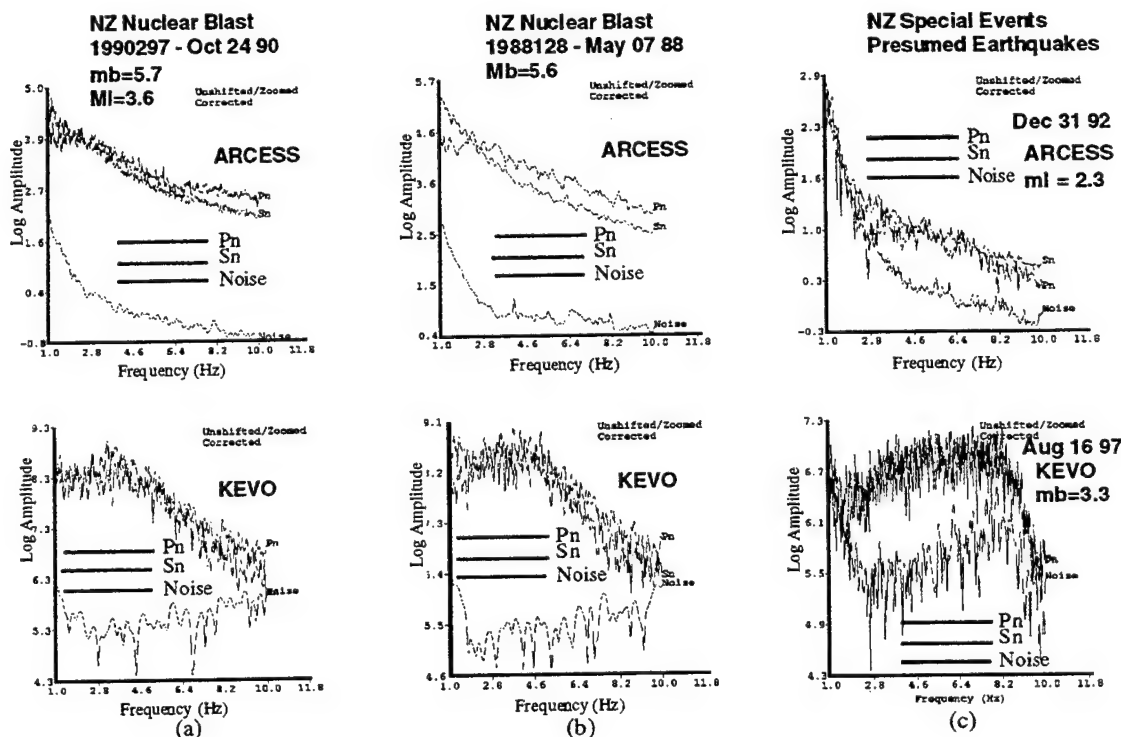


Figure 33: Comparisons of spectra recorded at ARCESS and KEV for the same nuclear explosions (a, b). (c) Comparison of the December 31, 1992 event recorded at ARCESS with the August 16, 1997 event recorded at KEV.

Comparison of the ARCESS and KEV spectra for the explosions shows similarity in the general trend. The ARCESS spectra have less variance because they are averaged across the array. The frequency dependence in the  $Pn$  and  $Sn$  spectra are similar overall. The  $Sn$  spectra fall off faster with frequency than the  $Pn$  spectra with the cross over point at about

2.5 Hz. Thus, the  $Pn$  spectral level exceeds the  $Sn$  below 2.5 Hz and reverses above 2.5 Hz in agreement with  $Pn/Sn$  plotted versus frequency. This pattern is the basic discriminant for identifying nuclear explosions, i.e., the  $Pn$  spectral level exceeds the  $Sn$  spectral level and the slopes of the  $Pn$  spectra are shallower than that of the  $Sn$  spectra. At low frequency, this pattern is reversed and shows that significant shear-wave energy is generated by nuclear explosions.

The KEV spectra for the nuclear explosions have almost exactly the same shape as those of the ARCESS spectra, although the variance of the spectra is higher because the KEV spectra and the overall bandwidth and signal-to-noise ratio are lower for KEV than for ARCESS. The noise level at KEV does increase somewhat with frequency above 5 Hz, whereas the ARCESS noise spectra fall off with frequency. The spectra for KEV seem to bend more with frequency than the ARCESS spectra, but this is an artifact of the dynamic range of the plot. Note, for example in Figure 33 (a), the KEV log amplitude range is 4.3 to 9.3, or 5 log units, whereas that for ARCESS is -0.8 to 5.0, or 5.8 log units. So, the ARCESS range is 0.8 larger than the KEV range, which is why the shapes of the ARCESS and KEV seem a little different. Close comparison of the explosion spectra in 33 (a) and (b) reveals that the ARCESS and KEV spectra are almost identical in shape and trend for the same nuclear explosions observed at the two sites.

However, the August 16, 1997 spectra are decidedly different in that they exhibit flat spectral characteristics that we have observed in earthquakes. For example, similar flat spectra were observed for the Vogtland earthquakes recorded at GERESS (Baumgardt, 1993a) as well as many of the closer earthquakes recorded at TEXAR, discussed in the previous section. Of course, the magnitudes for the nuclear explosions, which were 5.7 and 5.6 mb, were much larger than the Kara Sea body-wave magnitude of 3.3. Thus, some of the spectral flattening in the case of the Kara Sea event may be explained by source size scaling. However, we also include the ARCESS spectrum for the December 31, 1992 event near Novaya Zemlya that had a local magnitude of 2.3. The August 16 spectral levels at KEV increase with frequency, which is quite different than the December 31, 1992 event recorded at ARCESS. Because the explosion spectra at ARCESS and KEV are so similar, we conclude the site effects are about the same and the differences seen in Figure 33 (c) are source effects.

### **3.5 $Pn/Sn$ Ratio Analysis at KEV and ARCESS**

Based on the comparative spectral analysis of the common nuclear explosions in the previous section and the fact that common events recorded at ARCESS and KEV have almost

identical spectral shapes in the 1 to 10 Hz band, the two stations appear to have very similar site structure and propagation paths in this region. This indicates that direct comparisons can be made of events recorded at ARCESS to different events recorded at KEV as if they are the same station in the 1 to 10 Hz band. Based on this assumption, this study expands on the earlier one of Israelsson et al (1997) in that we compare the August 16, 1997 event, recorded at KEV, with the archive of events recorded at ARCESS, even though the August 16, 1997 event was not directly recorded at ARCESS.

Based on the incoherent beam analysis discussed above, we also decided to focus primarily on the stations ARCESS, and KEV, which we treat as a stand-in in for ARCESS. Special Event characterization should only be done using data from the stations with the best quality data and where the discriminants are known to perform well. As shown in Figure 32, the Apatity and NORESS station had poor signal-to-noise ratio for events in this region, and thus, we did not use them. Spitzbergen had a good signal, but as we will discuss below, the discriminants perform poorly there for reasons we understand.

Given that the spectra were similar, the rms incoherent beams and the measured amplitudes should also be similar. In the analysis that follows, we use the method we call “inter-region comparison”, discussed in the last section, of plotting KEV and ARCESS amplitude-ratio features on the same plot. The  $Pn$  and  $Sn$  amplitudes were computed in 7 frequency bands at KEV and 9 frequency bands for the ARCESS archived events, using the measurement of maximum rms amplitudes in the phase windows starting at the time picks of the phases, as discussed in the previous section.

Because  $Lg$  waves do not propagate in this region, the  $Pn/Sn$  ratio discriminant had to be used instead of the  $Pn/Lg$  ratio. Figure 34 shows scatter plots of  $Pn/Sn$  ratios plotted versus distance. Figure 34 (a) shows the various  $Pn/Sn$  ratio measurements in the 5-7 Hz band, made at both ARCESS and KEV, plotted versus distance, but uncorrected for distance, and Figure 34 (b) shows the same points after a distance correction. We use the distance correction for  $Pn/Sn$  amplitude ratios derived from relations for Scandinavia and western Eurasia given by Sereno (1991). As discussed earlier, the distance correction pulls down the  $Pn/Sn$  ratios at larger distances relative to the values at smaller distances. This correction is required for comparison of the August 16 Kara Sea event with mine blasts and earthquakes at about 400 km from ARCESS but not for comparison with nearby earthquakes and nuclear explosions, since they are at about the same distance, about 1100 km, as the August 16 Kara Sea event. The plus signs indicate the  $Pn/Sn$  ratios measured at both KEV and ARCESS for Novaya Zemlya nuclear blasts, and it is notable that the measure-

ments tend to cluster at the same value in this band. The August 16 event is well below the values for mine blasts and nuclear blasts, and falls well within the category of values for other earthquakes.

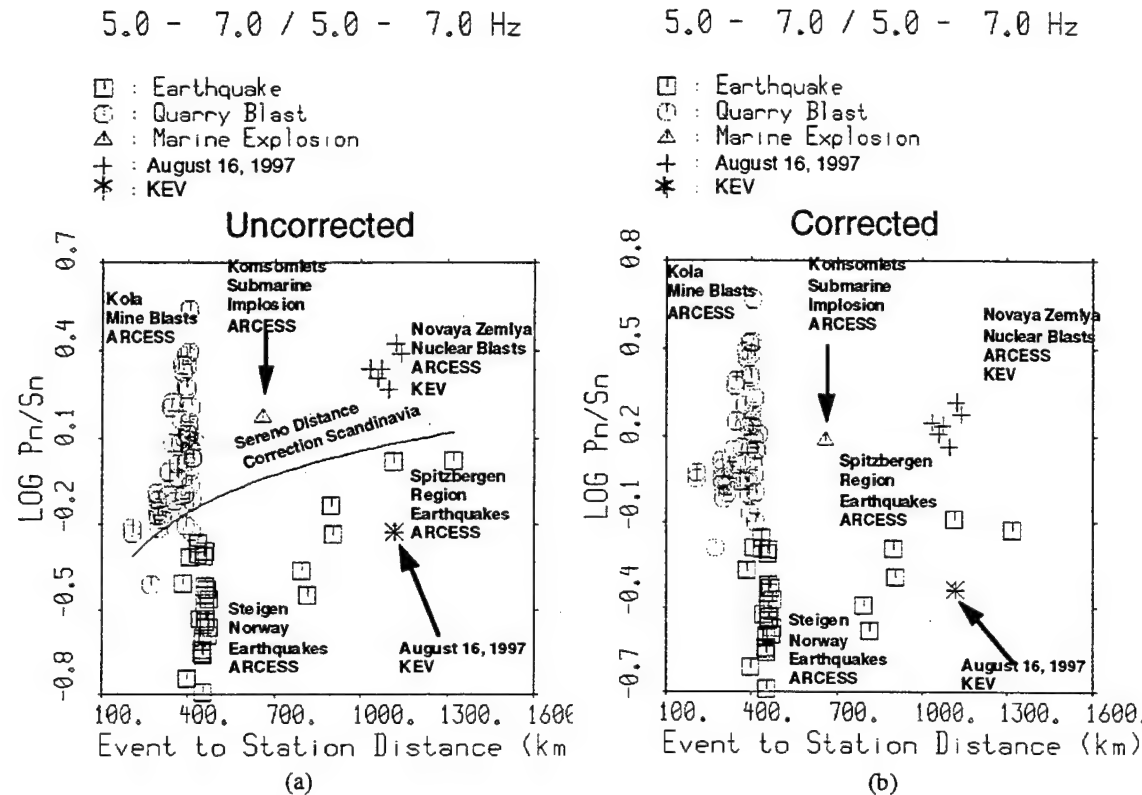


Figure 34: Plots of the  $\log_{10} P_n/S_n$  ratios for discriminants for the August 16, 1997 event, recorded at KEV, with nuclear explosions, mine blasts, earthquakes, and an underwater event (Komsomolets submarine sinking) recorded at ARCESS (a) With distance correction curve. (b) Ratios plotted after distance correction.

Also shown on the plot is the presumed Komsomolets submarine implosion (blue triangle) that occurred in the Norwegian Sea in 1989 and had been earlier analyzed in ISEIS. Implosions are known to have characteristics similar to explosions, so this event can serve as a useful example of an undersea explosion and can be used to determine if the August 16 event might have been an undersea blast in the Kara Sea. The  $P_n/S_n$  ratios for the Komsomolets event falls in the blast category, and higher than that of the August 16 Kara Sea event.

As we noted in earlier studies of the 31 December 1992 New Years Eve event in this region (Baumgardt, 1993b), the  $P_n/S_n$  amplitude ratios for mine blasts on the Kola Peninsula have high scatter. We were not able to clearly identify that earlier event as an earthquake, because of the partial overlap of the mine blast population with this event. However, the

August 16, 1997 event clearly has a lower ratio  $Pn/Sn$  ratio, after distance correction, than the mine blasts on the Kola and falls closer to the earthquake category.

Figure 35 (a) and (b) shows all the  $Pn/Sn$  ratios plotted versus frequency without and with distance corrections, respectively.

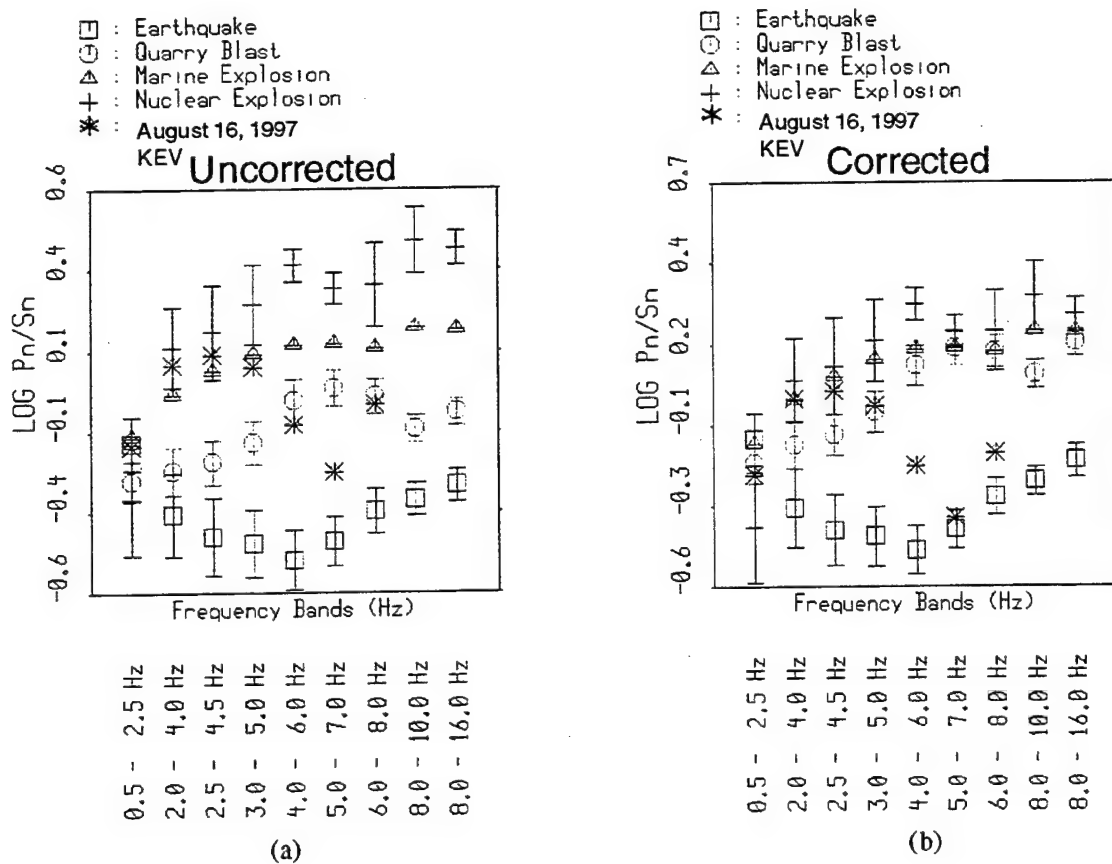


Figure 35: Plots of the  $\log_{10} Pn/Sn$  ratios for discriminants for the August 16, 1997 event, recorded at KEV, with nuclear explosions, mine blasts, earthquakes, and an underwater event (Komsomolets submarine sinking) recorded at ARCESS plotted versus filter frequency. (a) Not distance corrected. (b) Ratios plotted after distance correction.

In this display, we show the average  $Pn/Sn$  amplitude-ratio values for different source types and the error bars are the standard deviations. This display clearly shows that the August 16 event falls well below the earthquakes category at high frequency, above the 3 to 5 Hz band. The distance correction enhances the separation at high frequency. The ratios for the event suddenly decrease in the 5 to 7 Hz band that seems to be an unusual feature of earthquakes in the region. It is unlikely that such a feature would be produced by a nuclear explosion.

### 3.6 $Pn/Sn$ Amplitude Ratios At Spitzbergen

We now consider the amplitude ratios measured at the Spitzbergen array. As we pointed out above, this station recorded the August 16, 1997 Kara Sea event with the highest signal-to-noise ratio. We also plot  $Pn/Sn$  amplitude ratio features for events recorded at KEV and ARCESS and compare with those of Spitzbergen array. Since there are no nuclear explosions recorded at Spitzbergen, we would have to transport nuclear explosions from some other region, say ARCESS and KEV recordings of Novaya Zemlya events, to the Spitzbergen array. However, this can only be done if we can demonstrate that the sites and propagation path effects are similar for Spitzbergen, KEV, and ARCESS. In this section, we will show that, in fact, the sites are not equivalent and we cannot transport the ARCESS and KEV archive of features to Spitzbergen.

Figure 36 shows plots of 5 to 7 Hz  $Pn/Sn$  ratio versus distance, with distance corrections applied.

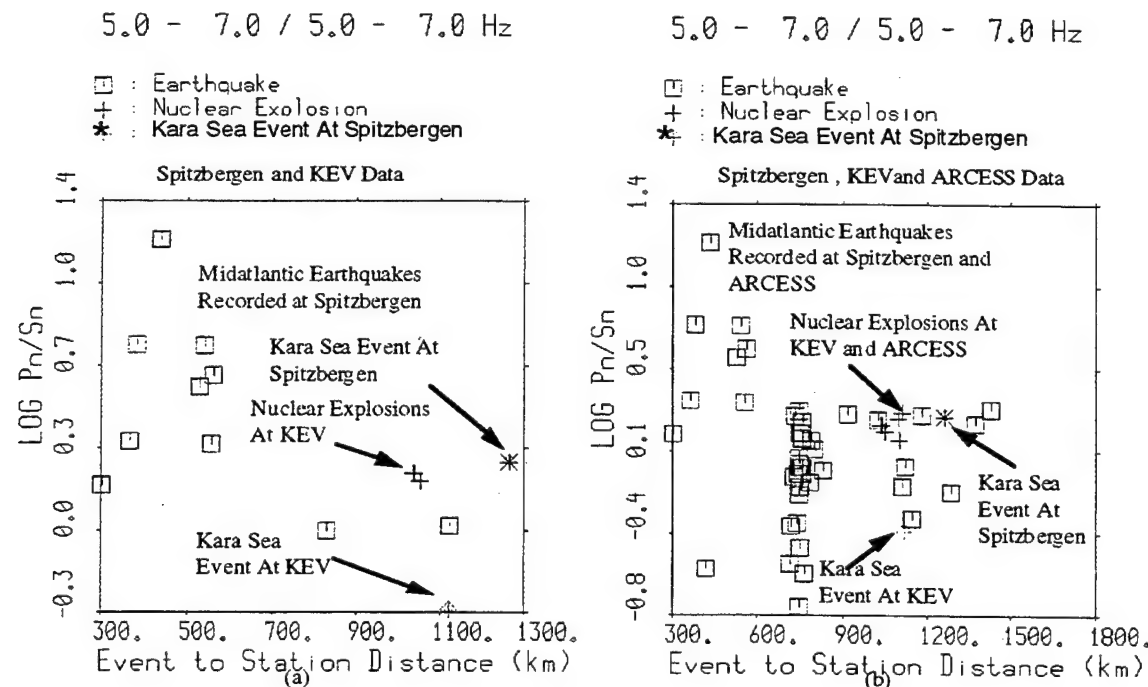


Figure 36: Plots of the  $\log_{10} Pn/Sn$  ratios for discriminants for the August 16, 1997 recorded at Spitzbergen (a) Comparison with mid-Atlantic ridge events recorded at Spitzbergen, and nuclear blasts recorded at KEV. Also, the August 16, 1997 event recorded at KEV is plotted. (b) Same as (a) but with ARCESS recordings of mid-Atlantic ridge events and nuclear blasts. All ratios are corrected to 700 km distance.

Figure 36 (a) compares the Spitzbergen  $Pn/Sn$  ratios for the Kara Sea events with the KEV ratio for the same event. We have also plotted a set of earthquakes close to Spitzbergen that

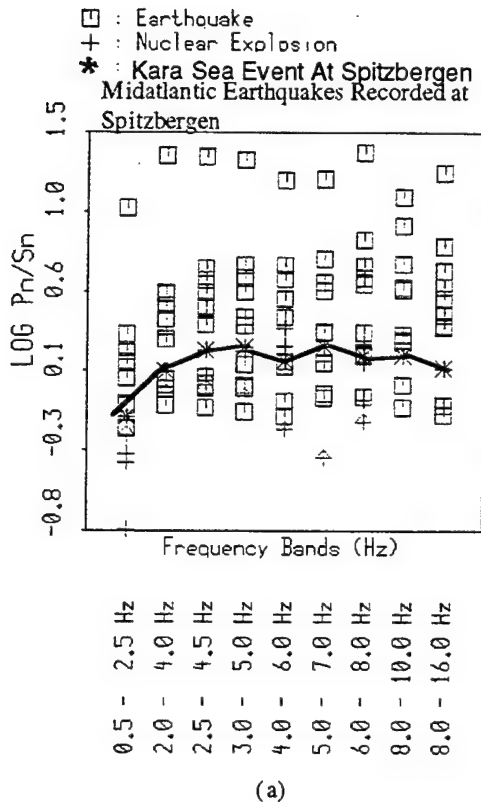
were located near the Mayan Ridge. We note that, even though the KEV and Spitzbergen sites were about the same distance from the Kara Sea event, the  $Pn/Sn$  ratio at Spitzbergen is almost a full log unit higher than the value at KEV. This difference appears to be caused by the  $Sn$  values being smaller at Spitzbergen than at KEV relative to the  $Pn$ . This comparison reveals a site difference between KEV and Spitzbergen in the  $Pn/Sn$  ratio which precludes transporting discriminants from KEV to Spitzbergen.

Also, we have plotted the nuclear explosion ratios for KEV on the plot, and we see that the ratios have similar values as the Kara Sea event recorded at Spitzbergen. However, there are also a number of earthquakes closer to Spitzbergen that have very high ratios which overlap nuclear explosions recorded at KEV. Again, there appears to be a strong site difference in  $Pn/Sn$  amplitude ratios between KEV and Spitzbergen.

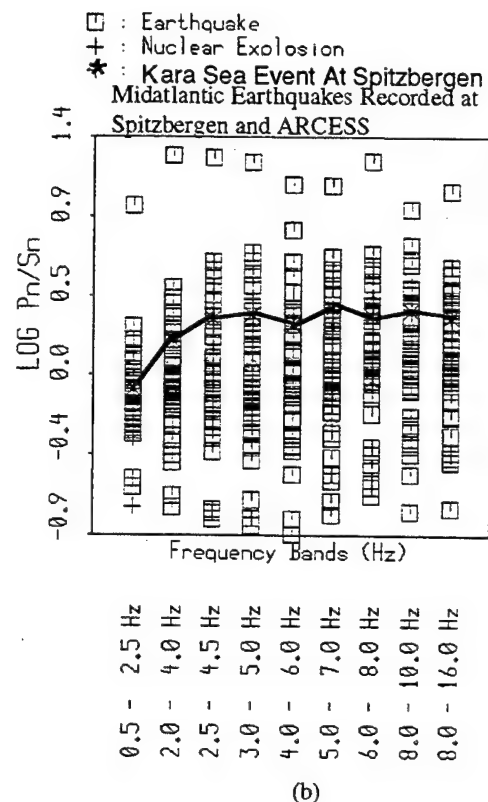
In Figure 36 (b), we have also plotted earthquakes near the mid-Atlantic ridge, recorded at ARCESS, as well as the Novaya nuclear explosions recorded ARCESS. All these points have been corrected for distance using the Scandinavian trends determined by Sereno (1991). These events do not discriminate, and have comparable values to the August 16, 1997 Kara Sea event. Also, it is impossible to characterize the Kara Sea event against the nearby earthquakes on the mid Atlantic ridge.

Figure 37 shows the same events plotted as a function of frequency band. The Kara Sea event is shown as the asterisks and the points are connected with a line. Figure 37 (a) only shows the Spitzbergen data, whereas in Figure 37 (b) we have included the ARCESS data. This plot also shows that the Spitzbergen measurements of  $Pn/Sn$  ratio cannot be distinguished from mid-Atlantic ridge earthquakes. But, we also cannot discriminate the event from nuclear blasts at ARCESS and KEV.

We suggest that the proximity of the Spitzbergen station to the mid-Atlantic ridge causes  $Sn$  waves from the ridge and from the Novaya Zemlya region to be strongly attenuated. This region is known to be more tectonically active, with likely higher mantle heat flow because of the upwelling at the mid-Atlantic ridge. Earthquakes near or on the ridge have severely attenuated  $Sn$  waves, and the  $Pn/Sn$  ratios of such events look like nuclear explosions. However, earthquakes recorded at the mid-Atlantic ridge should not be considered to be consistent with any earthquakes in the Novaya Zemlya region, because the latter is in a more stable platform tectonic region. Moreover, the Spitzbergen station itself should not be used for identification of events in the Novaya Zemlya region, using the  $Pn/Sn$  amplitude ratio, because  $Sn$  waves from both nuclear explosions and earthquakes recorded there would be highly attenuated at high frequency.



(a)



(b)

Figure 37: Plots of the  $\log_{10} Pn/Sn$  ratios for discriminants for the August 16, 1997 recorded at Spitzbergen and mid-Atlantic ridge earthquakes plotted versus frequency. The line connects the  $Pn/Sn$  ratio values for the Kara Sea event recorded at KEV. (a) Spitzbergen and KEV data, (b) Spitzbergen, KEV, and ARCESS data.

The point of this analysis is to emphasize that only data which provide discriminatory information should be used in discrimination. In principle, only one well-recorded measurement of a low  $Pn/Sn$  ratio would be required to identify an earthquake. Thus, KEV recorded  $Pn/Sn$  ratios less than 1 at KEV at frequencies above 4 Hz, and that should be sufficient to identify the event even if this cannot be done at any other station. This is only valid if nuclear explosions never produce  $Pn/Sn$  ratio less than 1 at frequencies above 4 Hz. At Novaya Zemlya, this seems to usually be the case. However, we have pointed out here and in numerous earlier studies the mine blasts can have low, earthquake-like  $Pn/Sn$  amplitude ratios at high frequency which appear to be caused by ripple fire-induced cracking and/or spall in the mines. Whether or not these kinds of effects can be produced frequently in nuclear explosions requires further investigation.

Finally, we also emphasize that high values of  $Pn/Sn$  ratio do not, by themselves, conclusively identify nuclear explosions because other effects, including attenuation and, in the

case of  $Lg$ , blockage can make earthquakes look like explosions. A convincing case must be made that no such phenomena affect the  $Pn/Sn$  ratio for earthquakes which could cause false identifications of nuclear explosions.

### **3.7 Was the Kara Sea Event An Underwater Explosion?**

We now consider the question of whether or not the Kara Sea event could have been an undersea detonation of a device on the sea bottom or buried beneath the sea bottom, given that the best seismic locations have placed the August 16 event in the Kara Sea in a region with about 225 m of water. If the event had been an explosion in the water or beneath the water, we would expect the signals to be much larger than a comparable explosion buried on land. However, the signals we observed for the August 16, 1997 Kara Sea event, were not unusually large.

Another way to characterize an underwater explosion is to examine spectral and cepstral features for evidence of bubble pulses and water column reverberations. For this, we draw on recent analysis of presumed underwater explosions in the southern part of Norway and Finland, discussed by Baumgardt and Der (1998).

One of the most direct ways of identifying underwater explosions is to detect bubble pulses. Baumgardt and Der (1998) looked for evidence of bubble pulses for undersea events recorded at the FINESA and NORESS. The pattern of multiple signals, produced by an underwater blast primary pulse and a series of correlated bubble pulses, are simpler than the multiple shots produced by ripple firing. The primary and first bubble pulse should act as delayed sources with each generating a full complement of regional phases, produced by mode conversion at the water/sea-bottom interface of acoustic waves in the water to seismic waves in the solid earth, and recorded seismically at regional distances.

Figure 38 (a) and (b) shows examples of spectra and cepstra for regional seismic phases from an event, recorded at FINESA and NORESS, from Baumgardt and Der (1998). The spectra in Figures 38 (a) and (b) reveal strong spectral scalloping evident in all the regional phases. To characterize this modulation, we analyzed cepstra computed using methods described by Baumgardt and Ziegler (1988). In brief, the linear trends of the spectra were removed and low-frequency blowup, due the removal of the instrument response, was smoothed. The logarithm of the instrument corrected amplitude spectrum was then Fourier transformed to produce the cepstra in Figures 38 (c) and (d).

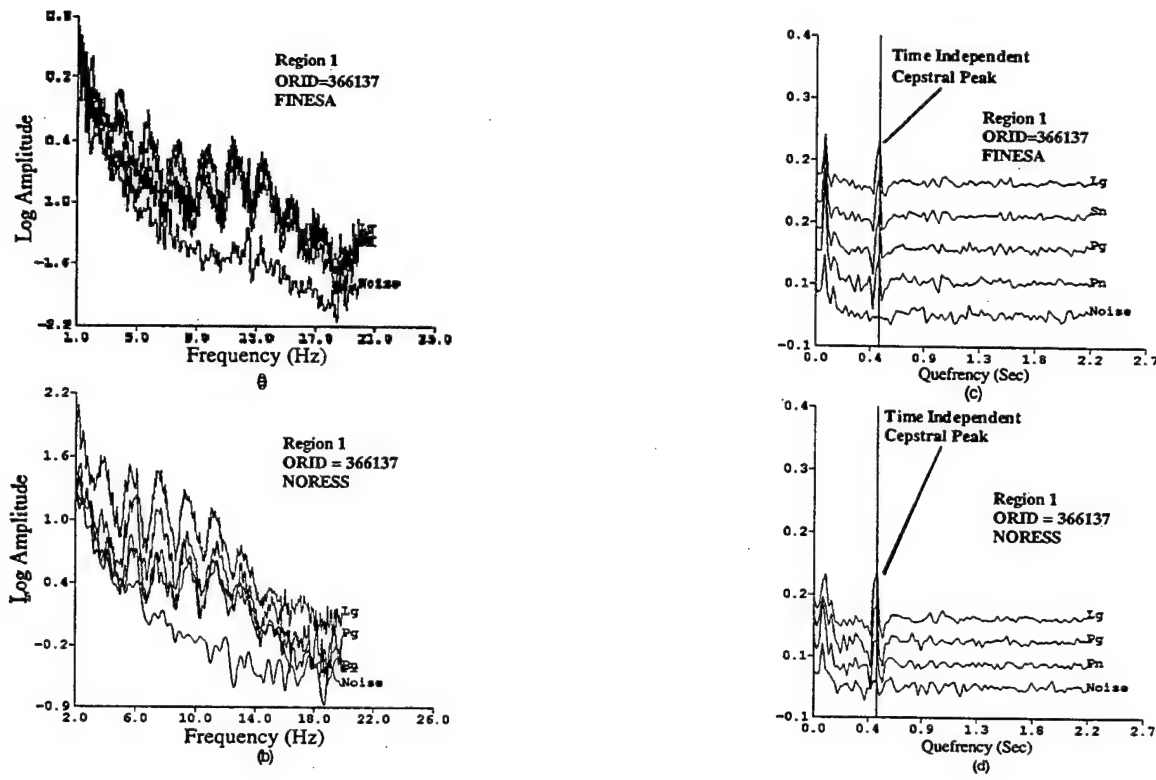


Figure 38: (a) Spectra for an event recorded at FINESA. (b) Spectra for the same event recorded at NORESS. (c) Cepstra computed for the event in (a). (d) Cepstra computed for the event in (b).

Time-independent spectral modulations should produce cepstral peaks that line up in quefrency for all associated phases. The vertical line in Figure 38 (c) and (d) marks the cepstral peaks that have the same quefrency at both the FINESA and NORESS arrays. The main cepstral peaks line up at frequencies of about 0.45 seconds, or 450 milliseconds. This cepstral peak is very strong at both arrays and indicates that the seismograms at both arrays consist of a series of pulse-echoes with time delays of 450 ms.

These plots are typical of several events, studied by Baumgardt and Der (1998), that occurred offshore but were detected by the seismic arrays NORESS and FINESA. The spectral scalloping is reminiscent of features seen on hydroacoustic recordings of explosions, which produce multiple arrivals from bubble pulses and water column reverberations. The cepstra, which are similar to autocorrelation functions, have spectral peaks which give the time delays between the primary pulse and the delayed pulse presumably produced by the bubble pulse.

time delays between the primary pulse and the delayed pulse presumably produced by the bubble pulse.

We next consider if such features appear for the spectra and cepstra of the signals from the Kara Sea event. Figure 39 shows plots of the spectra computed for all the stations. All spectra have been array averaged at the arrays and are single channel spectra for KEV. The spectra have smoothed by means of the Parzen window and the instrument responses have been removed.

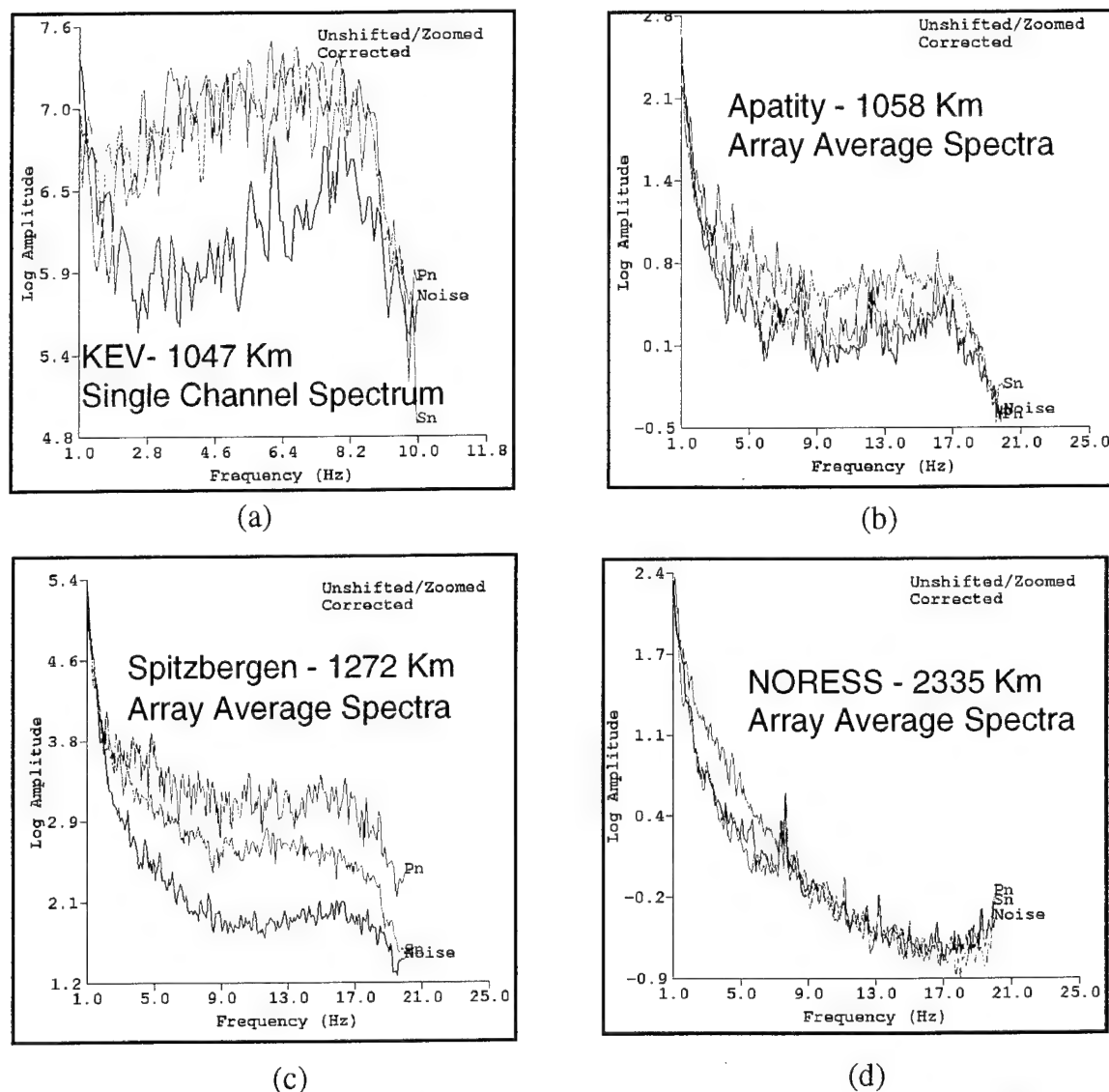


Figure 39: Plots of array averaged spectra for the recordings of the August 16, 1997 Kara Sea Event at four recording stations. (a) KEV, (b) Apatity, (c) Spitzbergen, and (d) NORESS.

In a recent study of the Middle East (Baumgardt, 1996), spectral/cepstral analysis of earthquakes in the Gulf of Aqaba revealed cepstral peaks that may have resulted from underwater reverberations. Presumably, these reverberations are produced when seismic waves from the earthquake convert to acoustic waves in the ocean, reverberate in the water column, and then convert back to seismic waves. Thus, it might be possible to determine or confirm if an earthquake is underwater by looking for underwater reverberations. However, we would not expect to see modulations as strong as those produced by bubble pulses and reverberations from underwater explosions.

The cepstra for the four events are shown in Figure 40.

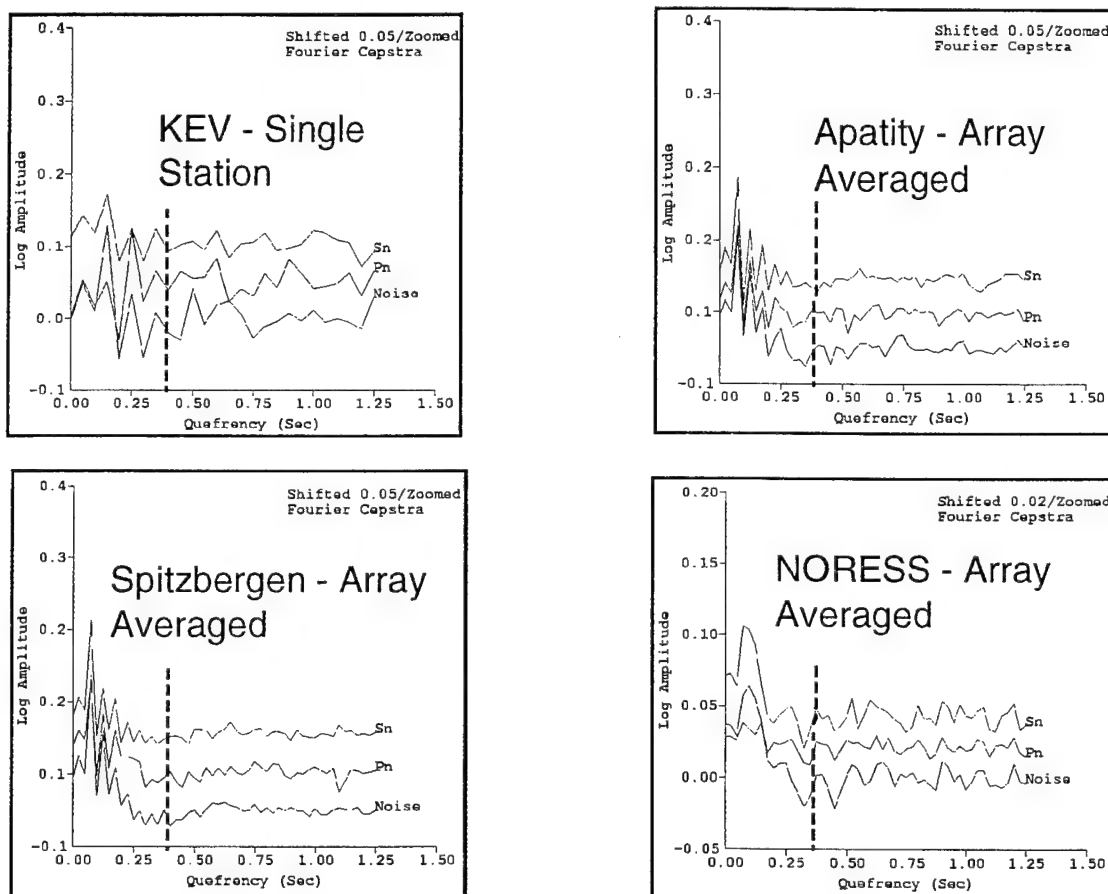


Figure 40: Cepstra for August 16, 1997 Kara Sea Event - 225 m Water Depth => 0.325 sec. (a) KEV, (b) Apatity, (c) Spitzbergen, (d) NORESS.

We look for evidence in these cepstra of such underwater reverberations. Each cepstrum has a vertical dashed line placed at the presumed time for the two-way water reverberation for 225 m of water, about 0.325 seconds. We see no evidence of any kind of consistent

peak at this time delay or near it for any of the cepstra that does not also appear in the spectra of the noise cepstra.

In Figure 30, we note that the paths for the four stations KEV, Apatity, Spitzbergen, and NORESS all have to cross the island. Thus, it is possible that there was not a sufficiently long coherent water column to produce observable water column reverberations. Ideally, we should analyze records due east of the location to look for such reflections. As a check for this, we also analyzed data at the station at NRI located east of the event location, as shown in Figure 30.

This path crosses straight over the eastern part of the Kara Sea. We had not originally studied this data because of its low quality and emergent signals. Figure 41 shows the incoherent beams (a) and spectra (b) for the signals recorded at NRI.

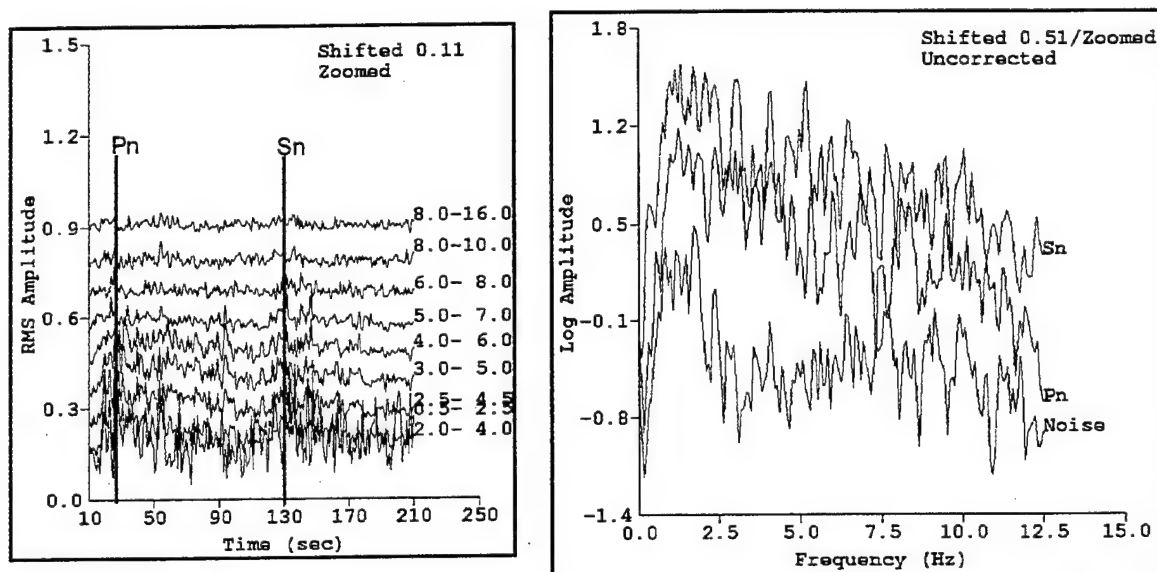


Figure 41: NRI incoherent beams (a) and Spectra (b) for propagation path east of the Kara Sea

The spectrum in Figure 41 is somewhat intriguing in that there is some scalloping in the phases. However, the apparent scalloping is distorted, and it is not clear that the scalloping is any different than the scalloping in the noise spectra. The signal levels are too weak and the bandwidth too limited to allow conclusive identification of scalloping. However, there is no evidence of the kinds of strong scalloping we have seen in underwater explosions caused by bubble pulses and reverberations.

### **3.8 Overall Conclusions**

We conclude overall that, based on analysis of the waveform characteristics, the August 16, 1997 event was an earthquake. The fact that the event was located in the Kara Sea clearly shows the event would not have been a normal test since it occurred well away from the test site. Based on the lack of clear spectral modulations and fairly weak signals, the event does not have any of the characteristics of underwater explosions. However, we were unable to confirm the undersea location with observation of underwater reverberations.

This study has shown the kinds of problems that will be encountered in Special Event analysis under the CTBT. In regions of limited data coverage and lacking a definitive understanding of the  $P/S$  amplitude ratio discrimination, we cannot often make conclusive arguments about event identification. In the case of Novaya Zemlya, we have an extensive archive of nuclear explosions but limited earthquakes. Other regions of the world might have the reverse, a large earthquake archive but no nuclear explosions. We have argued in this section that discriminants must be transported, and that it may often be necessary to combine data recorded at different stations. The limitations of this approach were shown for the case of the Spitzbergen recordings of the August 16, 1997 Kara Sea event, where it would be impossible to discriminate earthquakes and nuclear explosions.

Finally, we conclude that discrimination of Special Events can and should be done only with stations with good discriminatory capability. We do not, for example, believe that data from NRI or Spitzbergen should be used, the former because of low signal-to-noise ratio and the latter because of poor discrimination capability caused by strong  $S_n$  attenuation. The fact that one station, KEV, observed strong earthquake-like characteristics should be sufficient to identify the event as an earthquake. This, of course, assumes all nuclear explosions will have high  $Pn/Sn$  ratios at high frequency. Whether this is true worldwide under all conditions is not yet well understood.

## REFERENCES

- Anderson, J., W.E. Farrell, K. Garcia, J. Given, and H. Swanger (1990). Center for Seismic Studies Version 3 Database: Schema Reference Manual, Technical Report C90-01, Center for Seismic Studies, Arlington, VA.
- Baumgardt, D.R. (1991). High frequency array studies of long range  $Lg$  propagation and the causes of  $Lg$  blockage and attenuation of the Eurasian continental craton, PL-TR-91-2059(II), 21 March 1991, ADA236984.
- Baumgardt, D.R. (1993a). Regional characterization of mine blasts, earthquakes, mine tremors, and nuclear explosions using the Intelligent Event Identification System, Final Report to ARPA, SAS-TR-94-12, ENSCO, Inc., Springfield, VA.
- Baumgardt, D.R. (1993b). Seismic waveform feature analysis and discrimination of the December 31, 1992 Novaya Zemlya event, in *The Novaya Zemlya Event of 31 December 1992 and Seismic Identification Issues, 15 th Annual Seismic Research Symposium, ARPA Report*, 30pp, PL-TR-93-2160, ADA271458.
- Baumgardt, D.R. (1995). Case studies of seismic discrimination problems and regional discriminant transportability, *PL-TR-95-2106*, Final Report, ENSCO, Inc., Springfield, VA, ADA302362.
- Baumgardt, D.R. (1996). Investigation of  $Lg$  blockage and the transportability of regional discriminants in the Middle East, *PL-TR-96-2294*, Scientific Report No. 1, ENSCO, Inc., Springfield, VA, ADA323818.
- Baumgardt, D.R. and Z. Der (1994). Investigation of the transportability of the  $P/S$  ratio discriminant to different tectonic regions, *Scientific Report No. 1*, PL-TR-94-2299, 6 December 1994, ENSCO, Inc, ADA292944.
- Baumgardt D.R. and Z. Der (1998), Identification of presumed shallow underwater chemical explosions using land-based arrays. *Bull. Seism. Soc. Am.* (in press).
- Baumgardt, D.R. and M.S. Karafotis (1995). Seismic discrimination and information fusion using Bayesian belief networks, Final Report, *SAS-TR-95-119*, ENSCO, Inc., Springfield, VA.

Baumgardt, D.R. and K.A. Ziegler (1988). Spectral evidence of source multiplicity in explosions: application to regional discrimination of earthquakes and explosions, *Bull. Seism. Soc. Am.*, **78**, 1773-1795.

Baumgardt, D.R. and G. Young (1990). Regional seismic waveform discriminants and case based event identification using regional arrays, *Bull. Seism. Soc. Am.*, **80**, Part B, 1874-1892.

Baumgardt, D.R., S. Carter, M. Maxson, J. Carney, K. Ziegler, and N. Matson (1991b). Design and development of the intelligent event identification system, *PL-TR-91- 22298(I)*, Final Report, Volumes I,II, and III, ENSCO, Inc., Springfield, VA, I:ADA248381; II: ADA248934; III: ADA248374.

Bonner, J. E. Herrin, and G. G. Sorrells (1997). Regional discrimination studies: Phase III, *PL-TR-97-2064*, Southern Methodist University, Dallas, TX, ADA328228.

Goldstein, P. (1995). Slopes of P-to S-wave spectral ratios - a broadband regional seismic discriminant and a physical model, *Geophys. Res. Letters*, **22**, 3147-3150.

Israelsson, H. M.D. Fisk, X. Yang, and R.G. North (1997). The August 16, 1997 event in the Kara Sea, *CMR-97/38*, Center for Monitoring Research, Arlington, VA.

Murphy, J.R. and T.J. Bennett (1982). A discrimination analysis of short-period regional seismic data recorded at Tonto Forest Observatory, *Bull. Seism. Soc. Am.*, **72**, 1351-1366.

Richards, P.G. and W.Y. Kim (1997). Testing the nuclear test-band treaty, *Nature*, **389**, 781-782.

Ryall, A.S., D.R. Baumgardt, M.D. Fisk, F. Riviere-Barbier (1996). Resolving regional discrimination problems: some case histories, in *Monitoring a Comprehensive Test Ban Treaty*, E.S. Huysebye and A.M. Dainty, 721-741, NATO ASI Series, Kluwer Academic Publishers.

Sereno, T.J. (1991). Simulation of the detection and location capability of regional seismic networks in the Soviet Union, Final Report, *SAIC-91/1061*, SAIC, San Diego, CA.

Stump, B.W. and D.C. Pearson (1997). Comparison of single-fired and delay-fired explosions at regional and local distances, Proceedings of the 19th Annual Seismic Research

Symposium on Monitoring a Comprehensive Test Ban Treaty, 23-25 September 1997,  
Orlando, Fla., pp 668-677.

Wuster, J. (1993). Discrimination of chemical explosions and earthquakes in central  
Europe - a case study, *Bull. Seism. Soc. Am.*, **83**, 1184-1212.

THOMAS AHRENS  
SEISMOLOGICAL LABORATORY 252-21  
CALIFORNIA INST. OF TECHNOLOGY  
PASADENA, CA 91125

AIR FORCE RESEARCH LABORATORY  
ATTN: VSOE  
29 RANDOLPH ROAD  
HANSCOM AFB, MA 01731-3010 (2 COPIES)

AIR FORCE RESEARCH LABORATORY  
ATTN: RESEARCH LIBRARY/TL  
5 WRIGHT STREET  
HANSCOM AFB, MA 01731-3004

AIR FORCE RESEARCH LABORATORY  
ATTN: AFRL/SUL  
3550 ABERDEEN AVE SE  
KIRTLAND AFB, NM 87117-5776 (2 COPIES)

RALPH ALEWINE  
NTPO  
1901 N. MOORE STREET, SUITE 609  
ARLINGTON, VA 22209

MUAWIA BARAZANGI  
INSTOC  
3126 SNEE HALL  
CORNELL UNIVERSITY  
ITHACA, NY 14853

T.G. BARKER  
MAXWELL TECHNOLOGIES  
8888 BALBOA AVE.  
SAN DIEGO, CA 92123-1506

DOUGLAS BAUMGARDT  
ENSCO INC.  
5400 PORT ROYAL ROAD  
SPRINGFIELD, VA 22151

THERON J. BENNETT  
MAXWELL TECHNOLOGIES  
11800 SUNRISE VALLEY  
SUITE 1212  
RESTON, VA 22091

WILLIAM BENSON  
NAS/COS  
ROOM HA372  
2001 WISCONSIN AVE. NW  
WASHINGTON DC 20007

JONATHAN BERGER  
UNIV. OF CALIFORNIA, SAN DIEGO  
SCRIPPS INST. OF OCEANOGRAPHY IGPP, 0225  
9500 GILMAN DRIVE  
LA JOLLA, CA 92093-0225

ROBERT BLANDFORD  
AFTAC  
1300 N. 17TH STREET  
SUITE 1450  
ARLINGTON, VA 22209-2308

LESLIE A. CASEY  
DEPT. OF ENERGY/NN-20  
1000 INDEPENDENCE AVE. SW  
WASHINGTON DC 20585-0420

CENTER FOR MONITORING RESEARCH  
ATTN: LIBRARIAN  
1300 N. 17th STREET, SUITE 1450  
ARLINGTON, VA 22209

ANTON DAINTY  
HQ DSWA/PMA  
6801 TELEGRAPH ROAD  
ALEXANDRIA, VA 22310-3398

CATHERINE DE GROOT-HEDLIN  
UNIV. OF CALIFORNIA, SAN DIEGO  
IGPP  
8604 LA JOLLA SHORES DRIVE  
SAN DIEGO, CA 92093

DIANE DOSER  
DEPT. OF GEOLOGICAL SCIENCES  
THE UNIVERSITY OF TEXAS AT EL PASO  
EL PASO, TX 79968

DTIC  
8725 JOHN J. KINGMAN ROAD  
FT BELVOIR, VA 22060-6218 (2 COPIES)

MARK D. FISK  
MISSION RESEARCH CORPORATION  
735 STATE STREET  
P.O. DRAWER 719  
SANTA BARBARA, CA 93102-0719

LORI GRANT  
MULTIMAX, INC.  
311C FOREST AVE. SUITE 3  
PACIFIC GROVE, CA 93950

HENRY GRAY  
SMU STATISTICS DEPARTMENT  
P.O. BOX 750302  
DALLAS, TX 75275-0302

DAVID HARKRIDER  
BOSTON COLLEGE  
INSTITUTE FOR SPACE RESEARCH  
140 COMMONWEALTH AVENUE  
CHESTNUT HILL, MA 02167

MICHAEL HEDLIN  
UNIVERSITY OF CALIFORNIA, SAN DIEGO  
SCRIPPS INST. OF OCEANOGRAPHY  
9500 GILMAN DRIVE  
LA JOLLA, CA 92093-0225

EUGENE HERRIN  
SOUTHERN METHODIST UNIVERSITY  
DEPT. OF GEOLOGICAL SCIENCES  
DALLAS, TX 75275-0395

VINDELL HSU  
HQ/AFTAC/TTR  
1030 S. HIGHWAY A1A  
PATRICK AFB, FL 32925-3002

THOMAS JORDAN  
MASS. INST. OF TECHNOLOGY  
BLDG 54-918  
CAMBRIDGE, MA 02139

LAWRENCE LIVERMORE NAT'L LAB  
ATTN: TECHNICAL STAFF (PLS ROUTE)  
PO BOX 808, MS L-208  
LIVERMORE, CA 94551

LAWRENCE LIVERMORE NAT'L LAB  
ATTN: TECHNICAL STAFF (PLS ROUTE)  
PO BOX 808, MS L-200  
LIVERMORE, CA 94551

THORNE LAY  
UNIV. OF CALIFORNIA, SANTA CRUZ  
EARTH SCIENCES DEPARTMENT  
EARTH & MARINE SCIENCE BUILDING  
SANTA CRUZ, CA 95064

I. N. GUPTA  
MULTIMAX, INC.  
1441 MCCORMICK DRIVE  
LARGO, MD 20774

THOMAS HEARN  
NEW MEXICO STATE UNIVERSITY  
DEPARTMENT OF PHYSICS  
LAS CRUCES, NM 88003

DONALD HELMBERGER  
CALIFORNIA INST. OF TECHNOLOGY  
DIV. OF GEOL. & PLANETARY SCIENCES  
SEISMOLOGICAL LABORATORY  
PASADENA, CA 91125

ROBERT HERRMANN  
ST. LOUIS UNIVERSITY  
DEPT. OF EARTH & ATMOS. SCIENCES  
3507 LACLEDE AVENUE  
ST. LOUIS, MO 63103

RONG-SONG JIH  
HQ DSWA/PMA  
6801 TELEGRAPH ROAD  
ALEXANDRIA, VA 22310-3398

LAWRENCE LIVERMORE NAT'L LAB  
ATTN: TECHNICAL STAFF (PLS ROUTE)  
PO BOX 808, MS L-175  
LIVERMORE, CA 94551

LAWRENCE LIVERMORE NAT'L LAB  
ATTN: TECHNICAL STAFF (PLS ROUTE)  
PO BOX 808, MS L-202  
LIVERMORE, CA 94551

LAWRENCE LIVERMORE NAT'L LAB  
ATTN: TECHNICAL STAFF (PLS ROUTE)  
PO BOX 808, MS L-205  
LIVERMORE, CA 94551

LAWRENCE LIVERMORE NAT'L LAB  
ATTN: TECHNICAL STAFF (PLS ROUTE)  
PO BOX 808, MS L-221  
LIVERMORE, CA 94551

ANATOLI L. LEVSHIN  
DEPARTMENT OF PHYSICS  
UNIVERSITY OF COLORADO  
CAMPUS BOX 390  
BOULDER, CO 80309-0309

JAMES LEWKOWICZ  
WESTON GEOPHYSICAL CORP.  
325 WEST MAIN STREET  
NORTHBORO, MA 01532

LOS ALAMOS NATIONAL LABORATORY  
ATTN: TECHNICAL STAFF (PLS ROUTE)  
PO BOX 1663, MS F665  
LOS ALAMOS, NM 87545

GARY MCCARTOR  
SOUTHERN METHODIST UNIVERSITY  
DEPARTMENT OF PHYSICS  
DALLAS, TX 75275-0395

BRIAN MITCHELL  
DEPARTMENT OF EARTH & ATMOSPHERIC SCIENCES  
ST. LOUIS UNIVERSITY  
3507 LACLEDE AVENUE  
ST. LOUIS, MO 63103

JOHN MURPHY  
MAXWELL TECHNOLOGIES  
11800 SUNRISE VALLEY DRIVE  
SUITE 1212  
RESTON, VA 22091

ROBERT NORTH  
CENTER FOR MONITORING RESEARCH  
1300 N. 17th STREET, SUITE 1450  
ARLINGTON, VA 22209

JOHN ORCUTT  
INST. OF GEOPH. & PLANETARY PHYSICS  
UNIV. OF CALIFORNIA, SAN DIEGO  
LA JOLLA, CA 92093

PACIFIC NORTHWEST NAT'L LAB  
ATTN: TECHNICAL STAFF (PLS ROUTE)  
PO BOX 999, MS K6-40  
RICHLAND, WA 99352

PACIFIC NORTHWEST NAT'L LAB  
ATTN: TECHNICAL STAFF (PLS ROUTE)  
PO BOX 999, MS K5-12  
RICHLAND, WA 99352

KEITH PRIESTLEY  
DEPARTMENT OF EARTH SCIENCES  
UNIVERSITY OF CAMBRIDGE  
MADINGLEY RISE, MADINGLEY ROAD  
CAMBRIDGE, CB3 OEZ UK

LOS ALAMOS NATIONAL LABORATORY  
ATTN: TECHNICAL STAFF (PLS ROUTE)  
PO BOX 1663, MS F659  
LOS ALAMOS, NM 87545

LOS ALAMOS NATIONAL LABORATORY  
ATTN: TECHNICAL STAFF (PLS ROUTE)  
PO BOX 1663, MS C335  
LOS ALAMOS, NM 87545

KEITH MC LAUGHLIN  
CENTER FOR MONITORING RESEARCH  
SAIC  
1300 N. 17TH STREET, SUITE 1450  
ARLINGTON, VA 22209

RICHARD MORROW  
USACDA/IVI  
320 21ST STREET, N.W.  
WASHINGTON DC 20451

JAMES NI  
NEW MEXICO STATE UNIVERSITY  
DEPARTMENT OF PHYSICS  
LAS CRUCES, NM 88003

OFFICE OF THE SECRETARY OF DEFENSE  
DDR&E  
WASHINGTON DC 20330

PACIFIC NORTHWEST NAT'L LAB  
ATTN: TECHNICAL STAFF (PLS ROUTE)  
PO BOX 999, MS K6-48  
RICHLAND, WA 99352

PACIFIC NORTHWEST NAT'L LAB  
ATTN: TECHNICAL STAFF (PLS ROUTE)  
PO BOX 999, MS K6-84  
RICHLAND, WA 99352

FRANK PILOTTE  
HQ AFTAC/TT  
1030 S. HIGHWAY A1A  
PATRICK AFB, FL 32925-3002

JAY PULLI  
BBN SYSTEMS AND TECHNOLOGIES, INC.  
1300 NORTH 17TH STREET  
ROSSLYN, VA 22209

DELAINE REITER  
AFRL/VSOE (SENCOM)  
73 STANDISH ROAD  
WATERTOWN, MA 02172

MICHAEL RITZWOLLER  
DEPARTMENT OF PHYSICS  
UNIVERSITY OF COLORADO  
CAMPUS BOX 390  
BOULDER, CO 80309-0309

CHANDAN SAIKIA  
WOODWARD-CLYDE FED. SERVICES  
566 EL DORADO ST., SUITE 100  
PASADENA, CA 91101-2560

SANDIA NATIONAL LABORATORY  
ATTN: TECHNICAL STAFF (PLS ROUTE)  
DEPT. 9311  
MS 1159, PO BOX 5800  
ALBUQUERQUE, NM 87185-1159

SANDIA NATIONAL LABORATORY  
ATTN: TECHNICAL STAFF (PLS ROUTE)  
DEPT. 5736  
MS 0655, PO BOX 5800  
ALBUQUERQUE, NM 87185-0655

AVI SHAPIRA  
SEISMOLOGY DIVISION  
IPRG  
P.O.B. 2286 NOLON 58122 ISRAEL

MATTHEW SIBOL  
ENSCO, INC.  
445 PINEDA CT.  
MELBOURNE, FL 32940

JEFFRY STEVENS  
MAXWELL TECHNOLOGIES  
8888 BALBOA AVE.  
SAN DIEGO, CA 92123-1506

TACTEC  
BATTELLE MEMORIAL INSTITUTE  
505 KING AVENUE  
COLUMBUS, OH 43201 (FINAL REPORT)

LAWRENCE TURNBULL  
ACIS  
DCI/ACIS  
WASHINGTON DC 20505

PAUL RICHARDS  
COLUMBIA UNIVERSITY  
LAMONT-DOHERTY EARTH OBSERV.  
PALISADES, NY 10964

DAVID RUSSELL  
HQ AFTAC/TTR  
1030 SOUTH HIGHWAY A1A  
PATRICK AFB, FL 32925-3002

SANDIA NATIONAL LABORATORY  
ATTN: TECHNICAL STAFF (PLS ROUTE)  
DEPT. 5704  
MS 0979, PO BOX 5800  
ALBUQUERQUE, NM 87185-0979

SANDIA NATIONAL LABORATORY  
ATTN: TECHNICAL STAFF (PLS ROUTE)  
DEPT. 5704  
MS 0655, PO BOX 5800  
ALBUQUERQUE, NM 87185-0655

THOMAS SERENO JR.  
SAIC  
10260 CAMPUS POINT DRIVE  
SAN DIEGO, CA 92121

ROBERT SHUMWAY  
410 MRAK HALL  
DIVISION OF STATISTICS  
UNIVERSITY OF CALIFORNIA  
DAVIS, CA 95616-8671

DAVID SIMPSON  
IRIS  
1200 NEW YORK AVE., NW  
SUITE 800  
WASHINGTON DC 20005

BRIAN SULLIVAN  
BOSTON COLLEGE  
INSITUTE FOR SPACE RESEARCH  
140 COMMONWEALTH AVENUE  
CHESTNUT HILL, MA 02167

NAFI TOKSOZ  
EARTH RESOURCES LABORATORY  
M.I.T.  
42 CARLTON STREET, E34-440  
CAMBRIDGE, MA 02142

GREG VAN DER VINK  
IRIS  
1200 NEW YORK AVE., NW  
SUITE 800  
WASHINGTON DC 20005

FRANK VERNON  
UNIV. OF CALIFORNIA, SAN DIEGO  
SCRIPPS INST. OF OCEANOGRAPHY  
9500 GILMAN DRIVE  
LA JOLLA, CA 92093-0225

JILL WARREN  
LOS ALAMOS NATIONAL LABORATORY  
GROUP NIS-8  
P.O. BOX 1663  
LOS ALAMOS, NM 87545      (5 COPIES)

RU SHAN WU  
UNIV. OF CALIFORNIA, SANTA CRUZ  
EARTH SCIENCES DEPT.  
1156 HIGH STREET  
SANTA CRUZ, CA 95064

JAMES E. ZOLLWEG  
BOISE STATE UNIVERSITY  
GEOSCIENCES DEPT.  
1910 UNIVERSITY DRIVE  
BOISE, ID 83725

TERRY WALLACE  
UNIVERSITY OF ARIZONA  
DEPARTMENT OF GEOSCIENCES  
BUILDING #77  
TUCSON, AZ 85721

DANIEL WEILL  
NSF  
EAR-785  
4201 WILSON BLVD., ROOM 785  
ARLINGTON, VA 22230

JIAKANG XIE  
COLUMBIA UNIVERSITY  
LAMONT DOHERTY EARTH OBSERV.  
ROUTE 9W  
PALISADES, NY 10964